

2018

The Progressive Evolution of the Champlain Thrust Fault Zone: Insights from a Structural Analysis of its Architecture

Matthew Merson
University of Vermont

Follow this and additional works at: <https://scholarworks.uvm.edu/graddis>



Part of the [Geology Commons](#)

Recommended Citation

Merson, Matthew, "The Progressive Evolution of the Champlain Thrust Fault Zone: Insights from a Structural Analysis of its Architecture" (2018). *Graduate College Dissertations and Theses*. 896.
<https://scholarworks.uvm.edu/graddis/896>

This Thesis is brought to you for free and open access by the Dissertations and Theses at ScholarWorks @ UVM. It has been accepted for inclusion in Graduate College Dissertations and Theses by an authorized administrator of ScholarWorks @ UVM. For more information, please contact donna.omalley@uvm.edu.

THE PROGRESSIVE EVOLUTION OF THE CHAMPLAIN THRUST FAULT ZONE:
INSIGHTS FROM A STRUCTURAL ANALYSIS OF ITS ARCHITECTURE

A Thesis Presented

by

Matthew Quintin Merson Jr.

to

The Faculty of the Graduate College

of

The University of Vermont

In Partial Fulfillment of the Requirements
for the Degree of Master of Science
Specializing in Geology

May, 2018

Defense Date: March 22, 2018
Thesis Examination Committee:

Keith Klepeis, Ph.D., Advisor
Mandar Dewoolkar, Ph.D., Chairperson
Laura Webb, Ph.D.
Cynthia J. Forehand, Ph.D., Dean of the Graduate College

ABSTRACT

Near Burlington, Vermont, the Champlain Thrust fault placed massive Cambrian dolostones over calcareous shales of Ordovician age during the Ordovician Taconic Orogeny. Although the Champlain Thrust has been studied previously throughout the Champlain Valley, the architecture and structural evolution of its fault zone have never been systematically defined. To document these fault zone characteristics, a detailed structural analysis of multiple outcrops was completed along a 51 km transect between South Hero and Ferrisburgh, Vermont.

The Champlain Thrust fault zone is predominately within the footwall and preserves at least four distinct events that are heterogeneous in both style and slip direction. The oldest stage of structures—stage 1—are bedding parallel thrust faults that record a slip direction of top-to-the-W and generated localized fault propagation folds of bedding and discontinuous cleavages. This stage defines the protolith zone and has a maximum upper boundary of 205 meters below the Champlain Thrust fault surface. Stage 2 structures define the damage zone and form two sets of subsidiary faults form thrust duplexes that truncate older recumbent folds of bedding planes and early bedding-parallel thrusts. Slickenlines along stage 2 faults record a change in slip direction from top-to-the-W to top-to-the-NW. The damage zone is ~197 meters thick with its upper boundary marking the lower boundary of the fault core. The core, which is ~8 meters thick, is marked by the appearance of mylonite, phyllitic shales, fault gouge, fault breccia, and cataclastic lined faults. In addition, stage 3 sheath folds of bedding and cleavage are preserved as well as tight folds of stage 2 faults. Stage 3 faults include thrusts that record slip as top-to-the-NW and -SW and coeval normal faults that record slip as top-to-the-N and -S. The Champlain Thrust surface is the youngest event as it cuts all previous structures, and records fault reactivation with any top-to-the-W slip direction and a later top-to-the-S slip. Axes of mullions on this surface trend to the SE and do not parallel slickenlines.

The Champlain Thrust fault zone evolved asymmetrically across its principal slip surface through the process of strain localization and fault reactivation. Strain localization is characterized by the changes in relative age, motion direction along faults, and style of structures preserved within the fault zone. Reactivation of the Champlain Thrust surface and the corresponding change in slip direction was due to the influence of pre-existing structures at depth. This study defines the architecture of the Champlain Thrust fault zone and documents the importance of comparing the structural architecture of the fault zone core, damage zone, and protolith to determine the comprehensive fault zone evolution.

DEDICATION

“Any scientist worth listening to must be something of a poet. Must possess the ability to communicate to the rest of us his sense of love and wonder at what his work discovers.”

---Edward Abbey---

The work that this document represents is dedicated to Lilah and Crosby.

They are the reason.

ACKNOWLEDGEMENTS

There is no one I can thank more than my wife, Michelle. Your undying, unwavering, unconditional love, support, and care is the reason I can do anything worthwhile. I can only hope to love you the same way in return.

Thank you, Keith Klepeis. You are truly an incredible leader. Your support, encouragement, and example will be something that I will always try to emulate.

Thank you, Joseph Allen. You instilled in me a passion and a drive to understand the complexities of our Earth. You are more than a teacher, you are a mentor.

I also wish to thank my parents, Quintin and Cathy. You have supported me through every adventure. Thank you for being the parents that I strive to be.

This project was partially funded through the University of Vermont's College of Arts and Sciences **Faculty Research Support Award (FRSA)** awarded to Keith Klepeis.

TABLE OF CONTENTS

DEDICATION.....	ii
ACKNOWLEDGEMENTS	iii
LIST OF TABLES	vi
LIST OF FIGURES	vii
CHAPTER 1: INTRODUCTION.....	1
CHAPTER 2: GEOLOGIC BACKGROUND	4
2.1: Introduction	4
2.2: Regional Tectonic History	7
2.3: The Champlain Thrust and Hinesburg Thrust.....	12
2.4: Fault Zone Development.....	14
2.5: Strain Localization	15
2.6: Thrust Ramps	16
2.7: Fault Reactivation	17
CHAPTER 3: THE ARCHITECTURE OF THE CHAMPLAIN THRUST FAULT ZONE	19
3.1: Introduction	19
3.2: Lessors Quarry, South Hero, Vermont.....	25
3.3: The Beam, South Hero, Vermont.....	28
3.4: Ferrisburgh Quarry, Ferrisburgh, Vermont.....	30
3.5: “The Driveway” and “The Flea Market”, Charlotte, Vermont	32
3.6: Lone Rock Point, Burlington, Vermont	37
3.7: Fault Zone Architecture	54
3.8: Relative Strain Description and Distribution	58
3.9: Conclusion.....	63
CHAPTER 4: THE PROGRESSIVE EVOLUTION OF THE CHAMPLAIN THRUST FAULT ZONE	65
4.1: Introduction	65
4.2: Fault Zone Evolution.....	66
4.3: Change in Motion Direction Along Faults.....	68
4.4: Change in Structural Style	71
4.5: Champlain Thrust Fault Reactivation	75
CHAPTER 5: SUMMARY AND FUTURE WORK.....	81
5.1: Introduction	81
5.2: Fault Zone Architecture Summary.....	81

5.3: Fault Zone Evolution Summary	82
5.4: Future Work	85
COMPREHENSIVE BIBLIOGRAPHY	87
APPENDIX I	95
APPENDIX II.....	96

LIST OF TABLES

	Page
3.1	24
Field location and relative age (stage) of structures preserved throughout the Champlain Thrust fault zone within northwestern Vermont	
3.2	60
Defining characteristics and examples of relative strain zones within the Champlain Thrust fault zone	

LIST OF FIGURES

	Page
1.1	2
Vermont bedrock units of various ages. The Champlain Thrust, exposed along the western edge of Vermont, is a low-angle frontal thrust associated with the Taconic orogeny. The Champlain Thrust fault emplaces massive Cambrian carbonate and siliciclastic units atop Ordovician shales.	
1.2	4
Four theoretical end member models that describe shear zone evolution through time. A) Type 1 model indicates that active deformation accumulates at shear zone boundaries. B) Type 2 model indicates that active deformation localizes towards the center of the shear zone. C) Type 3 model indicates that active deformation is homogeneously distributed through the shear zone through time. D) Type 4 model indicates that active deformation evenly grows through the fault zone through time. (Means, 1995; Vitale and Mazzoli, 2008). Figure adapted from Fossen and Cavalcante (2017).	
2.1	7
Approximate terrane boundaries associated with late Proterozoic through late Devonian orogenic events in present day New England and Southern Quebec. Boundaries and terrane names from Karabinos et al. (2017).	
2.2	8
Simplified tectonic model of orogenic events in New England during early to mid-Paleozoic. Modified from Karabinos et al. (2017).	
2.3	9
Mapped bedrock belts across Vermont. Modified from Kim et al. (2011).	
2.4	13
Lithostratigraphic column of rock units associated with the Champlain Thrust and Hinesburg Thrust faults exposed in northwest Vermont. Modified from Kim et al. (2011).	
2.5	14
A simplified model of fault zone architecture and components. Modified from Mitchell and Faulkner (2009) and Caine et al. (2010).	
3.1	21
Location of field sites analyzed for determining the extent and characteristics of the Champlain Thrust fault zone exposed in northwestern Vermont. Map adapted from Ratcliffe et al. (2011).	
3.2	22
The calculated depth of each field site below the westward projection of the Champlain Thrust surface. The top of the bar represents location for an assumed 10° constant dip of the fault surface and the bottom bar represents an assumed 15° constant dip (Stanley, 1990).	
3.3	23
Photograph of the heavily fractured Champlain Thrust hanging wall exposed at Lone Rock Point. Fractures are predominately sub-vertical with three common orientations: NE striking, SE striking, and SW striking.	
3.4	23
Photograph of a localized region of the hanging wall that preserves a < 1-meter damage zone of foliated rock with minor faults and fractures that cut foliation. Due to the extreme asymmetry of fault zone width across the Champlain Thrust fault, this project focuses primarily on the complex fault zone preserved in the footwall.	
3.5	26
A) Composite map of structures seen throughout Lessors Quarry. B) Equal area stereographic projections of early and late stage 1 structures including bedding, dissolution cleavage, early and late faults, and fault zone cleavage. Slickenline orientations from late stage 1 faults indicate slip was top-to-the-NW.	

3.6	27
Bedding at Lessors Quarry consists of interbedded layers of light-grey limestone and a dark-grey to brown fossiliferous limestone. Bedding is cut by an early dissolution cleavage that has ~17cm spacing.	
3.7	29
A) Illustrated composite of early and late stage 1 structures preserved at “the beam”. Late stage 1 faults form a series of five stacked duplexes involving a 30-centimeter thick micrite layer. B) Equal area stereographic projections of stage 1 structures including bedding, early cleavage, late stage thrust faults, and late stage 1 fault zone cleavage. Slickenline orientations from late stage 1 faults indicate slip as top-to-the-NW.	
3.8	31
A) Composite diagram of early and late stage 1 structures preserved at the Ferrisburgh Quarry. Late stage 1 faults are bedding parallel and cut an early stage 1 dissolution cleavage. B) Equal area stereographic projections of early and late stage 1 structures include bedding, early dissolution cleavage, and late stage faults. Slickenlines preserved on late stage 1 faults indicate slip of top-to-the-west.	
3.9	33
Bedding of the Stony Point Shale exposed at the “flea market” and “the driveway” are composed of alternating layers of dolostone, brown-weathered shale, and black-weathered shales. Bedding thickness varies across the outcrops and was used to determine the presence of two mappable sub-units. A) Unit 1 consists of beds that average 0.5–11 centimeters thick, whereas B) unit 2 consists of beds that average 0.5–35 centimeters thick.	
3.10	34
A–B) Structural map for portions of the “flea market” road cut along Route 7. Bedding is incorporated into early stage 2a folds that generated an axial planar cleavage. Late stage 2a faults cut bedding and early stage 2a folds. C) Equal area stereographic projections indicate that the early stage 2a folds are cylindrical with axes gently plunging toward the NE, and late stage 2a faults record slip as top-to-the-NW.	
3.11	35
A) Structure map of “the driveway” along Route 7. Bedding thickness variability was used to determine the presence of two mappable units. Unit 1 consists of beds 0.5 – 11 cm thick. Unit 2 consists of beds 0.5–35 cm thick. Early stage 2a folds incorporate bedding, late stage 1 faults, and generated an axial planar cleavage. Late stage 2a faults cut all earlier structures. B) Equal area stereographic projection of stage 1 and stage 2 faults and fold characteristics.	
3.12	37
Variability of cleavage spacing within shale and dolostone layers at “the driveway” and the “flea market”. Cleavage spacing within the shales is sub-centimeter, whereas cleavage spacing within the dolostone is ~2 cm near the hinge zone of folds and ~10 cm near inflection point. This cleavage refraction indicates the role that various rock type with various mechanical properties plays on cleavage formation (Treagus, 1988).	
3.13	39
A north to south profile of the Champlain Thrust fault surface exposed at Lone Rock Point. The elevation (\pm 1 meter) of the fault surface above a mid-summer water level of Lake Champlain was measured using an arc laser range finder in 2-meter increments along a horizontal transect. For location of aerial image see Figure 3.1.	
3.14	40
A) Structural map of Lone Rock Point section 1. Early stage 2a axial planar cleavage and late stage 2a faults are folded by early stage 2b folds and cut by late stage 2b thrust faults. These late stage 2b thrusts form a series of stacked duplexes at both the centimeter and meter scales. B) Equal area stereographic projections of structures indicate that both late stage 2a and 2b faults record a top-to-the-NW slip. Early stage 2b folds are predominately NW verging with axes plunging from NE-SE.	

3.15	41
A) Structural map of Lone Rock Point section 2. Late stage 2b faults cut and displace late stage 2a faults and early stage 2b folds of axial planar cleavage. Late stage 3a faults are also present and cut late stage 2b faults and associated stage 2b cleavage. B) Equal area stereographic projections of faults indicate that late stage 2a faults and late stage 2b faults have similar orientations and both record top-to-the-NW slip. Early stage 2b folds are W to NW verging folds with axes oriented to the NE and SE.	
3.16	42
A) Structural map of Lone Rock Point section 3. Late stage 2a faults and axial planar cleavage are cut and folded by late stage 2b faults. Late stage 3a normal faults cut late stage 2b faults and early stage 2a axial planar cleavage. B) Equal area stereographic projections of structures indicate both late stage 2a and 2b faults are of similar orientation with slip of top-to-the-NW. Late stage 3a normal faults record slip of top-to-the-north. Late stage 2b folds of cleavage are north verging folds with axes oriented to the NE, E, and a few toward the south.	
3.17	43
A) Structural map of Lone Rock Point section 4. Late stage 2b faults are cut by late stage 3a thrust and normal faults. Stage 2b transformed cleavage is incorporated into early stage 3a folds. B) Equal area stereographic projections of structures indicate that late stage 2b and late stage 3a thrust faults record slip as top-to-the-NW, whereas late stage 3a normal faults record slip top-to-the-N and top-to-the-S. Early stage 3a folds are NNW verging with axes predominately plunging to the SE.	
3.18	44
A) Early stage 2a folds incorporated bedding and generated an axial planar cleavage. These folds are primarily preserved at distances greater than 15 meters below the Champlain Thrust fault surface. B) Early stage 2b folds incorporated 2a cleavage and 2a faults. Early 2b folds are the dominant generation of folds preserved at Lone Rock Point.	
3.19	47
Illustrated image of early and late stage 3a structures from Lone Rock Point section 4 (See figure 3.17). Early stage 3a folds incorporate bedding and stage 2b modified cleavage. Late stage 3a thrust and normal faults cut these folds. Thrust faults record slip top-to-the-NW; whereas normal faults record slip top-to-the-N and top-to-the-S.	
3.20	48
Late stage 3a thrusts and normal faults are considered coeval. A) Late stage 3a normal faults are observed to cut late stage 3a thrusts. B) Late stage 3a thrusts are also observed to cut late stage 3a normal faults	
3.21	48
Cleavage intensification zone. Cleavage spacing is on the millimeter scale and contains discontinuous veins and no other measurable structures.	
3.22	49
A) Structural map of early and late stage 3b structures and associated rock types. Early stage 3b fault zone cleavage is incorporated into early stage 3b folds and cut by late stage 3b faults. B) Equal area stereographic projections indicate these faults record a unique NE-SW direction of motion. 3b fold axes plunge to the NE, E, and SE, with a few plunging to the NW. For image location, see Figure 3.15.	
3.23	51
Images of various early and late stage 3b structures. Early stage 3b structures include fault breccia, fault gouge, mylonite, and boudin structures. Late stage 3b structures include cataclastic lined faults and sheath folds.	
3.24	52
A) The variations in fault strike and dip indicate that the Champlain Thrust fault at Lone Rock Point is gently folded. B) Stereographic projection of Champlain Thrust fault surface with slickenline and mullion orientations. The oldest generation of slickenlines preserved on the Champlain Thrust fault indicate that motion was top-to-the-west, whereas the youngest generation indicates that motion was top-to-the-south. These directions do not match the axes orientations of fault mullions.	

3.25	53
Images of slickenlines preserved on the Champlain Thrust fault surface. A) The oldest generation of slickenlines is highly weathered with a slickenstep indicating that oldest recorded motion is top-to-the-west. B) The youngest generation is less weathered with predominant slickensteps indicating that the youngest recorded motion was top-to-the-south. Both images are looking up at the bottom of the Champlain Thrust fault surface, and both slickenline sets were separated by ~0.5 m.	
3.26	55
A scaled composite diagram of structures preserved within the footwall and hanging wall of the Champlain Thrust fault from each of the six field sites. The distance below the Champlain Thrust fault corresponds the calculated location of each location (Figure 3.2).	
3.27	57
Boundaries of the Champlain Thrust fault zone within northwestern Vermont.	
3.28	61
Distribution of relative strain zones across Lone Rock Point sections 1 and 2. High strain zones are localized around major faults and surround regions of intermediate strain. Very high strain and ultra-high strain are confined to the top 8 meters of the footwall.	
3.29	62
Distribution of relative strain zones within Lone Rock Point sections 3 and 4. High strain zones is the dominant zone exposed, with very high and ultra-high strain zones constrained to within 4 meters of the Champlain Thrust fault surface.	
3.30	64
Composite diagram of Champlain Thrust fault zone with relative strain distribution. Strain increases as the Champlain Thrust is approached from the protolith in the footwall. Strain zone thickness decreases towards the fault surface indicating a progressive localization of strain.	
4.1	67
A modified model of the Champlain Thrust fault zone as a type 2 shear zone. This type of shear zone records a time progressive localization of strain towards the active slip surface. In this model for the Champlain Thrust, strain localizes into narrower zones over time and increases in intensity. Adapted from Fossen and Cavalcante (2017).	
4.2	70
Simple models for each stage of Champlain Thrust fault zone evolution. Colors in block diagram indicate zone of active deformation and relative strain intensity at that stage. Center squares indicate type of structures that formed during that stage. Equal area lower hemisphere stereonet of slickenline orientations preserved on thrust faults (or normal where indicated). Contours are generated using Kamb contour method with intervals of 2. Mean vectors are plotted for slickenlines clusters with a 95% confidence interval.	
4.3	77
A block diagram of a lateral ramp along a thrust fault. A lateral ramp is defined as a portion of a fault plane that cuts bedding and has a strike direction parallel to transport direction (Boyer, 1982). Along a lateral ramp, faults exhibit strike-slip components, yet slickenlines preserved on the fault plane should be a consistent orientation. Slickenlines along the Champlain Thrust fault record motion in two distinct orientations, therefore suggesting reactivation was not due to a lateral ramp.	
4.4	78
A) Two different ways that newly formed thrust faults can propagate through rift-basin sediments over pre-existing extensional structures. Both images depict complex deformation within the thrust fault's footwall and hanging wall. Modified from Bonini et al. (2012). B) Block diagram of proposed Champlain Thrust evolution as a result of basin inversion. Reactivation of the Champlain Thrust fault surface, and heterogenous motion recorded in the fault zone, was likely influenced by buried pre-existing extensional structures. Slickenline projections mimic orientations from measured data.	

CHAPTER 1: INTRODUCTION

The Champlain Thrust fault zone exposed in northwest Vermont preserves brittle and ductile structures that record the history of deformation that occurred at the leading edge of a fold-and-thrust belt. The goal of this project is to determine the spatial and temporal evolution of the Champlain Thrust fault zone through a macroscale analysis of its architecture.

In general, fault zones preserve critical information regarding recent to ancient tectonic processes while also directly influencing modern sub-surface processes. The overall extent, motion history, strain accumulation, total displacement, and possible reactivation of faults are all recorded during the structural evolution of the fault zone. In addition to preserving information regarding its deformational history, fault zones within the upper crust directly influence sub-surface fluid flow (Eichhubl and Boles, 2000; Wall, 2006; Bense et al., 2013). These fluids include groundwater aquifers (Anderson and Bakker, 2008; Bense et al., 2008; Mundy et al., 2016), contaminant plumes (Ryan et al., 2013), natural gas (Paul et al., 2009; Hennings et al., 2012), and injected waste fracking fluids (Ellsworth, 2013; Keranen et al., 2014; Yeck et al., 2016). Recent studies have been conducted that analyze the hydrogeologic effects the Champlain Thrust fault has on local groundwater flow (Mundy et al., 2016). This study focuses the structural evolution of the Champlain Thrust fault zone to understand how a fault zone develops at the leading edge of a mountain building event.

The Champlain Thrust fault is a low-angle frontal thrust of the Taconic orogeny (ca. 475-450 Ma) in northwest Vermont (Stanley, 1987; Hayman and Kidd, 2002) (Figure

1.1). East of the Champlain Thrust, many structures associated with the Taconic orogeny have been deformed or overprinted by younger orogenic events (Tremblay and Pinet, 2016). The Champlain Thrust fault records no apparent deformation associated with later events, therefore providing the opportunity to determine the progressive evolution of a fault zone that developed during a single orogenic event.

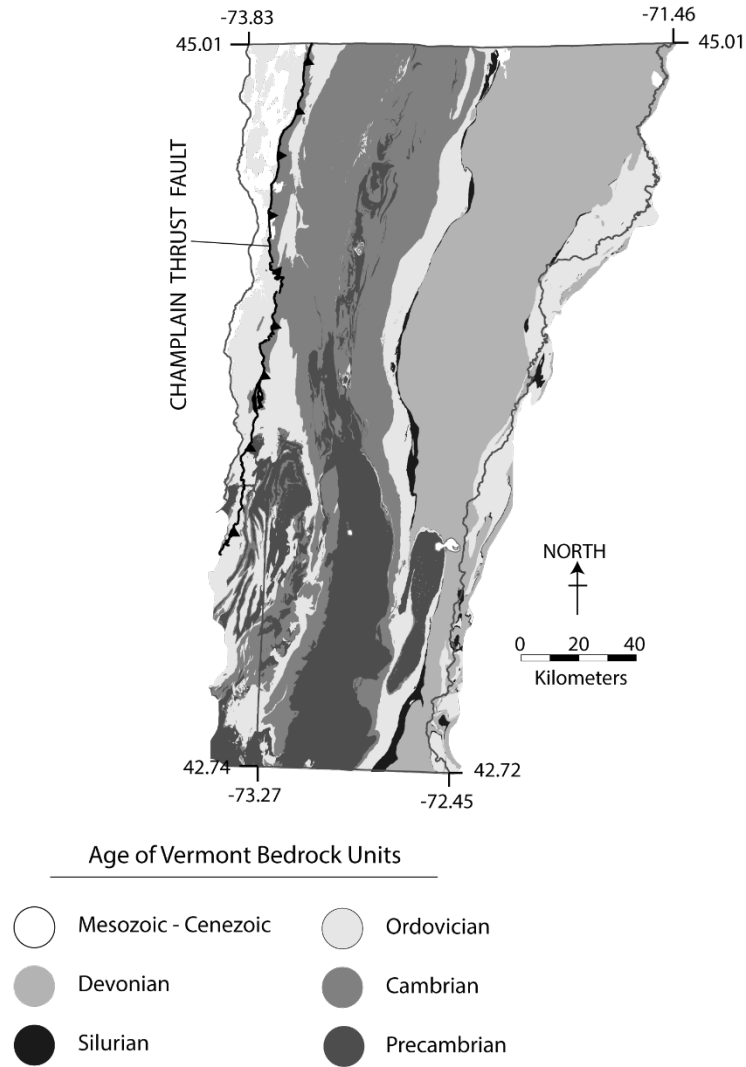


Figure 1.1: Vermont bedrock units of various ages. The Champlain Thrust, exposed along the western edge of Vermont, is a low-angle frontal thrust associated with the Taconic orogeny. The Champlain Thrust fault emplaces massive Cambrian carbonate and siliciclastic units atop Ordovician shales.

The Champlain Thrust fault surface and portions of the fault zone in close proximity to the principal slip surface have been previously mapped and characterized (Rowley, 1982; Stanley and Ratcliffe, 1985; Stanley, 1987). However, the full extent of structures and their evolution within the fault zone have yet to be described. Outcomes of this project will provide new insights into the following questions regarding the Champlain Thrust fault zone: (1) Where are the boundaries of the fault zone and what are the structures that define them? And, (2) How did the fault zone evolve through space and time?

Combined, the structures that define fault zone boundaries refer to its overall architecture. Through this study, I will be able to determine if the structural architecture of the Champlain Thrust fault zone is homogenous throughout its extent or if there are changes in structural style or motion preserved within its architecture.

Four theoretical reference models describing shear zone evolution through time have been previously derived (Means, 1995; Vitale and Mazzoli, 2008; Fossen and Cavalcante, 2017) (Figure 1.2). These end member models describe Type 1–4 shear zones and indicate how a shear zone grows during times of active deformation. Type 1 shear zones thicken over time by accumulating deformation at their active boundaries (Figure 1.2A). Type 2 shear zones thicken over time by accumulating deformation towards their center (Figure 1.2B). Type 3 shear zones remain a constant thickness by deformation being homogeneously distributed during active deformation (Figure 1.2C). Type 4 shear zones thicken evenly during active deformation (Figure 1.2D). I used these criteria for shear zone development to determine which model best describes the evolution of the Champlain Thrust fault zone spatially and temporally.

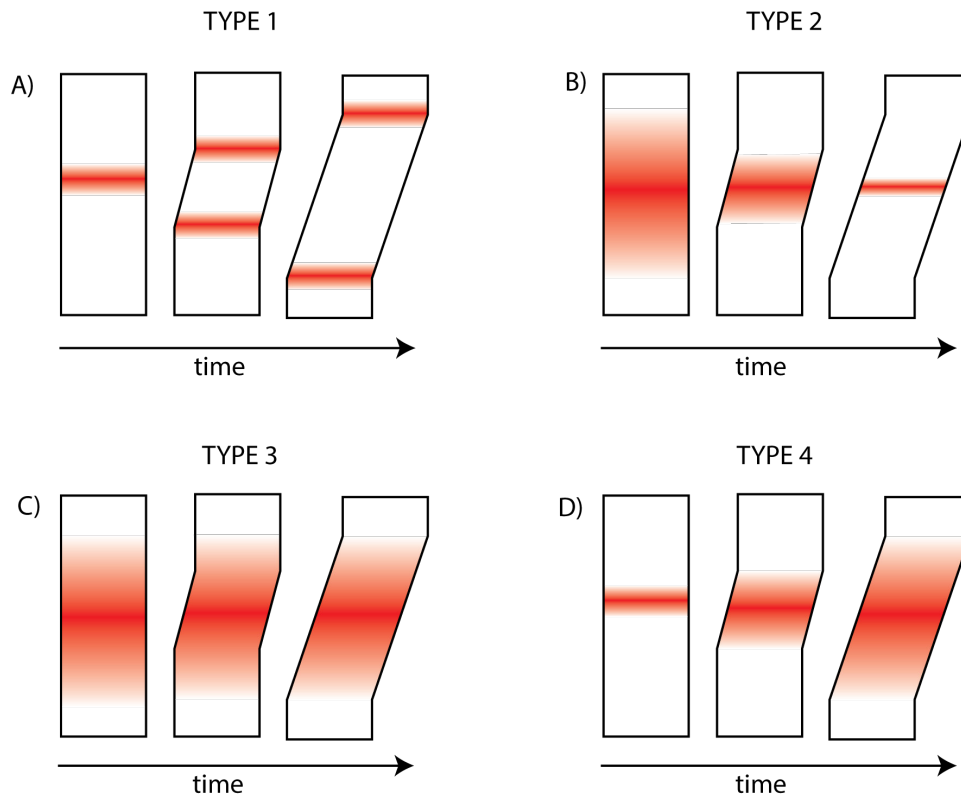


Figure 1.2: Four theoretical end member models that describe shear zone evolution through time. A) Type 1 model indicates that active deformation accumulates at shear zone boundaries. B) Type 2 model indicates that active deformation localizes towards the center of the shear zone. C) Type 3 model indicates that active deformation is homogeneously distributed through the shear zone through time. D) Type 4 model indicates that active deformation evenly grows through the fault zone through time. (Means, 1995; Vitale and Mazzoli, 2008). Figure adapted from Fossen and Cavalcante (2017).

Previous studies of fault zones from around the world have documented how the evolution of a fault zone can be inferred by distinguishing its overall architecture (Chester and Logan, 1986; Caine et al., 1996; Kim et al., 2004; Faulkner et al., 2010; Choi et al., 2016; O’Hara et al., 2017). To answer the questions associated with the Champlain Thrust fault zone, I completed a detailed structural analysis of various exposures of the Champlain Thrust fault zone. At each location I generated outcrop-scale structural maps that display the spatial distribution of faults, folds, and cleavages. I recorded the orientation and sense-

of-shear preserved on these structures to determine changes in style and motion within the fault zone. I used the principle of cross-cutting relations to determine the relative age of each structure and used that information to understand how the structures within the fault zone changed through time. Finally, I qualitatively defined various relative strain zones and used the spatial distribution of those zones as well as the relative age of structures preserved within each zone to determine how strain localized during fault zone evolution. I joined these descriptions to develop a comprehensive model of fault zone architecture and used that model to interpret the evolution of the fault zone.

Through this project, I was able to determine previously unknown aspects of the Champlain Thrust fault zone including: (1) the approximate boundaries of the fault core, damage zone, and protolith; (2) the localization of strain towards the fault core characterized by a progressive change in motion history and a progressive change in structural style, and (3) a reactivation of the Champlain Thrust principal slip surface as an inferred result of propagating over a pre-existing extensional structure during basin inversion.

CHAPTER 2: GEOLOGIC BACKGROUND

2.1. Introduction

The northern New England and southern Quebec landscapes record a complex tectonic history that includes continental break-up, marine sediment deposition, plutonic and volcanic activity, and multiple mountain building events (Figure 2.1). In Vermont, this suite of geologic processes is recorded and deformed through a series of tectonic events that occurred during the late Proterozoic through the late Devonian (620–375 Ma) (Figure 2.2). These events include the rifting of Laurentia from Rodinia, the opening of the Iapetus Ocean and Taconic seaway, and the accretion of Gondwanan-derived microcontinents onto Laurentia driven by the closure of the Iapetus ocean (Tremblay and Pinet, 2016). Separate orogenic events occurred as a result of the Laurentian collision with the Shelburne Falls arc and Moretown terrane (Taconic, ca. 475–450 Ma), Ganderia (Salinic, ca. 450–410 Ma), and Avalonia (Acadian, ca. 380–370 Ma) (St-Julien and Hubert, 1975; Williams, 1979; Stanley and Ratcliffe, 1985; van Staal et al., 1998; Van Staal and Barr, 2012; De Souza et al., 2014; Macdonald et al., 2014; Tremblay and Pinet, 2016; Karabinos et al., 2017; Macdonald et al., 2017). The following section provides (1) a brief summary of tectonic events from oldest to youngest that attributed to the deposition and subsequent deformation Vermont's bedrock units up through the Late Devonian and (2) defining characteristics of key terms used within this project including: fault zone, strain localization, thrust ramps, and fault reactivation.

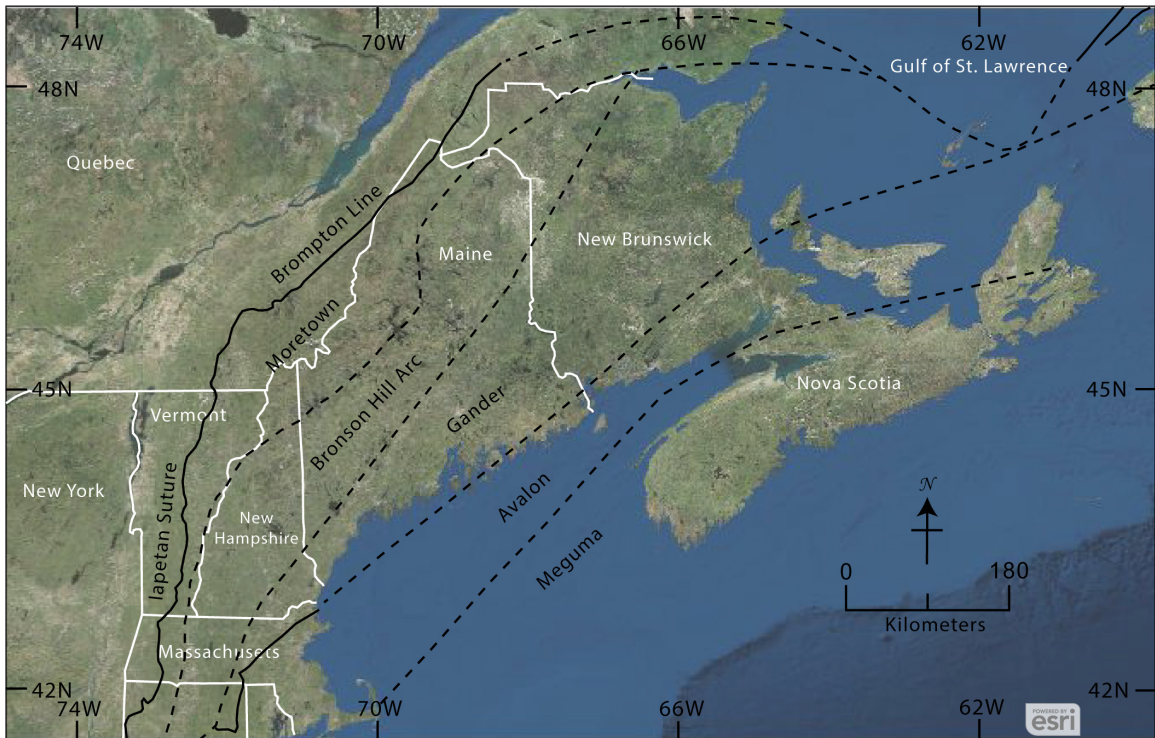


Figure 2.1: Approximate terrane boundaries associated with late Proterozoic through late Devonian orogenic events in present day New England and Southern Quebec. Boundaries and terrane names from Karabinos et al. (2017).

2.2 Regional Tectonic History

The oldest events were (1) the formation of the Laurentian margin, and (2) the subsequent opening of the Iapetus Ocean, due to the Neoproterozoic breakup of Rodinia through a system of low-angle detachment and transform faults (Allen et al., 2009). O'Brien and van der Pluijm (2012) used $^{40}\text{Ar}/^{39}\text{Ar}$ dating of pseudotachylyte preserved along normal faults within the present-day Quebec Appalachians and determined that the earliest rifting occurred between ca. 610 and 619 Ma. Volcanic and plutonic rocks have been used as evidence that rifting in western New England occurred between 570–555 Ma (Walsh and Aleinikoff, 1999; Karabinos et al., 2017), and magmatic rocks in southern

Quebec have been used as evidence for a rifting event occurring around ca. 558 Ma (Tremblay and Pinet, 2016). Within rift-generated basins, Neoproterozoic–Cambrian sediments were deposited atop magmatic and metamorphic rocks associated with the Grenville orogeny (1250–980 Ma). These sedimentary deposits define the present day Green Mountain bedrock belt in Vermont (Figure 2.3).

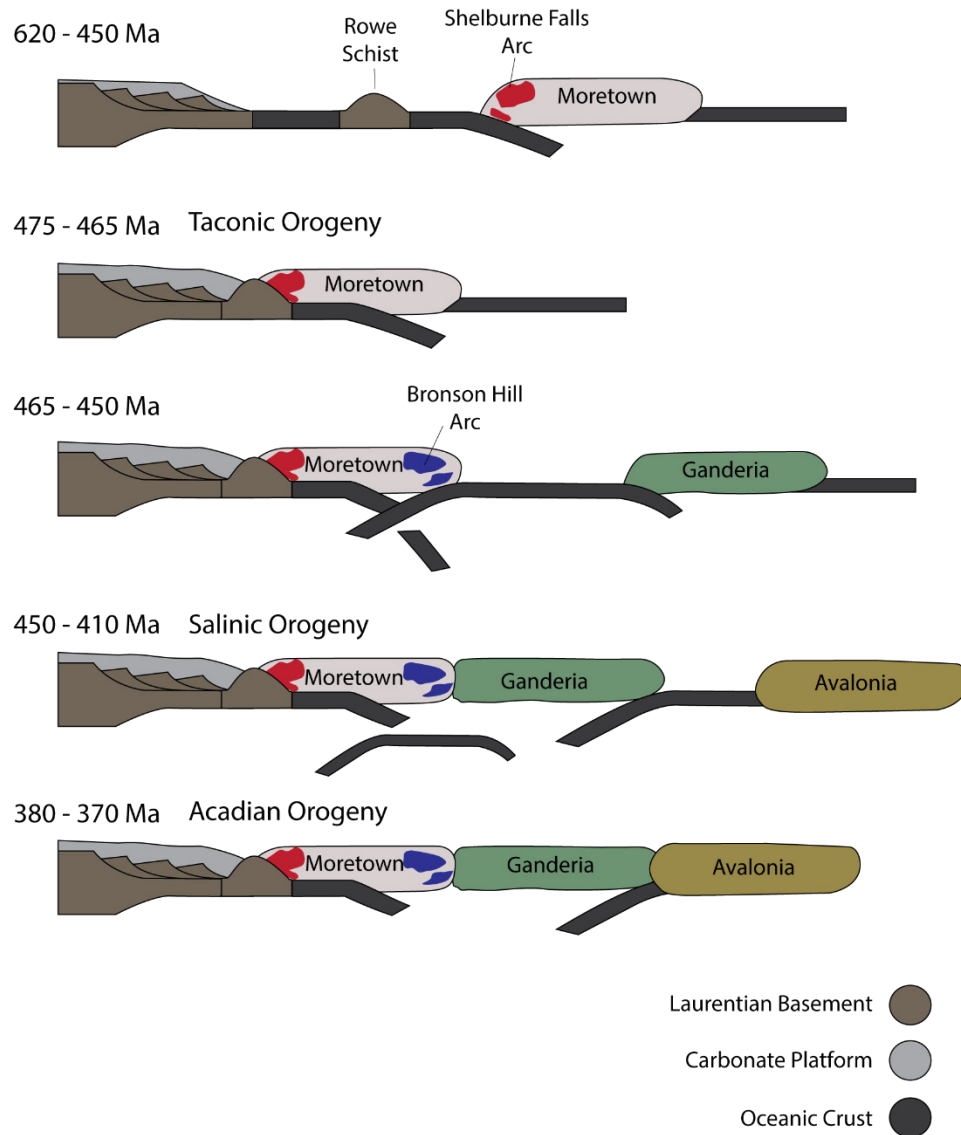


Figure 2.2: Simplified tectonic model of orogenic events in New England during early to mid-Paleozoic. Modified from Karabinos et al. (2017).

During the rift-drift transition, Cambrian–Ordovician clastic sedimentary and carbonate rocks were deposited as a carbonate platform along the passive Laurentian margin (Allen et al., 2010; Karabinos et al., 2017). These ancient carbonate platform rocks are the bedrock units that comprise Vermont’s Champlain Valley (Figure 2.3). The Taconic Seaway separated the Laurentian passive margin from the Neoproterozoic–Cambrian Rowe Schist (Stanley and Ratcliffe, 1985; Macdonald et al., 2014) which was separated from Gondwanan microcontinents to the east by the Iapetus Ocean (Karabinos et al., 2017) (Figure 2.2).

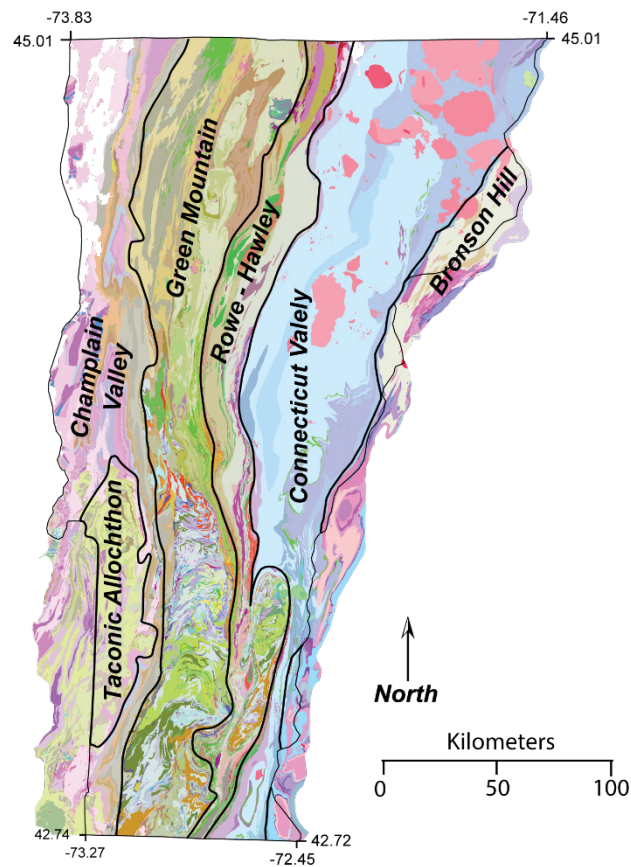


Figure 2.3: Mapped bedrock belts across Vermont. Modified from Kim et al. (2011).

During this time, an eastward dipping subduction zone (modern day coordinates) was active off the coast of the Laurentian margin below the Gondwanan-derived Moretown terrane ~500–475 Ma (Karabinos et al., 2017) (Figure 2.2). Subduction of oceanic lithosphere — the leading edge of Laurentia — resulted in the formation of the magmatic Shelburne Falls arc along the leading edge of the Moretown terrane (Karabinos et al., 1998; Macdonald et al., 2017). This subduction also attributed to the closure of the Iapetus Ocean and the subsequent collision along the Laurentian margin.

At 475 Ma, the Taconic orogeny began as a result from the collision between the Laurentian margin and the Moretown terrane (Karabinos et al., 2017; Macdonald et al., 2017) (Figure 2.2). This collision marks the suture zone of Laurentian–Gondwanan crust (Karabinos et al., 2017) and defines the Rowe-Hawley bedrock belt in present day Vermont. Arc-continent collision continued for ~15 M.y. (De Souza et al., 2014) or up to ~23 M.y. (Macdonald et al., 2017). It was during this collision that the Mesoproterozoic basement and overlying late Proterozoic–Cambrian rocks of the Green Mountain massif were thrust onto the foreland over the carbonate platform of the Champlain Valley (Ratcliffe et al., 2011; Karabinos et al., 2017). The Taconic Allochthon in southwest Vermont was also obducted onto the Laurentian margin during this time (Figure 2.3).

The next event occurred at ~465 Ma. At this time the east dipping subducting slab separated, and a reversal of polarity generated a westward dipping subduction zone beneath the Laurentian margin and the recently collided Moretown terranes (Karabinos et al., 2017) (Figure 2.2). By ~455 Ma, the Bronson Hill arc formed above the westward dipping subduction zone along the eastern edge of the accreted Moretown terrane (Karabinos et al.,

2017; Macdonald et al., 2017). Rocks associated with the Bronson Hill arc comprise the Bronson Hill bedrock belt along the eastern edge of Vermont (Figure 2.3). Large-scale sinistral oblique thrusting events ended the Taconic orogeny ~ 453–451 Ma (MacDonald et al., 2017).

The next major event occurred at ~450 Ma when the Gondwanan-derived Ganderia terrane docked against the composite Laurentian margin due to continued oceanic closure driven by the westward-dipping subduction zone (Tremblay and Pinet, 2016) (Figure 2.2). This docking event generated the Salinic Orogeny which is recorded through early stage (450–425 Ma) and late stage (425–410 Ma) deformation. Early deformation was predominately accommodated through hinterland-propagating backthrusts, folds, and retrograde metamorphism (Tremblay and Pinet, 2016). Slab delamination during the late stage of the Salinic orogeny generated a sedimentary basin through crustal extension (Rankin et al., 2007; Tremblay and Pinet, 2005, and 2016). Marine sediments were deposited within this basin and define the Connecticut Valley bedrock belt in eastern Vermont (Figure 2.3).

Late Devonian deformation ended with the Acadian orogeny (Figure 2.2). This is defined by the collision of the deformed Laurentian margin with Avalonia from ~380–370 Ma (Hussey et al., 2010; van Staal and Barr, 2012; Tremblay and Pinet, 2016; and references therein). Deformation generated from the Acadian orogeny includes west and east-propagating thrust faults (Tremblay and Pinet, 2016) and metamorphism of the Green Mountain, Rowe-Hawley, Connecticut Valley, and Bronson Hill bedrock belts of Vermont (Figure 2.3).

2.3 The Champlain Thrust and Hinesburg Thrust

In northwest Vermont, two exposed thrust faults record the western-directed crustal shortening that occurred during the Taconic orogeny—the Champlain Thrust fault and the Hinesburg Thrust. The Champlain Thrust fault emplaced early Cambrian to Middle Ordovician carbonate rocks atop Late Ordovician carbonate-rich shales (Figure 2.4) (Stanley and Sarkisian, 1972; Stanley, 1987), and has been mapped from the Catskill Plateau in eastern New York, along the western edge of Vermont, and into southern Quebec where it becomes known as the Logan’s Line (Keith, 1923; Stanley and Sarkisian, 1972; Rowley, 1983; Stanley and Ratcliffe, 1985; Stanley, 1987; Hayman and Kidd, 2002; Thompson and Thompson, 2003; Sejourne and Malo, 2007). In northwest Vermont, the hanging wall of the Champlain Thrust fault is the Lower Cambrian Dunham Dolostone, whereas south of Burlington Bay, the fault cuts up section ~700 meters into the basal member of the Middle Cambrian Monkton Quartzite (Stanley, 1987). Total displacement accommodated by the Champlain Thrust fault was estimated to be 60-80 kilometers with a total stratigraphic throw of ~2700 meters (Stanley, 1987).

The Hinesburg Thrust, exposed ~15 km to the east of the Champlain Thrust, emplaced Late Proterozoic–Early Cambrian rift clastic sediments atop weakly metamorphosed sedimentary rocks of the Champlain Valley (Stanley and Ratcliffe, 1985). The Hinesburg Thrust has been interpreted to have formed because of continual deformation along the axial plane of an overturned nappe fold (Dorsey et al., 1983). Total displacement accommodated by the Hinesburg Thrust was estimated to be ~6–7 kilometers (Stanley and Wright, 1997). Exposures of the Hinesburg Thrust and the Champlain Thrust

fault provide the opportunity to interpret the structural evolution of fault zones associated with the Taconic orogeny in northwest Vermont.

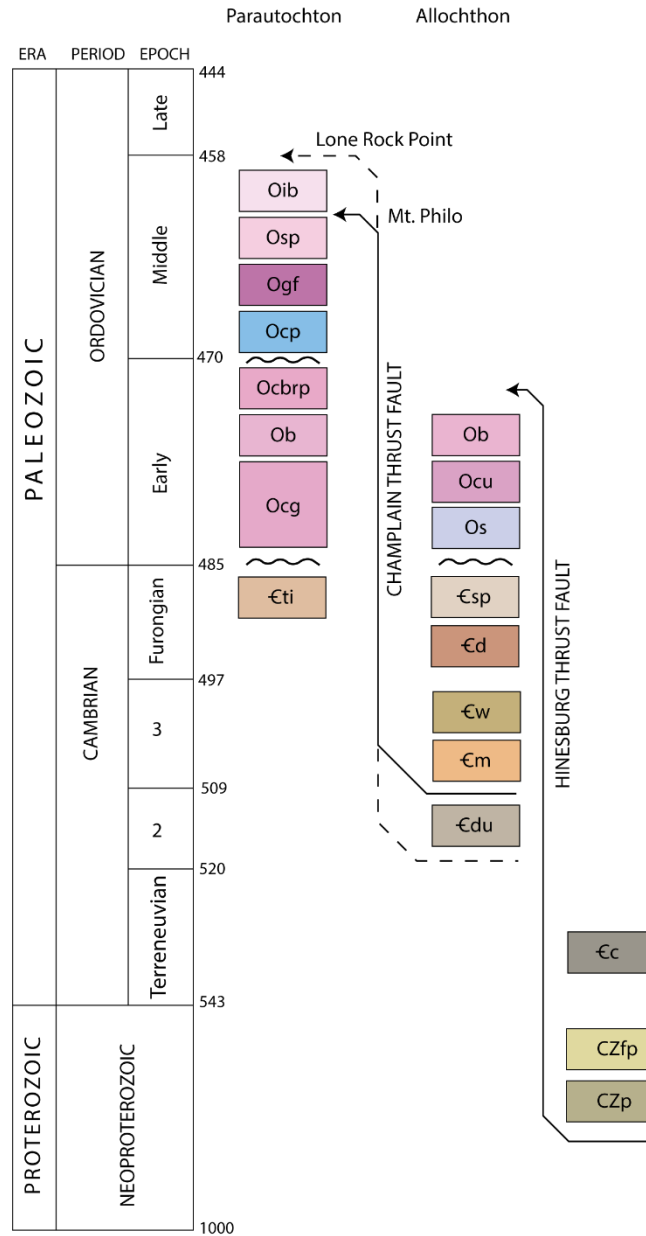


Figure 2.4: Lithostratigraphic column of rock units associated with the Champlain Thrust and Hinesburg Thrust faults exposed in northwest Vermont. Modified from Kim et al. (2011).

2.4 Fault Zone Development

Caine et al. (1996) defined a fault zone as being comprised of three separate components—the core, the damage zone, and the protolith (Figure 2.5). In brittle fault zones, the core is defined by a principal slip surface, or multiple slip surfaces (Choi et al., 2016), and may contain brittle fault rocks such as breccia, gouge, and cataclasite (Sibson 1977; Bastesen and Braathen, 2010). In ductile fault zones, the core may consist of a localized region of mylonite or highly-sheared rocks with gradational boundaries (Caine et al., 2010). The core, in both brittle and ductile fault zones, are zones of variable thickness that accommodated most of the displacement and associated strain during fault zone development.

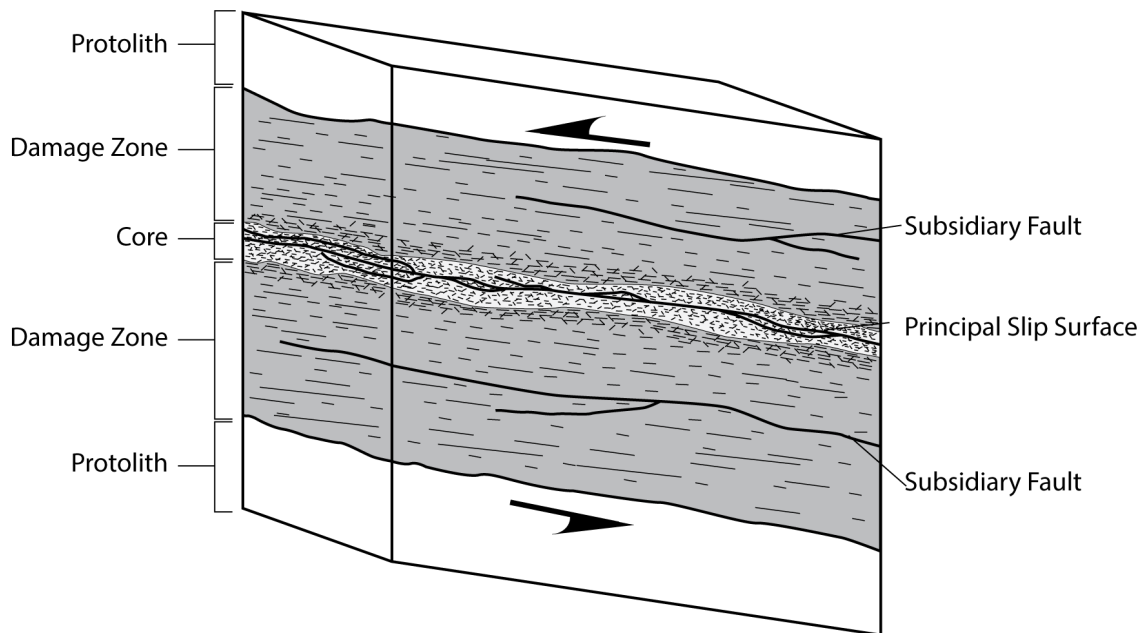


Figure 2.5: A simplified model of fault zone architecture and components. Modified from Mitchell and Faulkner (2009) and Caine et al. (2010).

In a brittle fault zone, the damage zone surrounds the fault core and contains subsidiary structures such as faults, folds, fractures and veins (Faulkner et al., 2010) (Figure 2.5). These subsidiary structures accommodate the remaining displacement and strain accumulation, with the thickness of the damage zone dependent on overall fault displacement (Mitchell and Faulkner, 2009). The presence of a damage zone within a purely ductile fault zone is more difficult to determine due to gradational contacts of ductile deformation and strain zones (Caine et al., 2010).

The protolith is defined as the country rock not effected by the fault or shear zone (Figure 2.5). However, structures such as faults, fractures, cleavages, and folds may be present within the protolith and any measurable changes in frequency, intensity, style, or relative age of these structures may indicate the transition into the damage zone (Riley et al., 2010; Choi et al., 2017).

2.5 Strain Localization

Strain refers to the distortion of a material through linear extension, shortening, shear, volumetric change, translation, rotation, or a combination thereof (Twiss and Moores, 1992). Strain localization is defined as the narrowing of zones that accommodate active deformation during fault zone evolution (Adam et al., 2004; Frost et al., 2009).

During evolution of a fault zone, strain can localize in various locations relative to the principal slip surface (Figure 1.2). Variations in strain localization patterns can be attributed to strain hardening or strain softening within the fault zone. Strain softening refers to the weakening of rocks as deformation is being accommodated (White et al.,

1980). Strain softening, and subsequent strain localization, is typically attributed to grain-size reduction (Montesi, 2013), geometric softening (Passchier and Trouw, 2005); reaction softening (Olio et al., 2010), and fluid-related softening (Finch et al., 2016). Identifying where strain localized in relation the principal slip surface, as well as the contributing mechanisms, will provide great insight to how the fault zone thickened or thinned during its progressive evolution and displacement.

2.6 Thrust Ramps

For this project, I refer to terms of thrust fault geometry defined by Butler (1982). Thrust faults are typically not consistently planar features, but rather a series of flats and ramps. Flats are defined as portions of the thrust fault that remain parallel to bedding or other layers during propagation (Butler, 1982). If a thrust fault cuts upwards in the transport direction and therefore cross-cuts bedding or layering, this is defined as a thrust ramp (Butler, 1982). Thrust ramps are considered hanging wall ramps if hanging wall layers are cut, and footwall ramps if the layer that are cut are within the footwall. Ramps are also defined by their orientation to overall transport direction. Ramps that are oriented perpendicular to transport direction are defined as frontal ramps, whereas ramps that are oriented parallel to transport direction are considered lateral ramps (Butler, 1982). Oblique ramps are defined as ramps that are oriented at some angle relative to overall transport direction (Butler, 1982).

Changes in thrust fault geometry can generate folds that accommodate deformation within the surrounding rock (Fossen, 2016). As displaced rock units move over frontal or

lateral ramps, a series of fault-bend-folds can form, some of which may stack and form a package of thrust duplexes (Suppe, 1983; Stanley, 1990). Fault-bend folds have been observed within fold-and-thrust belts from all over the world (Savage and Cooke, 2003; Suppe et al., 2004; Muñoz, 2017) and are important indicators to how fault geometry effects the structural evolution of the surrounding fault zone (Brandes and Tanner, 2014).

2.7 Fault Reactivation

Fault reactivation is defined as separate displacement events along a pre-existing fault plane with intervals of inactivity greater than 1 Ma. (Holdsworth et al., 1997). Fault reactivation can be evidenced through stratigraphic, structural, geochronological, or neotectonic characteristics (Holdsworth et al., 1997). Fault reactivation commonly occurs when extensional basins undergo compression—which is defined as basin inversion (Bonini et al., 2012).

The final state of basin inversion structures is typically complex as their formation was controlled by pre-existing structures (Bonini et al., 2012). During basin inversion, pre-existing normal faults can become reactivated as thrust faults—known as positive inversion (Cooper and Williams, 1989). Alternatively, pre-existing thrust or reverse faults that reactivate as normal faults during extension—a processes known as negative inversion (Harding, 1985). Pre-existing faults typically reactivate during shortening, however new faults can develop in the sedimentary cover of extensional basins (Turner and Williams, 2004). These faults and their kinematics may be influenced or controlled by the pre-existing structures over which they develop (Scisciani, 2009; Bonini et al., 2012).

Identifying fault reactivation and the influence of pre-, syn-, or post-orogenic faults or folds is critical to understanding the structural history of a fault zone that evolved in a region that experienced multiple orogenic events (Calamita, 2017).

CHAPTER 3: THE ARCHITECTURE OF THE CHAMPLAIN THRUST FAULT ZONE

3.1 Introduction

The overarching goal of this chapter is to provide a detailed description of the architecture of the Champlain Thrust fault zone through the structural analysis of various outcrops exposed throughout northwestern Vermont. Specifically, I use the data collected from the structural analysis to address three previously undescribed aspects of the Champlain Fault zone which include: (1) the structural characteristics of the fault core, damage zone, and protolith, (2) the spatial extent of the core damage and protolith boundaries within northwestern Vermont, and (3) the stage of development preserved within the fault zone. I will use these aspects to determine if the architecture of the Champlain Thrust fault zone is homogenous throughout its extent, or if there are changes of structural style or motion preserved.

In northwest Vermont, the Champlain Thrust fault is a multi-kilometer scaled structure associated with the leading edge of the Taconic orogeny (Stanley, 1987). It records no apparent deformation associated with later orogenic events that altered or overprinted similar structures to the east. Due to the absence of multi-orogenic deformation within its fault zone, the Champlain Thrust records how fault zones evolve in the upper crust at the forefront of a mountain building event.

Previous studies of the Champlain Thrust fault provide a great deal of information regarding its location, extent, deformed stratigraphy, orientation, and chronology (Keith, 1923; Keith, 1932; Clark, 1934; Cady, 1945; Welby, 1961; Stanley and Sarkisian, 1972,

Stanley, 1987). Other previous studies have provided detailed analysis of imbricate thrust fault formation (Stanley, 1990), lithological constraints of structure style (Kim et al., 2011), and hydrologic effects (Mundy et al., 2016) of localized parts of the Champlain Thrust fault zone.

For this project, I focused on six separate field sites and analyzed them using field-based structural analysis (Figure 3.1). These sites are separated by a geographical distance of 51 kilometers north-to-south, yet each site corresponds to a different depth below a westward projection of the previously mapped Champlain Thrust principal slip surface (Figure 3.2). The depth of each field site was calculated by projecting the Champlain Thrust westward at an assumed constant dip of 10° – 15° (Stanley, 1990) and accounting for elevation differences between the field site and the mapped location of the Champlain Thrust fault due east. This calculation also assumes constant planarity of the project fault surface.

In general, shear zone development and strain localization within a fault zone tend to occur within the rheological weaker layers or at lithologic contacts (Fossen and Cavalcante, 2017). This generality applies to the Champlain Thrust fault zone as most of the accommodated deformation is recorded in the carbonate-rich shales of the footwall. Though the hanging wall offers key information regarding overall stratigraphic throw, fault surface geometry, and syn-faulting deformation, it was only observed at Lone Rock Point (Figure 3.1). The massive Cambrian Dunham Dolostone of the hanging wall contains numerous sub-vertical fractures with three dominant orientations: NE, SE, and SW strikes (Figure 3.3). There are localized portions of the hanging wall—directly above the principal

slip surface—that reveal a <1-meter thick damage zone consisting of micro-faults that cut calcite veins and foliated rocks (Figure 3.4). Due to the very thin damage zone and homogeneity of structures above, this study focuses on the fault zone preserved within the footwall.

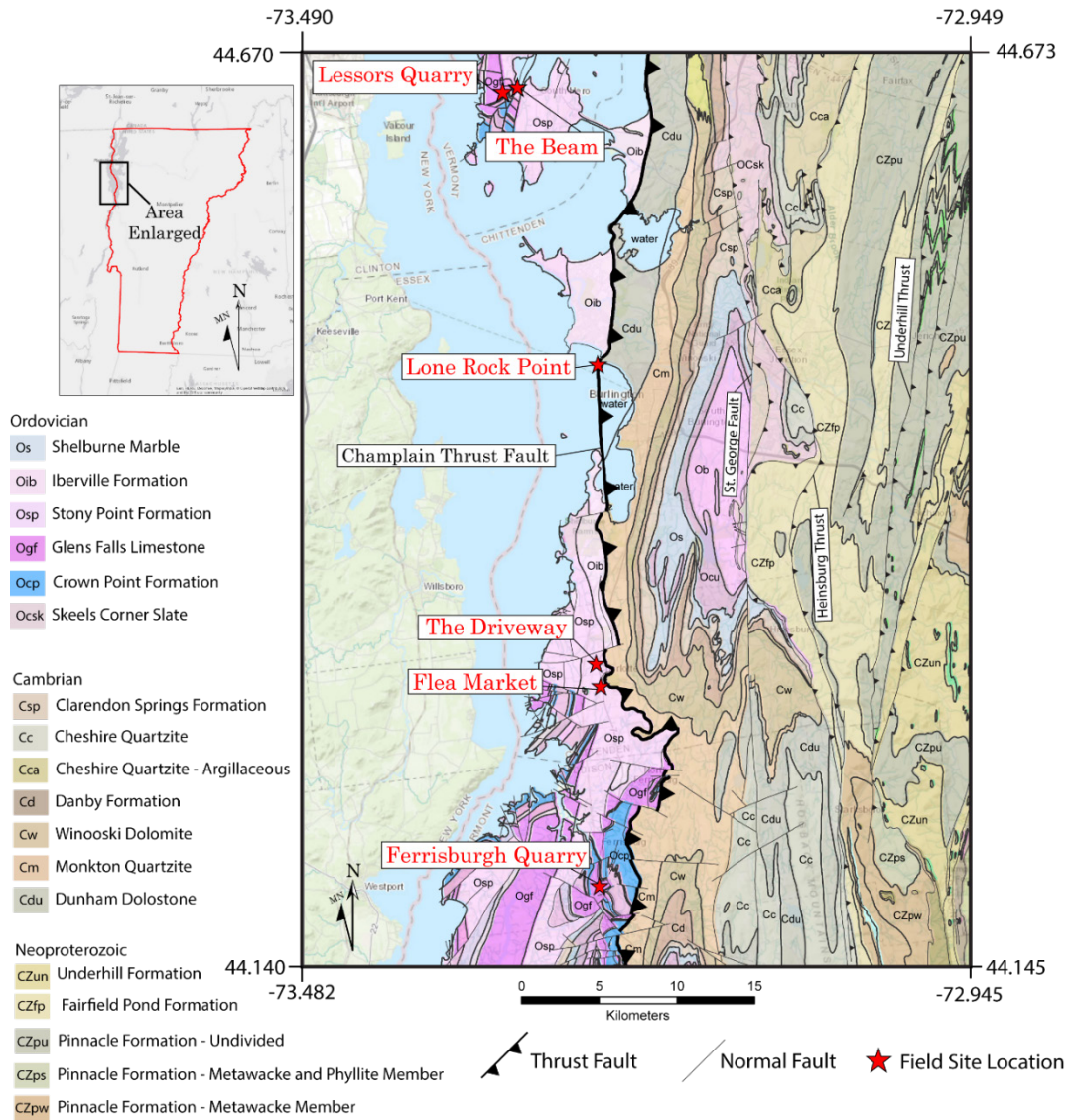


Figure 3.1: Location of field sites analyzed for determining the extent and characteristics of the Champlain Thrust fault zone exposed in northwestern Vermont. Map adapted from Ratcliffe et al. (2011).

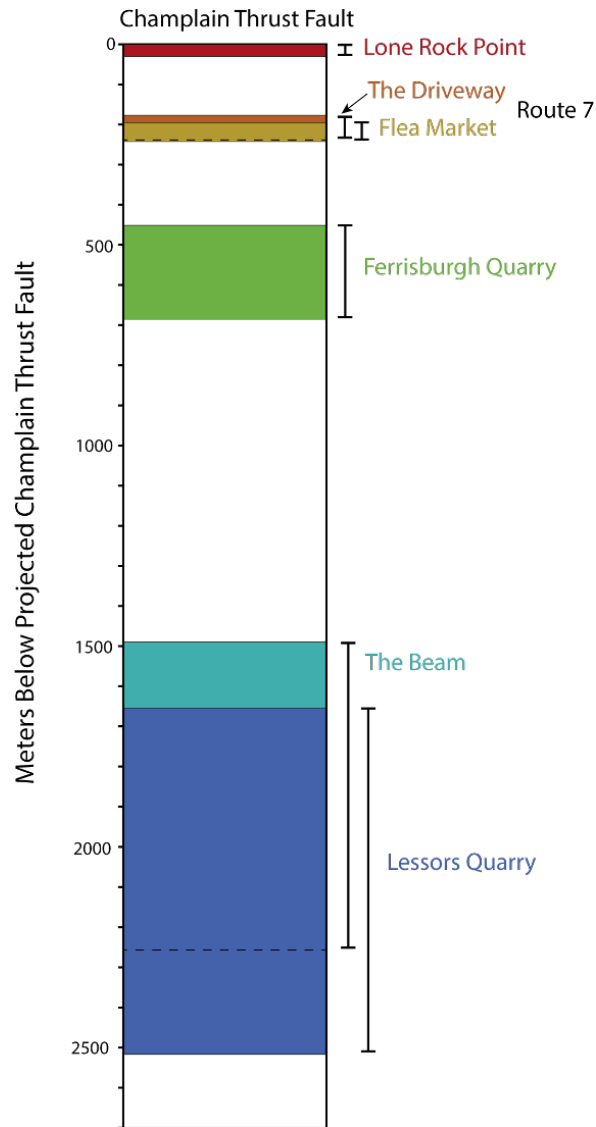


Figure 3.2: The calculated depth of each field site below the westward projection of the Champlain Thrust surface. The top of the bar represents location for an assumed 10° constant dip of the fault surface and the bottom bar represents an assumed 15° constant dip (Stanley, 1990).

Each of the six field sites analyzed for this project preserves multiple stages of deformation, some of which are recognized at multiple sites. I first determined the various types of structures preserved at each of the six field sites, and determined their relative age based on cross-cutting relations. I then generated structural maps for each of the six field

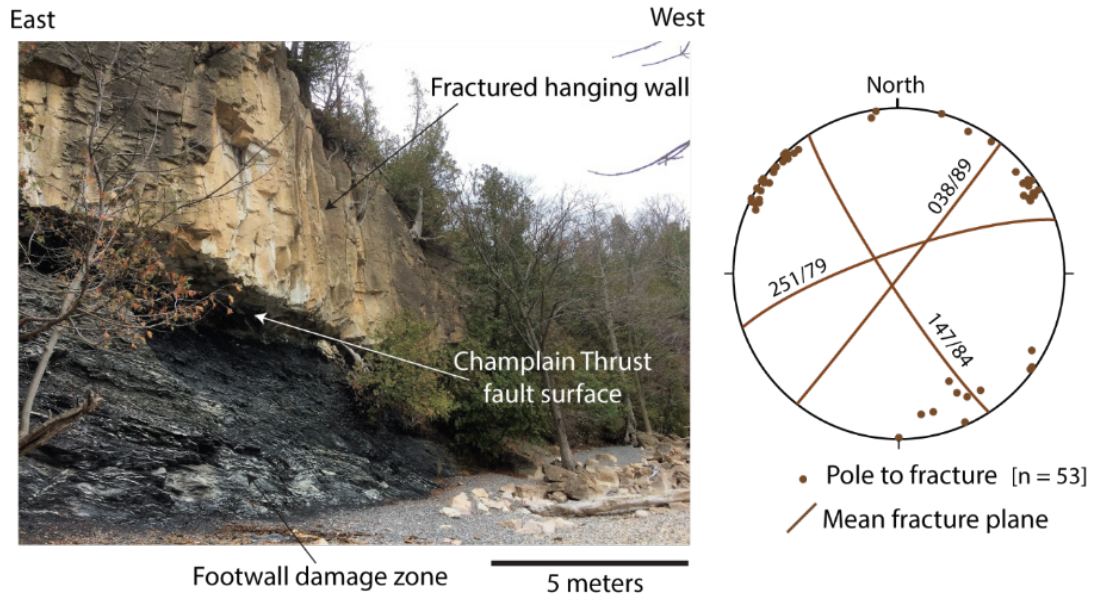


Figure 3.3: Photograph of the heavily fractured Champlain Thrust hanging wall exposed at Lone Rock Point. Fractures are predominately sub-vertical with three common orientations: NE striking, SE striking, and SW striking.

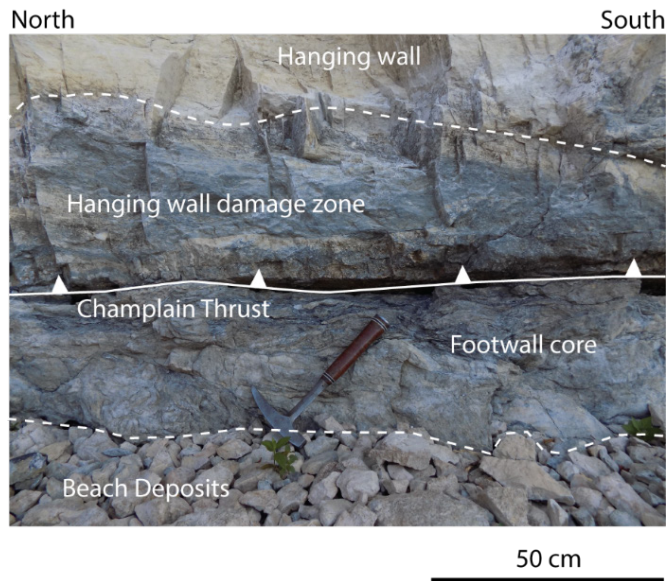


Figure 3.4: Photograph of a localized region of the hanging wall that preserves a < 1-meter damage zone of foliated rock with minor faults and fractures that cut foliation. Due to the extreme asymmetry of fault zone width across the Champlain Thrust fault, this project focuses primarily on the complex fault zone preserved in the footwall.

Table 3.1: Field location and relative age (stage) of structures preserved throughout the Champlain Thrust fault zone within northwestern Vermont

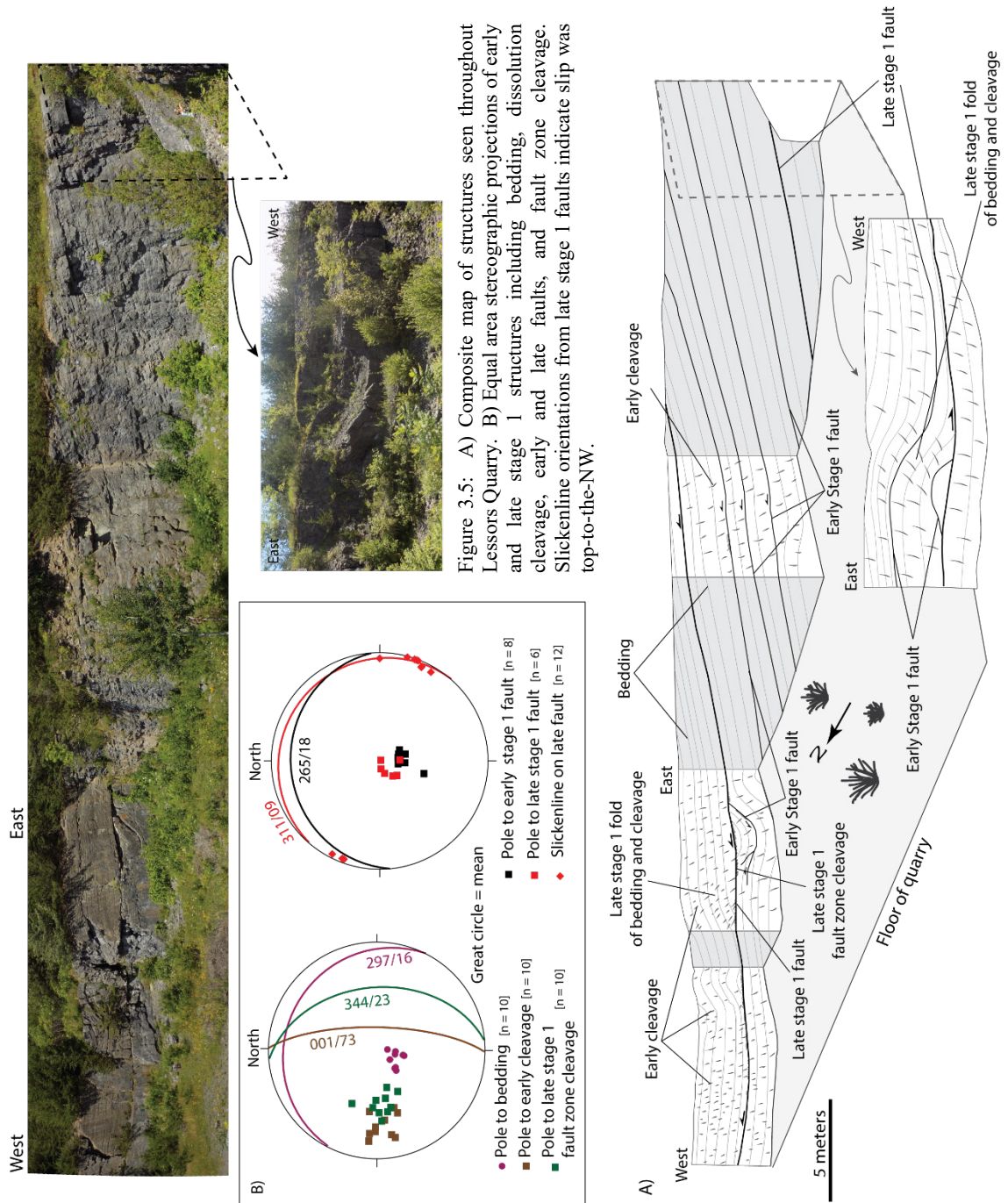
	PROTOLITH			DAMAGE ZONE			CORE		CHAMPALIN THRUST FAULT
				Lower	Upper	Lower	Upper	Surface	
	Lessons Quarry	The Beam	Ferrisburgh Quarry	Flea Market	The Driveway	Lone Rock Point	Lone Rock Point	Lone Rock Point	Lone Rock Point
EARLY	Dissolution cleavage Bedding parallel thrusts	Dissolution cleavage Bedding parallel thrusts	Dissolution cleavage Bedding parallel thrusts						
STAGE 1	Stacked fault-bend- folds of bedding and early cleavage top-to-the-WNW	Bedding parallel thrusts top-to-the-NW Stacked duplex in thick beds of micrite	Bedding parallel thrusts top-to-the-WNW No folds	Bedding parallel thrusts top-to-the-W	Bedding parallel thrusts top-to-the-W				
LATE									
EARLY				Cylindrical folds of bedding and Stage 1 faults with axial planar cleavage	Cylindrical folds of bedding and Stage 1 faults with axial planar cleavage	Rootless recumbent folds of bedding with axial planar cleavage	Axial planar cleavage deformed by stage 2b		
STAGE 2a				Thrust faults that cut early folds top-to-the-NNW	Thrust faults that cut early folds top-to-the-NNW	Bedding and cleavage parallel thrust faults top-to-the-NW			
LATE									
EARLY						Folds of axial planar cleavage and bedding	Folds of axial planar cleavage and bedding		
STAGE 2b						Thrust faults cut and rotate bedding, axial planar cleavage, and Stage 2a faults top-to-the-NW Stacked duplexes	Thrust faults cut and rotate bedding, axial planar cleavage, and Stage 2a faults top-to-the-NW Stacked duplexes		
LATE									
EARLY						Tight folds of bedding, stage 2b cleavage, and Stage 2b faults	Tight folds of bedding, stage 2b cleavage, and Stage 2b faults		
STAGE 3a						Thrust and normal faults that cut early folds	Thrust and normal faults that cut early folds	Normal faults that cut bedding and cleavage top-to-the-N & top-to-the-S	
LATE						Thrust top-to-the-NW Normal top-to-the-N & top-to-the-S	Thrust top-to-the-NW Normal top-to-the-N & top-to-the-S		
EARLY								Boudinaged layers, mylonite, fault zone cleavage, fault breccia	Fault mullions SE - trending
STAGE 3b								Rootless and sheath folds, thrust faults that cut cleavage top-to-the-SW	Fault gouge top-to-the-W & top-to-the-S
LATE									

sites to determine the spatial distribution of these structures. Finally, I combined the data describing the temporal and spatial characteristics of preserved structures to determine the overall architecture of the Champlain Thrust fault zone. Table 3.1 provides a brief description of the defining structures, relative ages, and locations of each of the deformation stages.

Key findings of this analysis include: (1) the thickness of the fault core is ~8 meters; (2) the thickness of the damage zone is ~197 to 430 meters; (3) the upper limit of the protolith is constrained to ~205–450 meters below the Champlain Thrust fault surface; (4) the record of at least 4 evolutionary stages; (5) relative strain localized through the footwall toward the fault surface during active deformation; (6) motion within the fault changes from top-to-the-west, -northwest, - north, -south, and -southwest; (7) changes in structural style from bedding-parallel faults and localized fault-bend-folds in the protolith, to duplex-forming thrust faults and associated folds in the damage zone, to anastomosing thrust faults and normal faults within the core; and (8) the Champlain Thrust fault records reactivation with a change in motion direction from top-to-the-west to top-to-the-south.

3.2 Lessors Quarry, South Hero, Vermont

Lessors Quarry (44° 38' 57.21" N; 73° 19' 44.50" W) (Figure 3.1), an abandoned quarry of the Glens Falls Limestone in South Hero, Vermont, corresponds to a calculated depth of 1.65–2.51 kilometers below the Champlain Thrust fault surface (Figure 3.2). Along the ~10-meter vertical exposures of north, east, and south oriented walls, early and late stage 1 structures are preserved. (Table 3.1) (Figure 3.5a).



Bedding is preserved throughout the quarry consists of interbedded layers of a light-grey weathered limestone averaging 9 cm thick and a dark-grey weathered fossiliferous limestone with an average thickness of 8 cm (Figure 3.6). Bedding is cut by an early stage

1 pressure-solution cleavage which is best observed along north wall of the quarry. Using the defining criteria based on cleavage spacing first described by Alvarez et al. (1978), these discontinuous cleavage planes are considered weak as they average ~30 cm in length and are spaced ~17 cm apart east to west. Filled with aligned clay minerals, this cleavage has an angle to bedding by ~67°, consistently strikes north, and steeply dips to the east at 73° (Figure 3.5b).

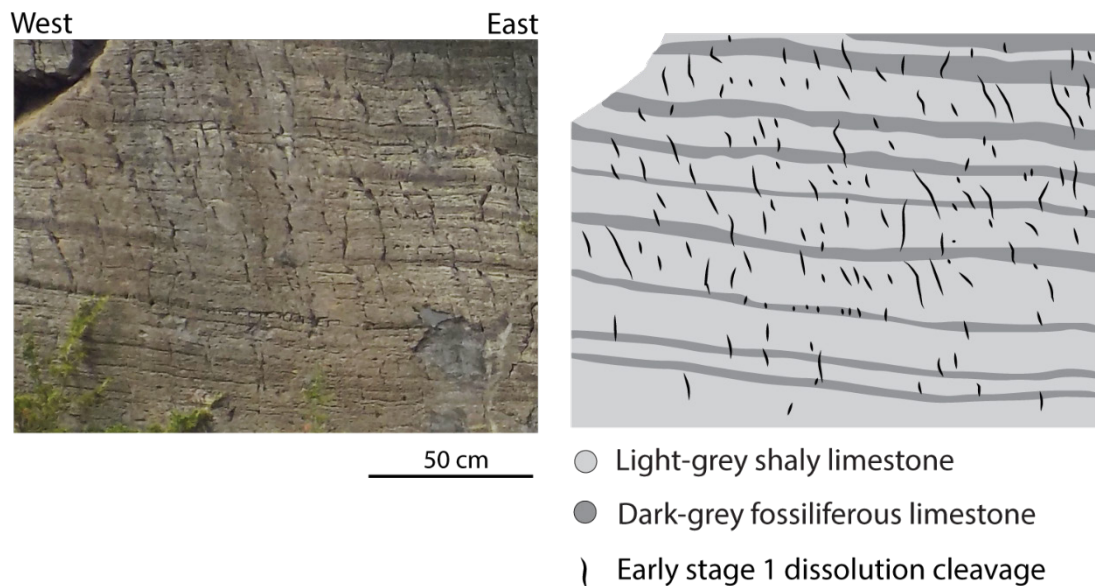


Figure 3.6: Bedding at Lessors Quarry consists of interbedded layers of light-grey limestone and a dark-grey to brown fossiliferous limestone. Bedding is cut by an early dissolution cleavage that has ~17cm spacing.

There are at least two generations of stage 1 faults preserved at this location. Early stage 1 faults are bedding-parallel thrusts that are best observed along the north, south, and east walls (Figure 3.5a). The exposure of these faults provides no detail on overall geometry or displacement indicators. These early stage 1 faults parallel bedding that has an average strike of 265° and a shallow 18° dip towards the north-east (Figure 3.5b). Along

the north wall, there is one preserved early stage 1 fault, and it is presently synformally folded and cut by a through-going late stage 1 fault. There are at least two separate late stage 1 faults preserved within the quarry, which are best observed along the south and north walls. These faults generated two stacked fault-bend-folds of bedding, early cleavage, and early faults, which rotated the early cleavage and bedding by $\sim 35^\circ$ to the west. Several components of a fault-bend-fold geometry are observed within the quarry and include a hanging wall flat, ramp, flat sequence, a footwall flat, flat, ramp sequence, and a syncline to anticline fold sequence (Suppe, 1983). The remaining hanging wall flat, footwall flat, and anticline to syncline fold sequence are inferred to exist to the east. The interlimb angles of the exposed syncline and anticline are approximately 110° – 140° . Based on slickenline orientation preserved along the late stage 1 faults and the exposed components of the fault-bend-fold, sense of shear was determined to be top-to-the-WNW (Figure 3.5b). These late stage 1 faults are lined with veins of white calcite that vary in thickness across the faults from sub-centimeter to ~ 10 centimeters.

3.3 “The Beam”, South Hero, Vermont

Early and late stage 1 structures are also observed at “the beam” ($44^\circ 39' 4.64''$ N; $73^\circ 18' 59.36''$ W) (Figure 3.1). First described by Stanley (1990), “the beam” corresponds to a calculated depth of 1.49–2.26 kilometers below projected Champlain Thrust fault surface (Figure 3.2). “The beam” is the non-technical name given to a ~ 3 -meter vertical exposure of the Middle Ordovician Cumberland Head Formation. Bedding consists of thin beds of a light-grey calcareous shale surrounding a 30-cm-thick micrite layer (Figure 3.7a).

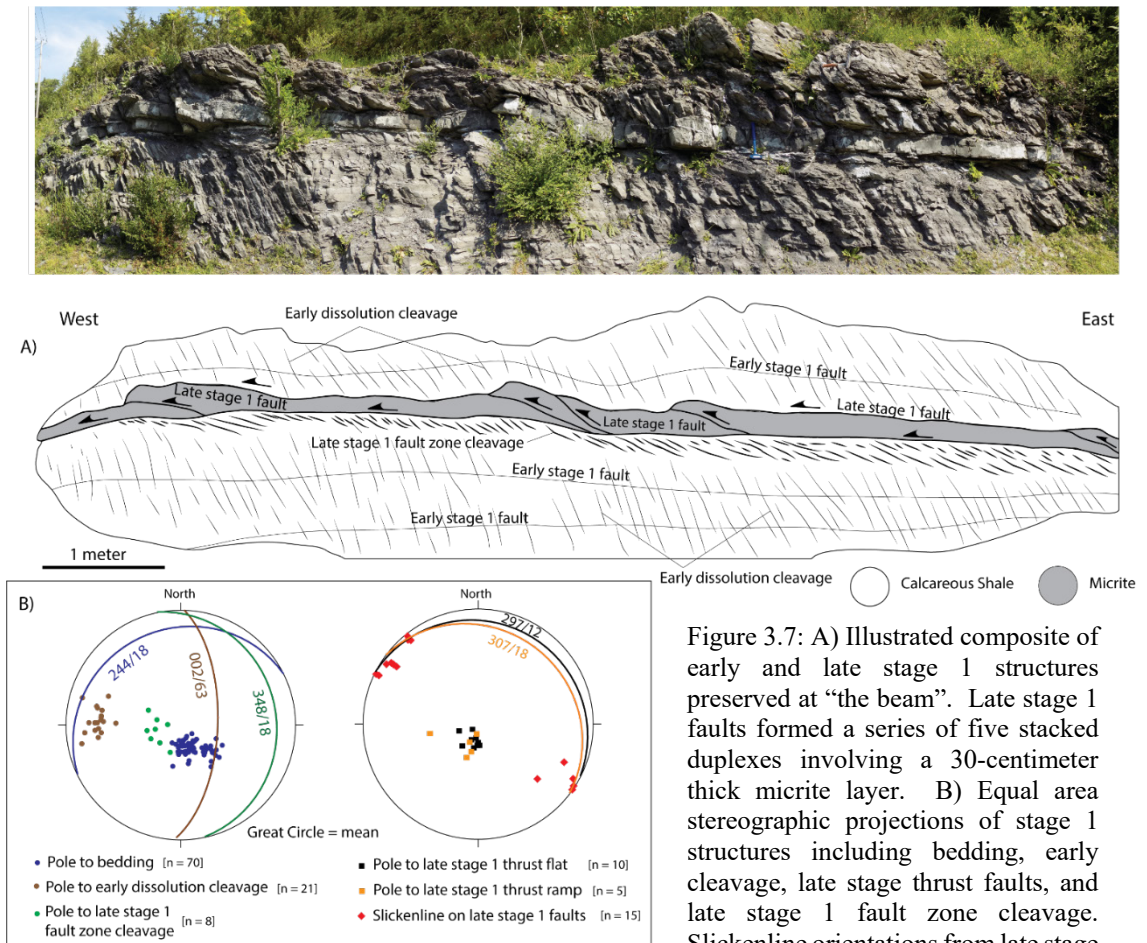


Figure 3.7: A) Illustrated composite of early and late stage 1 structures preserved at “the beam”. Late stage 1 faults formed a series of five stacked duplexes involving a 30-centimeter thick micrite layer. B) Equal area stereographic projections of stage 1 structures including bedding, early cleavage, late stage thrust faults, and late stage 1 fault zone cleavage. Slickenline orientations from late stage 1 faults indicate slip was top-to-the-NW.

Bedding has a mean strike towards the southwest and a shallow dip of 18° toward the northwest (Figure 3.7b). An early stage 1 dissolution cleavage cuts bedding and early stage 1 faults and is the predominant structure observed at “the beam”. This early cleavage has an average spacing of 5.6 cm and accommodated layer-parallel shortening on the range of 11–16% (Stanley, 1990). The early cleavage has a mean strike to the north, and dips moderately to the east at 63° . Early stage 1 bedding parallel faults are preserved and are lined with thin veins of sparry calcite.

Late stage 1 bedding-parallel thrust faults localized along the micrite layer and form a series of 5 thrust horses that stack in order from east to west (Stanley, 1990) (Figure 3.7a). The floor and roof thrusts are oriented with a mean strike to the northwest and a shallow 12° dip to the northeast, whereas the thrust ramps strike in a similar orientation, yet have a slightly steeper dip of 18° to the northeast (Figure 3.7b). The floor thrust of this duplex system hosts a localized fault-zone cleavage that dips 18° to the east and thick veins of calcite. Stanley (1990) described this vein thickness as evidence for the reactivation of the floor thrust during the development of each thrust duplex. Motion was interpreted to be progressive along this floor thrust for each duplex generation, whereas the thrust ramps and roof thrust were interpreted to be active only during the development of that specific associated duplex. Unlike Lessors Quarry, fault related folds are restricted only to the thrust horses within the centimeter scale micrite layer. Slickenlines preserved along these faults, along with a slight asymmetry of the early cleavage below the thrusts, indicate that slip along these late stage 1 faults was top-to-the-west-northwest (Figure 3.7b).

3.4 Ferrisburgh Quarry, Ferrisburgh, Vermont

An active quarry of the Glens Falls Limestone in Ferrisburgh, Vermont (44° 11' 21.21" N; 73° 14' 37.93" W) (Figure 3.1) corresponds to a calculated depth of 450–684 meters below the Champlain Thrust surface (Figure 3.2). Within the ~12 vertical meter exposure, early and late stage 1 structures are preserved (Figure 3.8a).

The Glens Falls Limestone at this location is a dark-grey to black limestone with veins of sparry calcite dispersed throughout. Bedding primarily strikes NNE, and dips

shallowly to the east at 04° (Figure 3.8b). A well-developed, moderate, early stage 1 dissolution cleavage is the predominant structure throughout the quarry and has an average spacing of 4.5 cm. These north-striking early cleavage planes dip 65° to the east and cut bedding (Figure 3.8b).

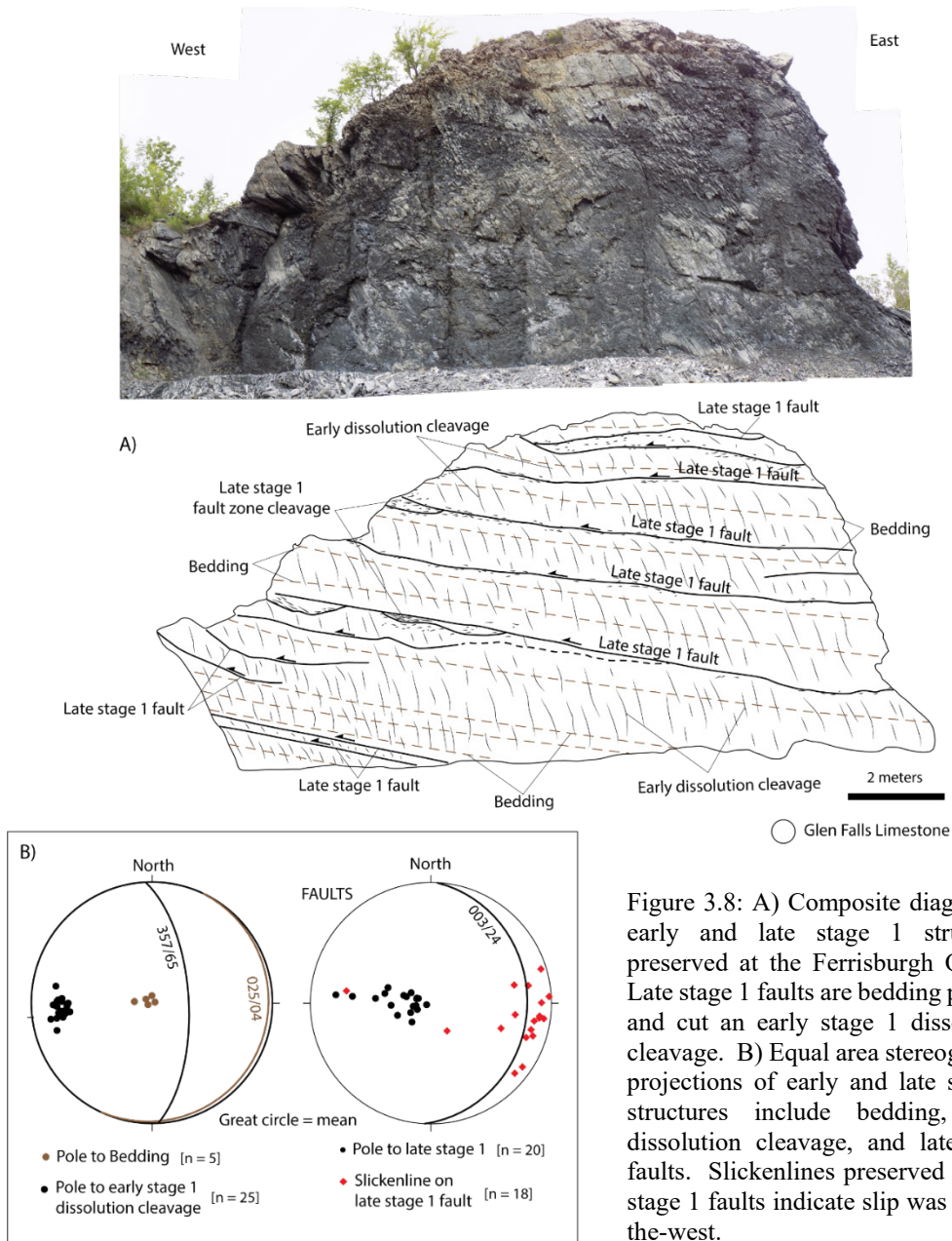


Figure 3.8: A) Composite diagram of early and late stage 1 structures preserved at the Ferrisburgh Quarry. Late stage 1 faults are bedding parallel and cut an early stage 1 dissolution cleavage. B) Equal area stereographic projections of early and late stage 1 structures include bedding, early dissolution cleavage, and late stage 1 faults. Slickenlines preserved on late stage 1 faults indicate slip was top-to-the-west.

Late stage 1 thrust faults are also preserved at this location (Figure 3.8a). These through going bedding-parallel thrusts strike to the north, dip moderately to the east at 21° , and cut the early stage 1 cleavage planes (Figure 3.8b). These faults are lined with thin veins of white calcite and preserved localized regions of an associated fault-zone cleavage. Slickenlines preserved along these faults, in conjunction with early cleavage asymmetry, indicate that motion was primarily top-to-the-west, with a few faults recording top-to-the-northwest slip (Figure 3.8b). Unlike the previously mentioned field sites that preserve stage 1 structures, there are no apparent folds associated with stage 1 structures at this quarry location.

3.5 “The Driveway” and “The Flea Market”, Charlotte, Vermont

Along Vermont’s Route 7, “the driveway” ($44^\circ 19' 4.64''$ N; $73^\circ 14' 53.44''$ W) and the “flea market” ($44^\circ 18' 17.02''$ N; $73^\circ 14' 38.89''$ W) (Figure 3.1) are two road-cut exposures of moderately deformed Middle Ordovician Stony Point Shale. “The driveway” corresponds to a calculated depth of 180–237 meters below the Champlain Thrust surface and “the driveway” corresponds to 194–243 meters below (Figure 3.2). At these locations, the hanging wall of the Champlain Thrust is composed of the massive Cambrian Monkton Formation—a heterolithic sandstone, siltstone and dolostone (Cady, 1945). At this location, the Monkton Formation is best exposed on the western side of Pease Mountain (Kim et al., 2011).

The Stony Point Shale at both field sites consists of alternating beds of blue-grey to light-brown dolostones, buff to dark-brown shale, and dark-grey to black calcareous

shales. Bedding thickness is highly variable across these outcrops and ranges from 0.5 to 35 cm (Figure 3.9). Based on similarity of bedding thickness, I determined the presence of two mappable sub-units. Areas where beds have an average thickness range of 0.5–11 cm were considered unit 1 (Figure 3.9a), whereas areas with beds of average thickness ranging from 0.5–35 cm were considered unit 2 (Figure 3.9b). When mapped across the Route 7 outcrops, the “flea market” consists of sub-unit 1 (Figure 3.10a), whereas “the driveway” consists of sub-unit 2 on the southern end of the exposure and sub-unit 1 at the northern end (Figure 3.11a).

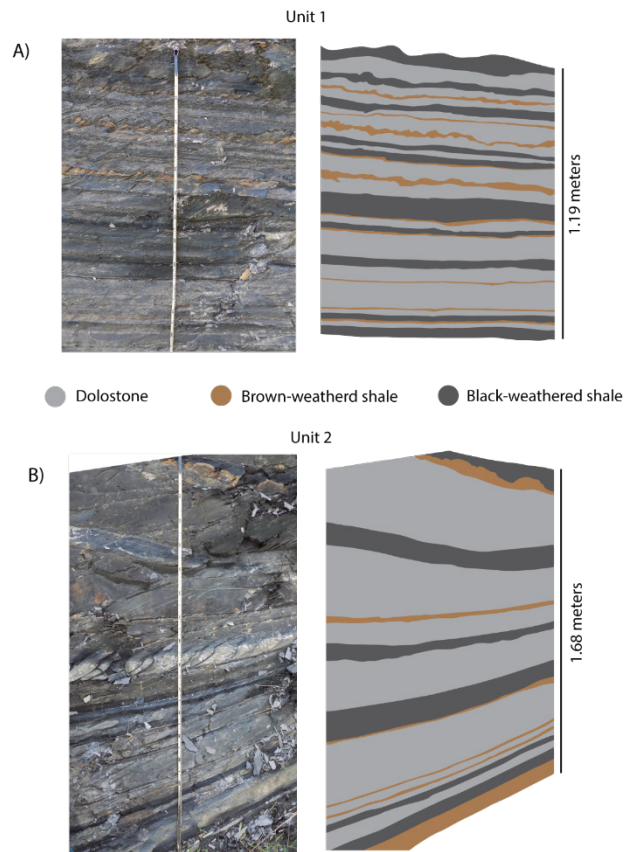


Figure 3.9: Bedding of the Stony Point Shale exposed at the “flea market” and “the driveway” are composed of alternating layers of dolostone, brown-weathered shale, and black-weathered shales. Bedding thickness varies across the outcrops and was used to determine the presence of two mappable sub-units. A) Unit 1 consists of beds that average 0.5 – 11 centimeters thick, whereas B) unit 2 consists of beds that average 0.5 – 35 centimeters thick.

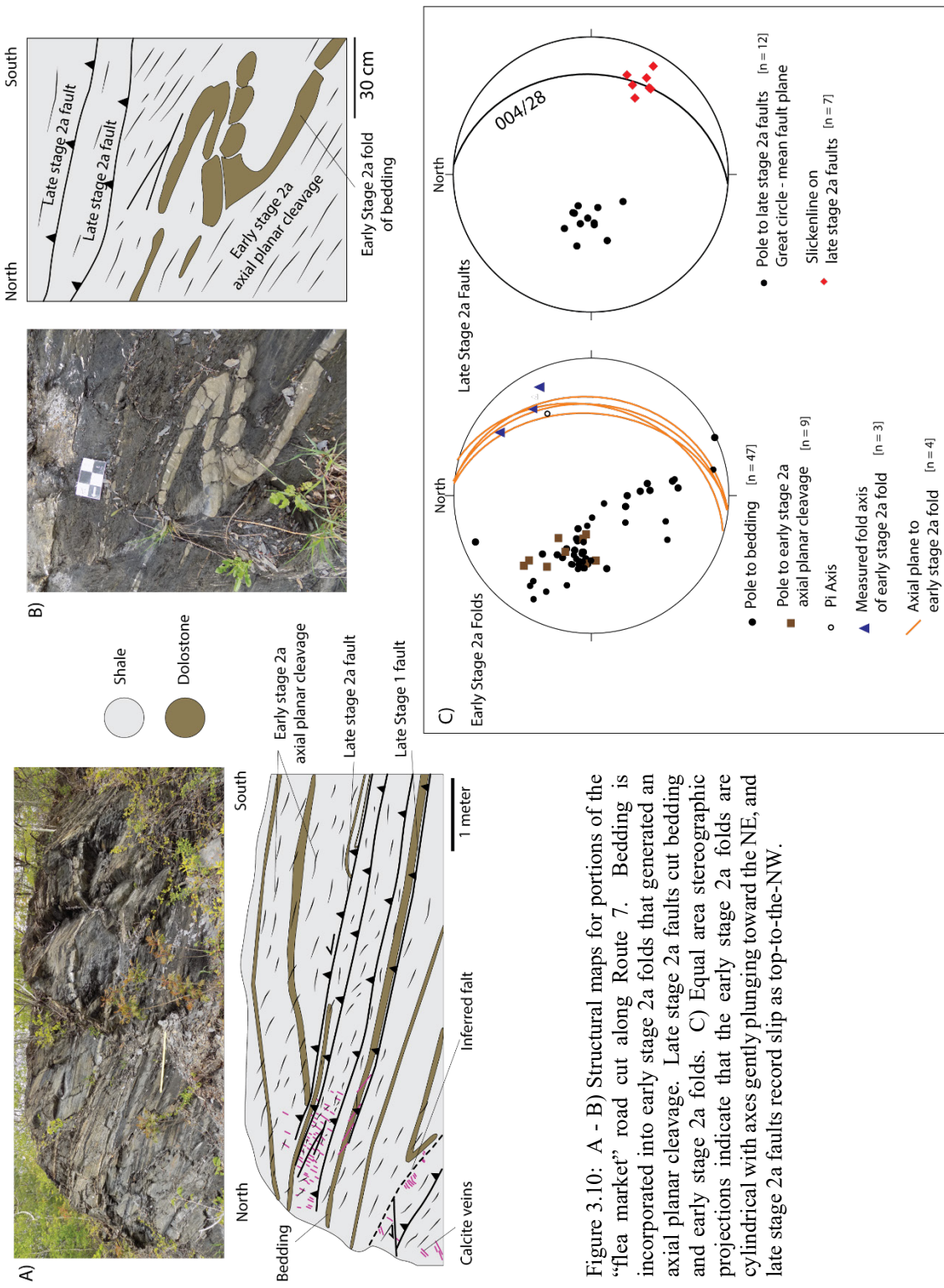


Figure 3.10: A - B) Structural maps for portions of the “flea market” road cut along Route 7. Bedding is incorporated into early stage 2a folds that generated an axial planar cleavage. Late stage 2a faults cut bedding and early stage 2a folds. C) Equal area stereographic projections indicate that the early stage 2a folds are cylindrical with axes gently plunging toward the NE, and late stage 2a faults record slip as top-to-the-NW.

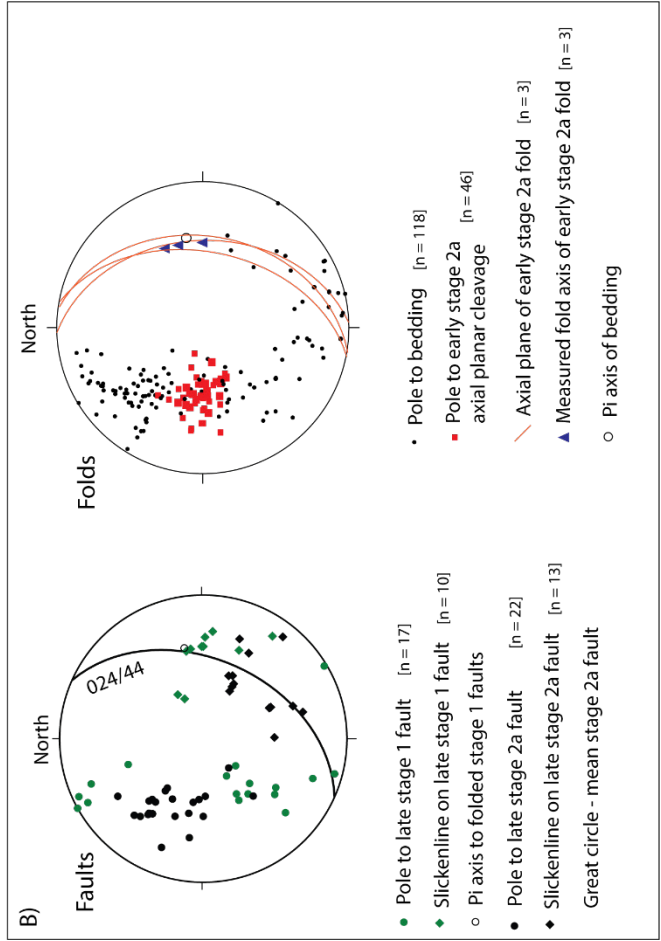
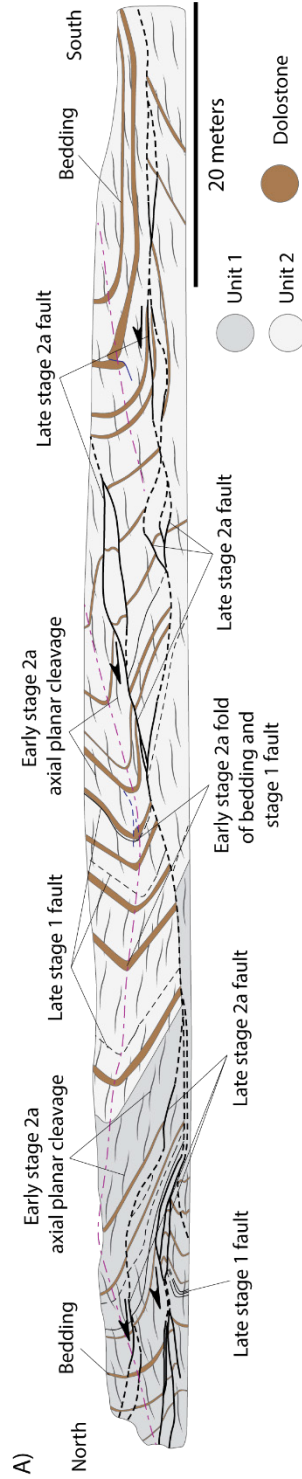


Figure 3.11: A) Structure map of "the driveway" along Route 7. Bedding thickness variability was used to determine the presence of two mappable units. Unit 1 consists of beds 0.5–11 cm thick. Unit 2 consists of beds 0.5–35 cm thick. Early stage 2a folds incorporate bedding, late stage 1 faults, and generated an axial planar cleavage. Late stage 2a faults cut all earlier structures. B) Equal area stereographic projection of stage 1 and stage 2 faults and fold characteristics.

At both Route 7 outcrops, late stage 1 bedding-parallel thrust faults are preserved and record a top-to-the-west direction of slip (Figures 3.10c, 3.11b). These late stage 1 faults are transformed and cut by younger stage 2a folds and faults. When plotted as poles on an equal-area stereonet, a calculated pi axis for late stage 1 faults plots in the same position as pi axes for early stage 2a folds (Figure 3.11b).

Early stage 2a folds incorporated bedding and late stage 1 faults, generated an axial planar cleavage, and vary in scale. At the “flea market”, early stage 2a folds are moderately to gently inclined to the east, gently plunging toward the northeast, and are 10–30 cm wide (Figure 3.10c). The interlimb angles of early stage 2a folds range from 19°–26°. Localized folds of dolostone layers are rootless and thicken towards the hinge zone, indicating flexural-flow (Figure 3.10b). At “the driveway”, stage 2a folds are moderately inclined to the east, moderately plunging toward the east, and are 5–10 m wide (Figure 3.11b). The interlimb angles of these larger scaled folds range from 34°–46°. Some stage 2a folds at “the driveway” also contain minor faults within the hinge zone (Figure 3.11a). The spacing of the generated axial planar cleavage varies between the shale and dolostone layers. Within the shale layers, cleavage spacing is sub-centimeter, yet within the folded dolostone layers, spacing ranges from 2 cm at the hinge zone to 10 cm near the inflection point (Figure 3.12). This cleavage refraction between shale layers and dolostone layers indicate how the difference in rock type, bedding thickness, and mechanical properties of various rock types influence structural style (Treagus, 1988).

Bedding, stage 1 faults, and early stage 2a folds are all cut by late stage 2a thrust faults that accommodate approximately 15–29 m of displacement (See Appendix 1 for

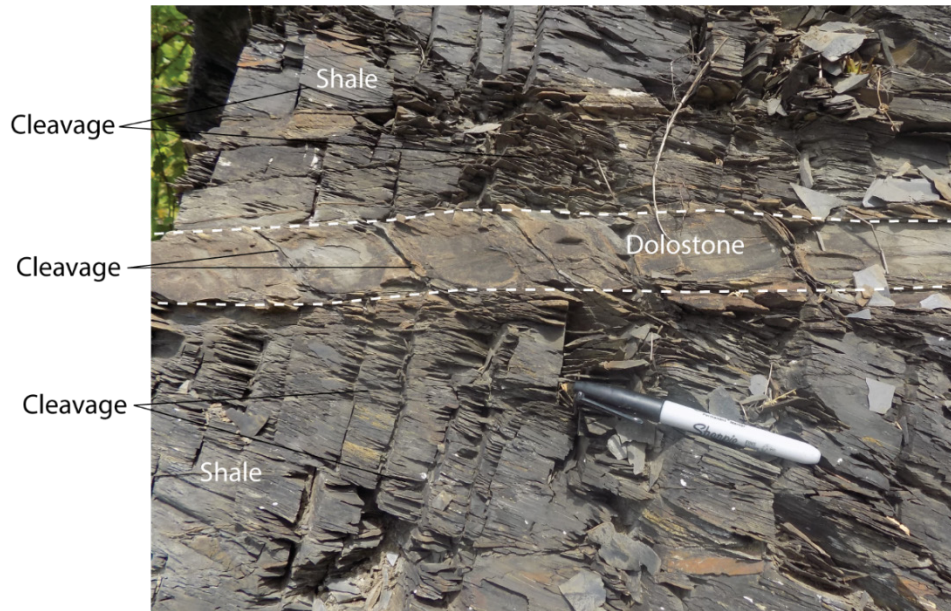


Figure 3.12: Variability of cleavage spacing within shale and dolostone layers at “the driveway” and the “flea market”. Cleavage spacing within the shales is sub-centimeter, whereas cleavage spacing within the dolostone is ~ 2 cm near the hinge zone of folds and ~ 10 cm near inflection point. This cleavage refraction indicates the role that various rock type with various mechanical properties plays on cleavage formation (Treagus, 1988).

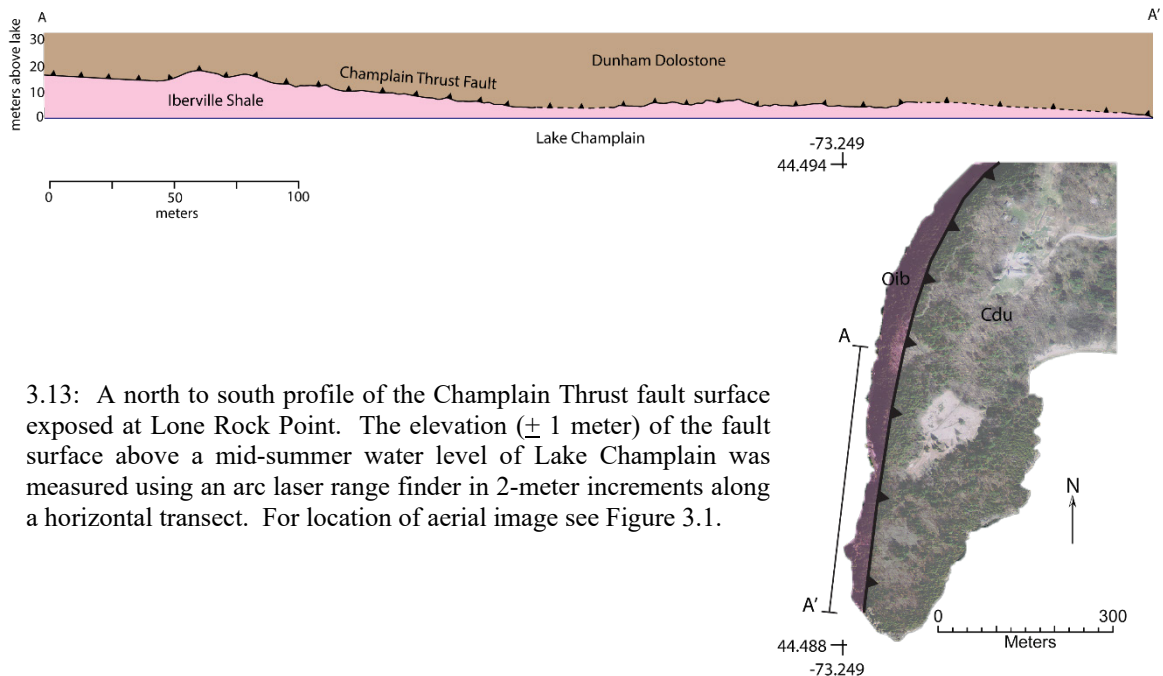
calculations). These through-going thrust faults anastomose across the outcrops with a mean strike to the northeast and a 28° – 44° dip to the southeast (Figure 3.10c, 3.11b). These late stage 2a faults record a top-to-the-NNW motion. Sense of shear was determined by slickenline orientations, offset bedding, and slicken steps preserved along fault planes. At the “flea market”, these late stage 2a faults generate thrust wedges of bedding and earlier faults (Figure 3.10a), whereas at “the driveway” the late stage 2a faults generate tight recumbent folds of bedding and localized regions of fault zone cleavage (Figure 3.11a).

3.6 Lone Rock Point, Burlington, Vermont

Lone Rock Point ($44^{\circ} 29' 27.68''$ N; $73^{\circ} 14' 56.12''$ W) (Figure 3.1) provides 10–30-meter vertical exposures of the highly deformed Ordovician Iberville Shale of the

footwall, the Champlain Thrust fault surface, and the slightly deformed base of the massive Cambrian Dunham Dolostone of the hanging wall. This inverted stratigraphy represents an interpreted stratigraphic throw of ~2,700 meters (Stanley, 1987). The Dunham Dolostone is a light-pink dolostone that weathers beige to buff colored. Using x-ray diffraction, Mundy et al. (2016) determined that this unit is comprised of 85% dolomite with calcite, quartz, and illite accessory minerals. Bedding within the dolostone is cryptic and not well observed in the cliff face exposures. The Iberville Shale is composed highly-cleaved interbedded marly-shales, slate, and dolostone with white-calcite veins observed both parallel and normal to layers. Using X-ray diffraction, Mundy et al. (2016) determined the mineralogical composition of the Iberville shale to be 75% calcite, 15% quartz, and 10% illite and other phyllosilicates.

To map the distribution of structures observed at the Lone Rock Point exposure, I first made a profile map of the Champlain Thrust's fault surface (Figure 3.13). Using an arc laser rangefinder, I measured the elevation (± 1 meter) of the fault surface above a mid-summer water level of Lake Champlain along a horizontal transect in 2-m increments. At the northernmost extent of the transect, the Champlain Thrust surface is at its highest elevation of 18 m above the Lake Champlain shore (Figure 3.13). Moving south from its highest point, the Champlain Thrust surface decreases in elevation by 14 m vertically across a 150 m horizontal distance—a 9% gradient. Continuing southward, the fault surface remains at 4 to 5 m above the lake until it finally dives below the Lake Champlain water level at the southernmost tip of the Lone Rock Point peninsula (Figure 3.13). Using the profile of the fault surface, I mapped the distribution and extent of all major faults,



3.13: A north to south profile of the Champlain Thrust fault surface exposed at Lone Rock Point. The elevation (± 1 meter) of the fault surface above a mid-summer water level of Lake Champlain was measured using an arc laser range finder in 2-meter increments along a horizontal transect. For location of aerial image see Figure 3.1.

folks, and cleavage trends along a 340 m transect. I divided this transect into four separate sections based on continuous footwall exposure (Figure 3.14–3.17). Sense of shear along the measured faults was determined based on a combination of observable displacement of bedding, veins, and cleavage, asymmetric cleavage planes, shear bands, and slicken steps.

The oldest structures preserved at Lone Rock Point are rootless recumbent folds of relict dolostone bedding that generated an axial planar cleavage (Figure 3.18a). These early stage 2a folds are 20-cm-wide with an interlimb angle of $\sim 20^\circ$ and are primarily observed in locations greater than 15 m below the Champlain Thrust fault surface. The spacing of the axial planar cleavage associated with the early 2a folds is ~ 2.8 cm. Late stage 2a thrust faults are also preserved within the footwall and are best preserved at distances greater than 12 m below the Champlain Thrust fault surface (Figure 3.14a). These faults are parallel to bedding and cleavage planes and record a top-to-the-northwest slip (Figures 3.14b, 3.15b, 3.16b).

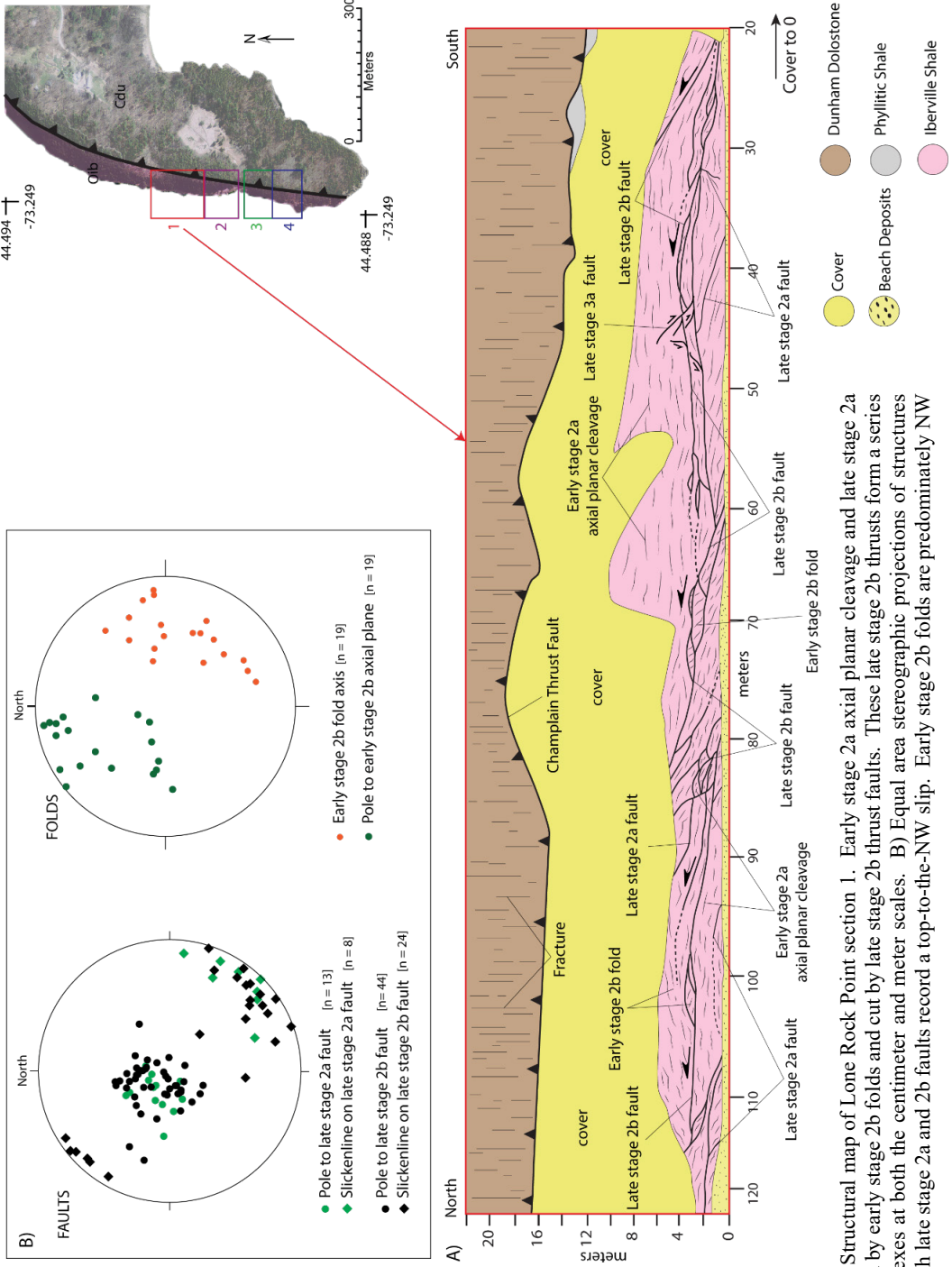


Figure 3.14: A) Structural map of Lone Rock Point section 1. Early stage 2a axial planar cleavage and late stage 2a faults are folded by early stage 2b folds and cut by late stage 2b thrust faults. These late stage 2b thrusts form a series of stacked duplexes at both the centimeter and meter scales. B) Equal area stereographic projections of structures indicate that both late stage 2a and 2b faults record a top-to-the-NW slip. Early stage 2b folds are predominately NW

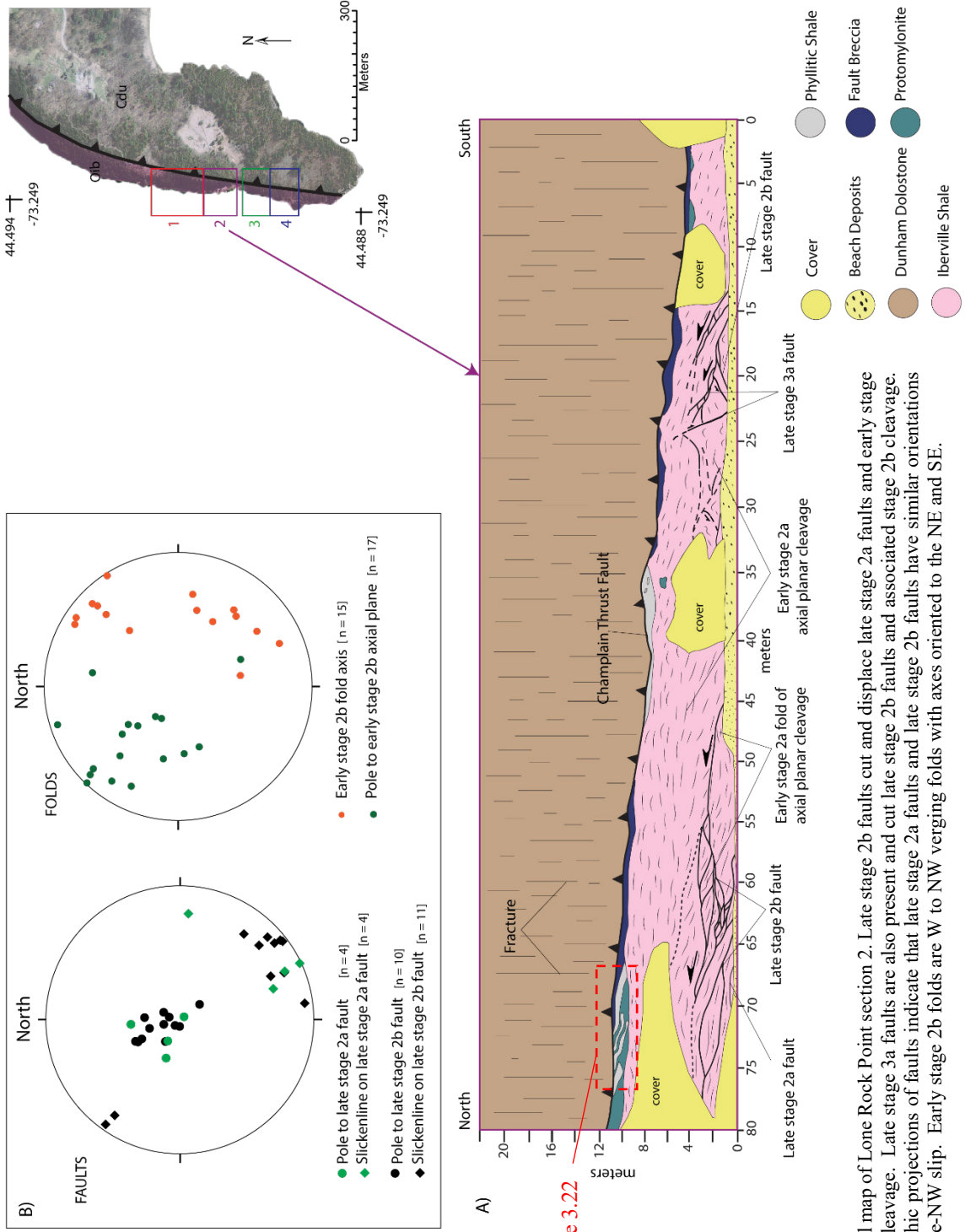


Figure 3.22

Figure 3.15: A) Structural map of Lone Rock Point section 2. Late stage 2b faults cut and displace late stage 2a faults and early stage 2b folds of axial planar cleavage. Late stage 3a faults are also present and cut late stage 2b faults and associated stage 2b cleavage. B) Equal area stereographic projections of faults indicate that late stage 2a faults and late stage 2b faults have similar orientations and both record top-to-the-NW slip. Early stage 2b folds are W to NW verging folds with axes oriented to the NE and SE.

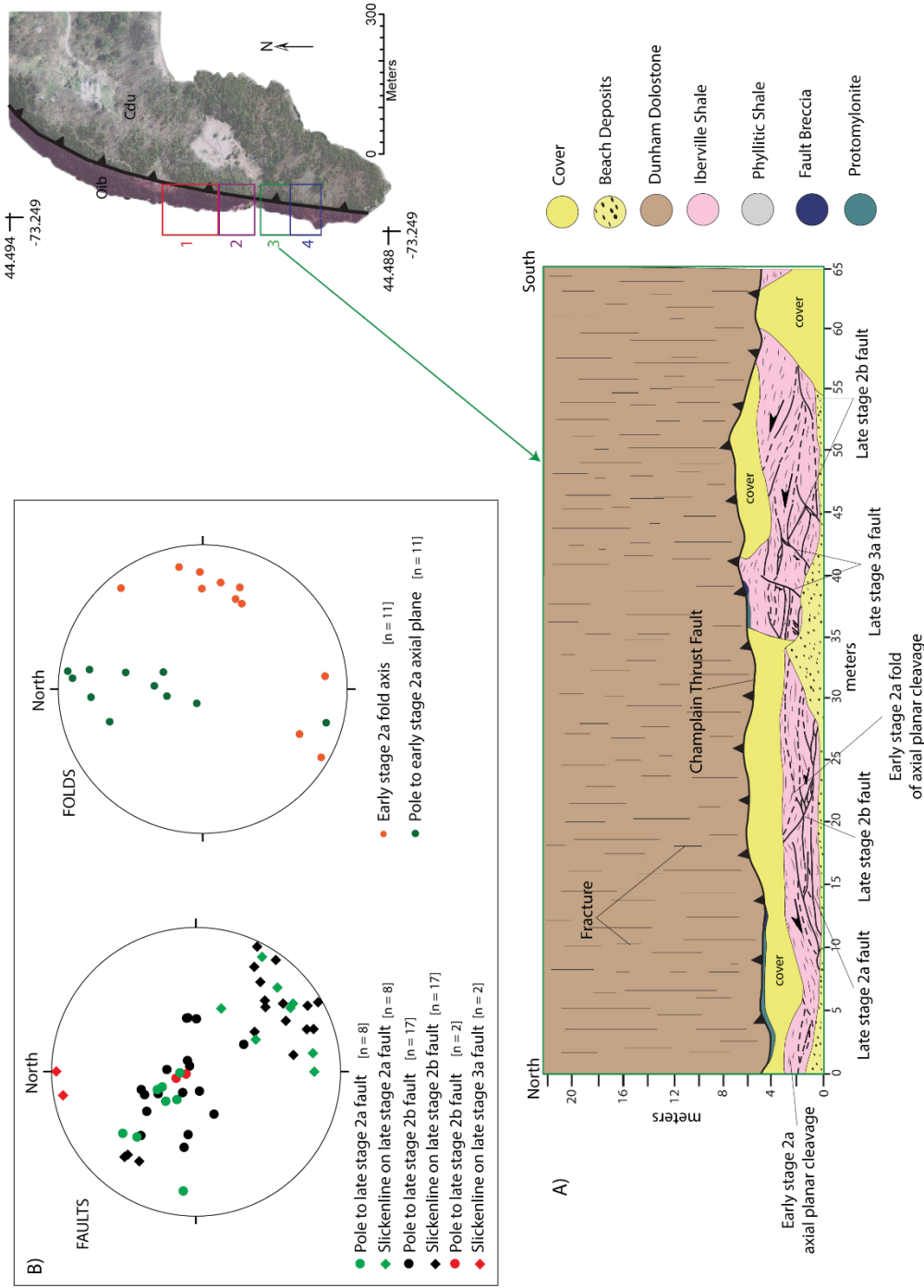


Figure 3.16: A) Structural map of Lone Rock Point section 3. Late stage 2a faults and axial planar cleavage are cut and folded by late stage 2b faults. Late stage 3a normal faults cut late stage 2b faults and early stage 2a axial planar cleavage. B) Equal area stereographic projections of structures indicate both late stage 2a and 2b faults are of similar orientation with slip of top-to-the-NW. Late stage 3a normal faults record slip of top-to-the-north. Late stage 2b folds of cleavage are north verging folds with axes oriented to the NE, E, and a few toward the south.

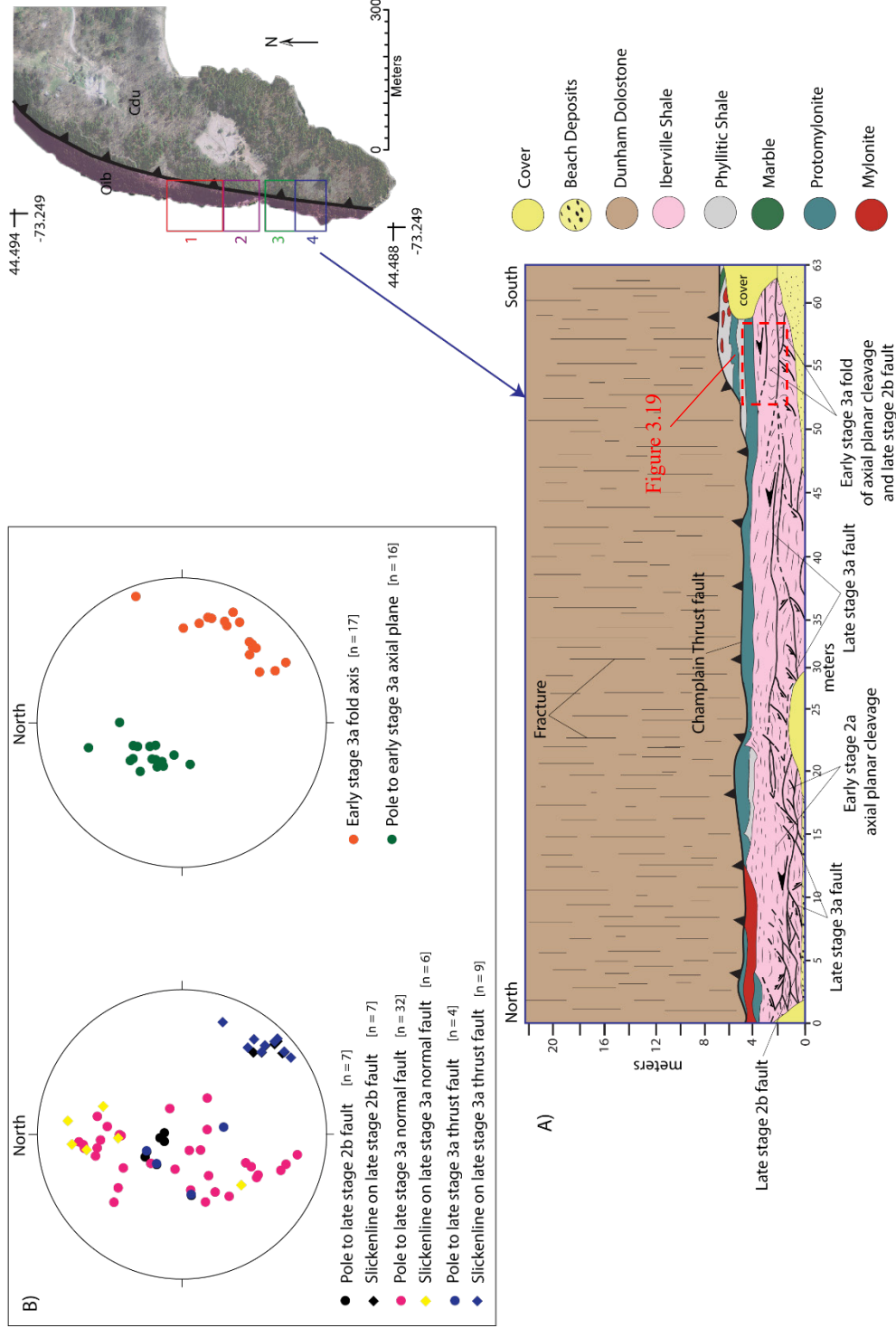


Figure 3.17: A) Structural map of Lone Rock Point section 4. Late stage 2b faults are cut by late stage 3a thrust and normal faults. Stage 2b transformed cleavage is incorporated into early stage 3a folds. B) Equal area stereographic projections of structures indicate that late stage 2b and late stage 3a thrust faults record slip as top-to-the-NW, whereas late stage 3a normal faults record slip top-to-the-N and top-to-the-S. Early stage 3a folds are NNW verging with axes predominately plunging to the SE.

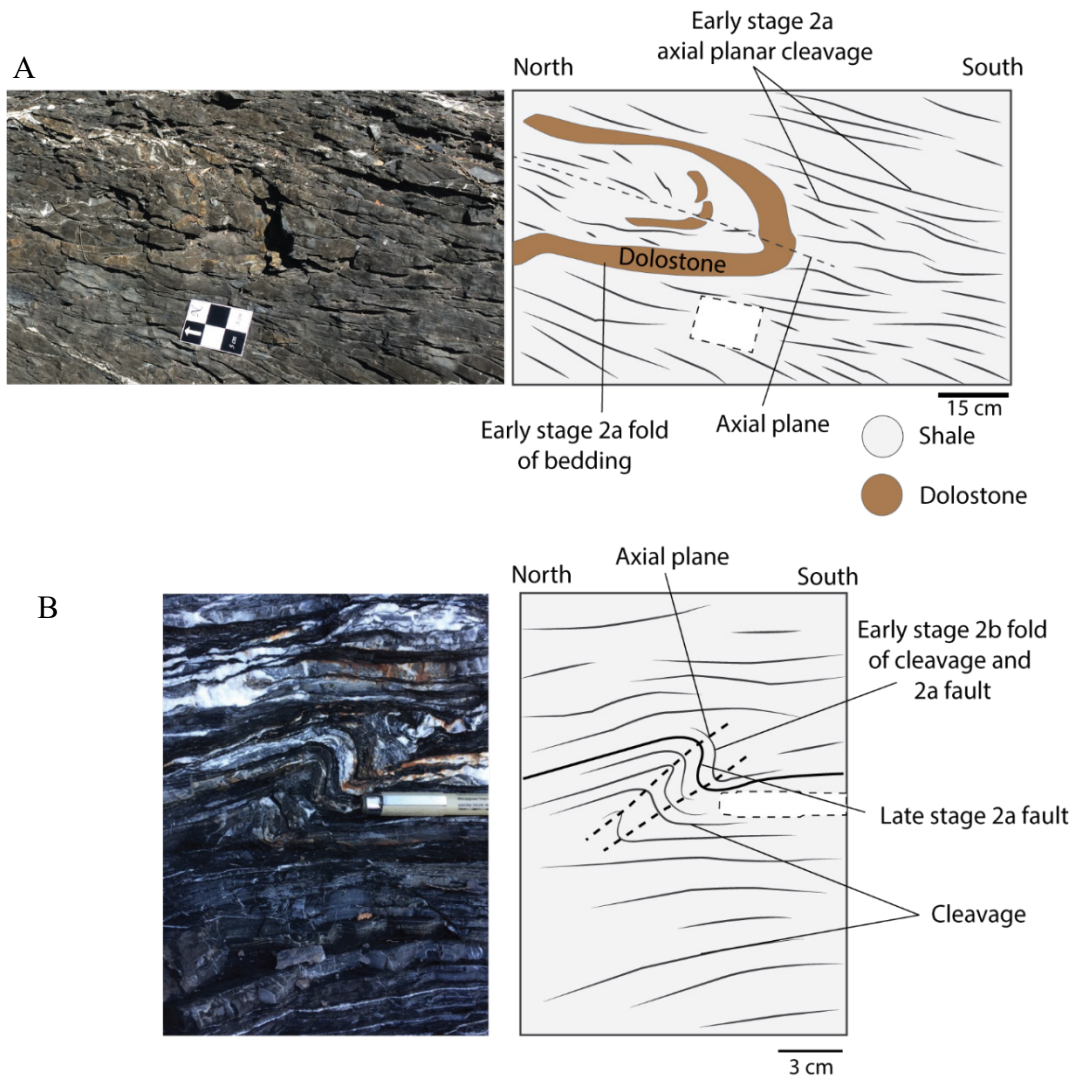


Figure 3.18: A) Early stage 2a folds incorporated bedding and generated an axial planar cleavage. These folds are primarily preserved at distances greater than 15 meters below the Champlain Thrust fault surface. B) Early stage 2b folds incorporated 2a cleavage and 2a faults. Early 2b folds are the dominant generation of folds preserved at Lone Rock Point.

Most of the stage 2a faults and folds are overprinted by early stage 2b folds and late stage 2b faults (Figures 3.14a, 3.15a, 3.16a). The early stage 2b folds, which incorporate bedding, early stage 2a cleavage, and late stage 2a faults, are the dominant fold generation preserved at Lone Rock Point (Figure 3.18b). These folds are predominately north–

northeast verging, moderately inclined to upright, with axes that plunge moderately to sub-horizontally to the northeast, east, and southeast (Figure 3.14b, 3.15b, 3.16b). These early stage 2b folds have an average interlimb angle of 59° and range in width from ~ 2 to tens of centimeters. These folds are associated with late stage 2b thrust faults (Figures 3.14a, 3.15a, 3.16a).

Late stage 2b thrust faults cut and transform bedding, early stage 2a cleavage, and late stage 2a faults. These late stage 2b faults record a top-to-the-northwest slip (Figure 3.14b, 3.15b, 3.16b, 3.17b) and generate localized fault-bound lozenges that stack along thrust faults that cut up towards the Champlain Thrust surface (Figure 3.14a, 3.15a). These packages of stacked lozenges are observed throughout Lone Rock Point and are best preserved at distances greater than 10 m from the Champlain Thrust surface. The observable geometry of these faults combined with their distribution on stereographic projections suggest that these late stage 2b faults are duplexes that stack at various scales. Though a common floor and roof thrust are not observed, the 2b thrusts that cut up toward the Champlain Thrust surface form ramps that cut earlier cleavage and stage 2a faults (Figure 3.14a, 3.15a). The smaller scaled lozenges that stack along these ramps also cut and transform bedding and early cleavage, but at a smaller scale. The thrust ramp that they are stacked on generates a common floor thrust for these smaller scaled duplexes. These smaller duplexes appear to mimic the larger duplex geometry in which they are nested. A series of these late stage 2b thrust duplexes has been mapped that spans ~ 120 meters (Figures 3.14a, 3.15a).

As the Champlain Thrust fault is approached from the footwall, stage 3a structures become dominant at distances less than 5 m from the fault surface (Figure 3.17a). Early stage 3a folds incorporate bedding, cleavage associated with 2b folds, and late stage 2b faults. These folds are west to northwest verging, gently to moderately inclined, and gently to sub-horizontally plunging to the east and southeast (Figure 3.17b). These folds are less than 10 cm wide with interlimb angles $\sim 50^\circ$. These early stage 3a folds are cut by late stage 3a faults.

Late stage 3a faults consist of both thrust faults and normal faults (Figure 3.19). Late stage 3a thrust faults are tightly spaced anastomosing faults that record a top-to-the-northwest slip, whereas late stage 3a normal faults record top-to-the-north and top-to-the-south slip (Figure 3.17b). Based on cross-cutting relations, both late stage 3a thrust and normal faults are interpreted to be coeval. Some late stage 3a thrusts are cut by normal faults (Figure 3.20a), yet in other places, late stage 3a thrusts cut late stage 3a normal faults (Figure 3.20b). These normal faults are primarily preserved within 5 m of the Champlain Thrust surface (Figure 3.16a, 3.17a). However, a few normal faults have been mapped at approximately 12 m from the Champlain Thrust surface (Figure 3.14a) and up to a few centimeters from the fault surface. No normal faults have been observed to cut or displace the Champlain Thrust fault surface, indicating that these late stage 3a faults are older than the last stage of motion along the Champlain Thrust.

Above stage 3a faults and folds is a zone of cleavage intensification that varies from tens of centimeters thick to < 6 meters thick (Figure 3.21). This zone contains a very strong cleavage with spacing on the millimeter scale. This zone is observed ~ 2 m below the

Champlain Thrust surface and though some discontinuous veins are preserved, no other measurable structures are observed.

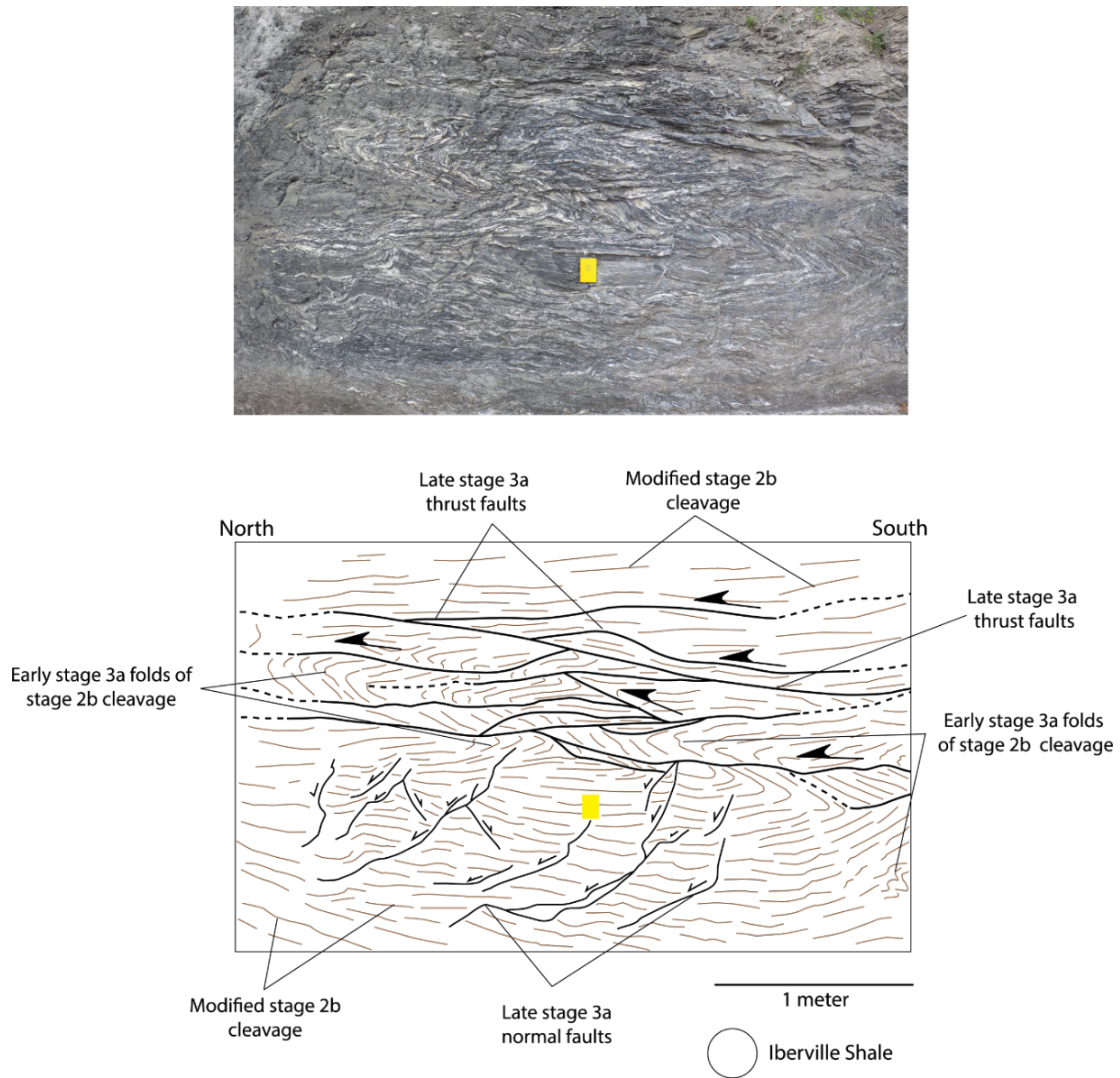


Figure 3.19: Illustrated image of early and late stage 3a structures from Lone Rock Point section 4 (See figure 3.17). Early stage 3a folds incorporate bedding and stage 2b modified cleavage. Late stage 3a thrust and normal faults cut these folds. Thrust faults record slip top-to-the-NW; whereas normal faults record slip top-to-the-N and top-to-the-S.

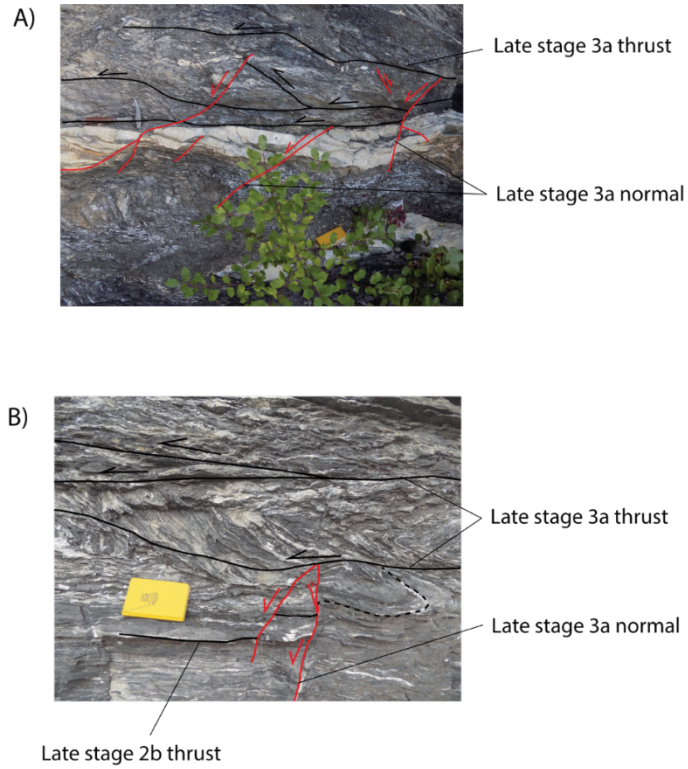


Figure 3.20: Late stage 3a thrusts and normal faults are considered coeval. A) Late stage 3a normal faults are observed to cut late stage 3a thrusts. B) Late stage 3a thrusts are also observed to cut late stage 3a normal faults

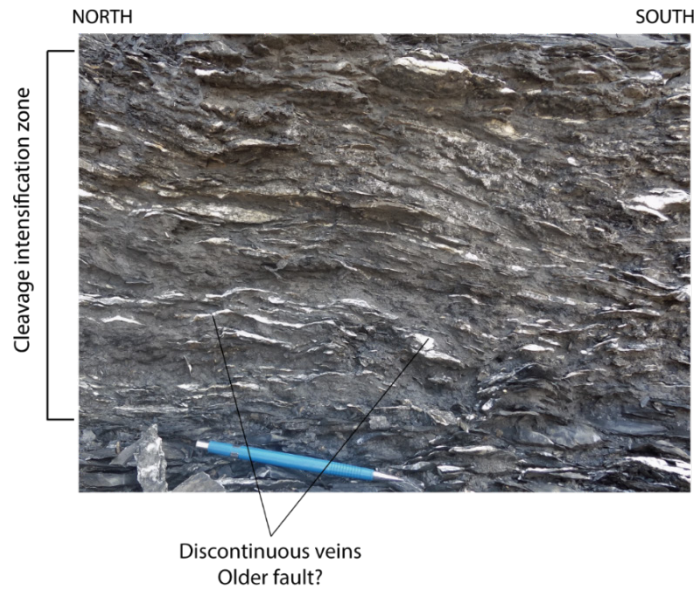


Figure 3.21: Cleavage intensification zone. Cleavage spacing is on the millimeter scale and contains discontinuous veins and no other measurable structures.

In localized lenses above this cleavage intensified zone are rocks of varying types with brittle and ductile tectonites not observed anywhere else within the footwall (Figure 3.22a) (Stanley, 1987). These rock types include marble, phyllitic-shale, and dolostone. Brittle tectonites include limestone breccia, fault gouge, and cataclastic lined faults.

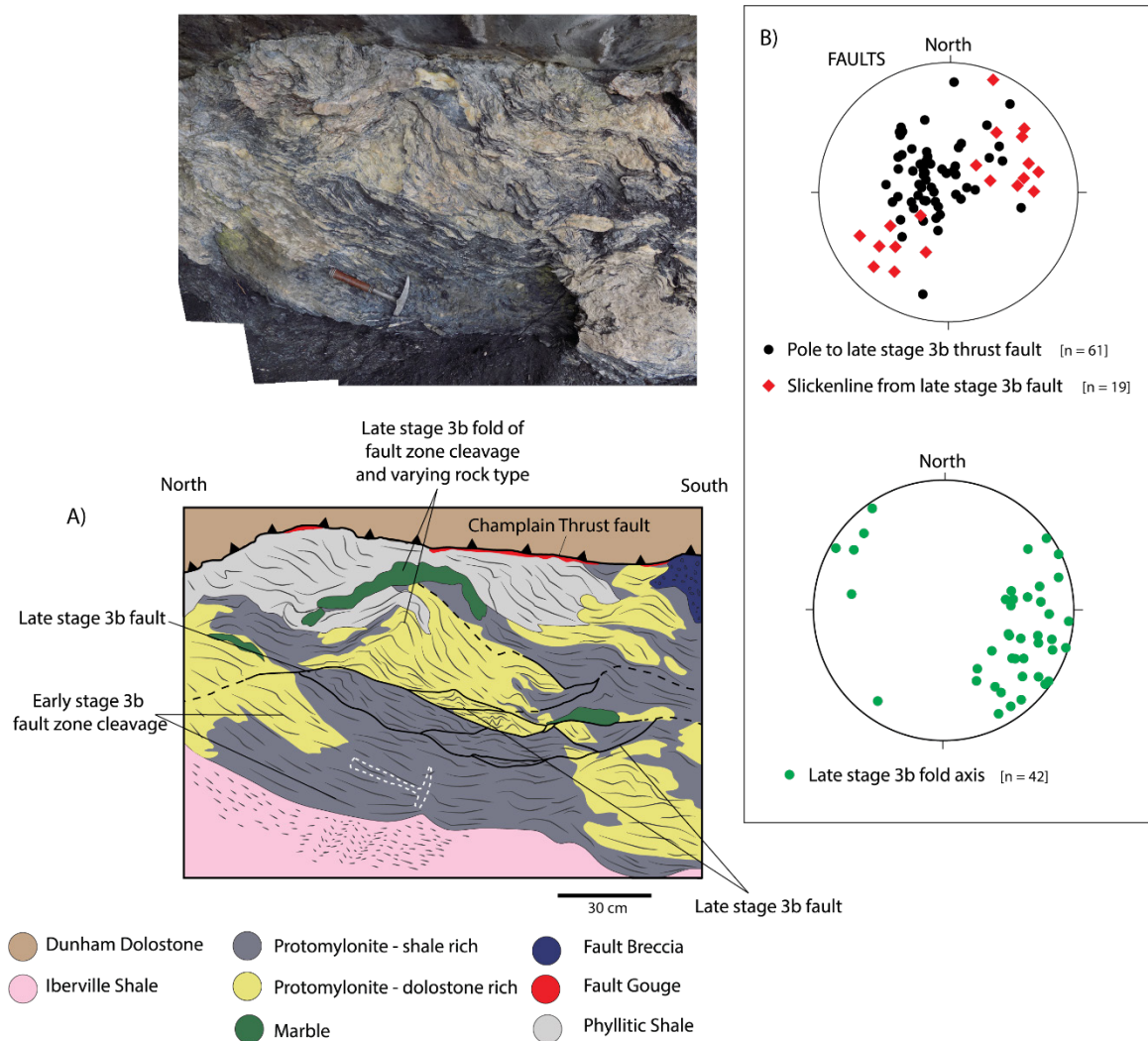


Figure 3.22: A) Structural map of early and late stage 3b structures and associated rock types. Early stage 3b fault zone cleavage is incorporated into early stage 3b folds and cut by late stage 3b faults. B) Equal area stereographic projections indicate these faults record a unique NE-SW direction of motion. 3b fold axes plunge to the NE, E, and SE, with a few plunging to the NW. For image location, see Figure 3.15.

Ductilely sheared rocks include protomylonite, mylonite and boudinaged layers of dolostones. Fault zone cleavage, tight folds, fault breccia, ductile shear zones, and boudin structures all constitute early stage 3b (Figure 3.23). The tight early stage 3b folds have axes orientations that range from the northeast, east, and southeast, with some axes trending toward the northwest (Figure 3.22b).

Late stage 3b structures include rootless sheath folds and cataclastic faults that cut early stage 3a fault zone cleavage and protomylonites (Figure 3.23). Late stage 3b faults are tightly spaced anastomosing faults that record top-to-the-southwest slip (Figure 3.22b). This motion direction is observed only along these late 3b faults and has not been observed at any other location within this study.

Finally, the Champlain Thrust fault—the contact of the Iberville Shale and the Dunham Dolostone—is considered the final stage of deformation as it cut all other structures within the footwall and hanging wall (Table 3.1). The orientation of the Champlain Thrust principal slip surface varies slightly across the Lone Rock Point (Figure 3.24a) and has a mean strike toward the north and shallow dip to the east at 13° (Figure 3.24b).

Slickenlines, although rare and predominately weathered, have been discovered along the bottom of the fault surface (Figure 3.25). Two main sets of slickenlines with different orientations were observed in the same location, separated by ~ 1 m. The relative age of these slickenlines was determined by the amount of apparent weathering effecting the appearance—the least weathered corresponds to the youngest generation. Both generations of slickenlines have observable chatter marks (slickensteps) preserved on the

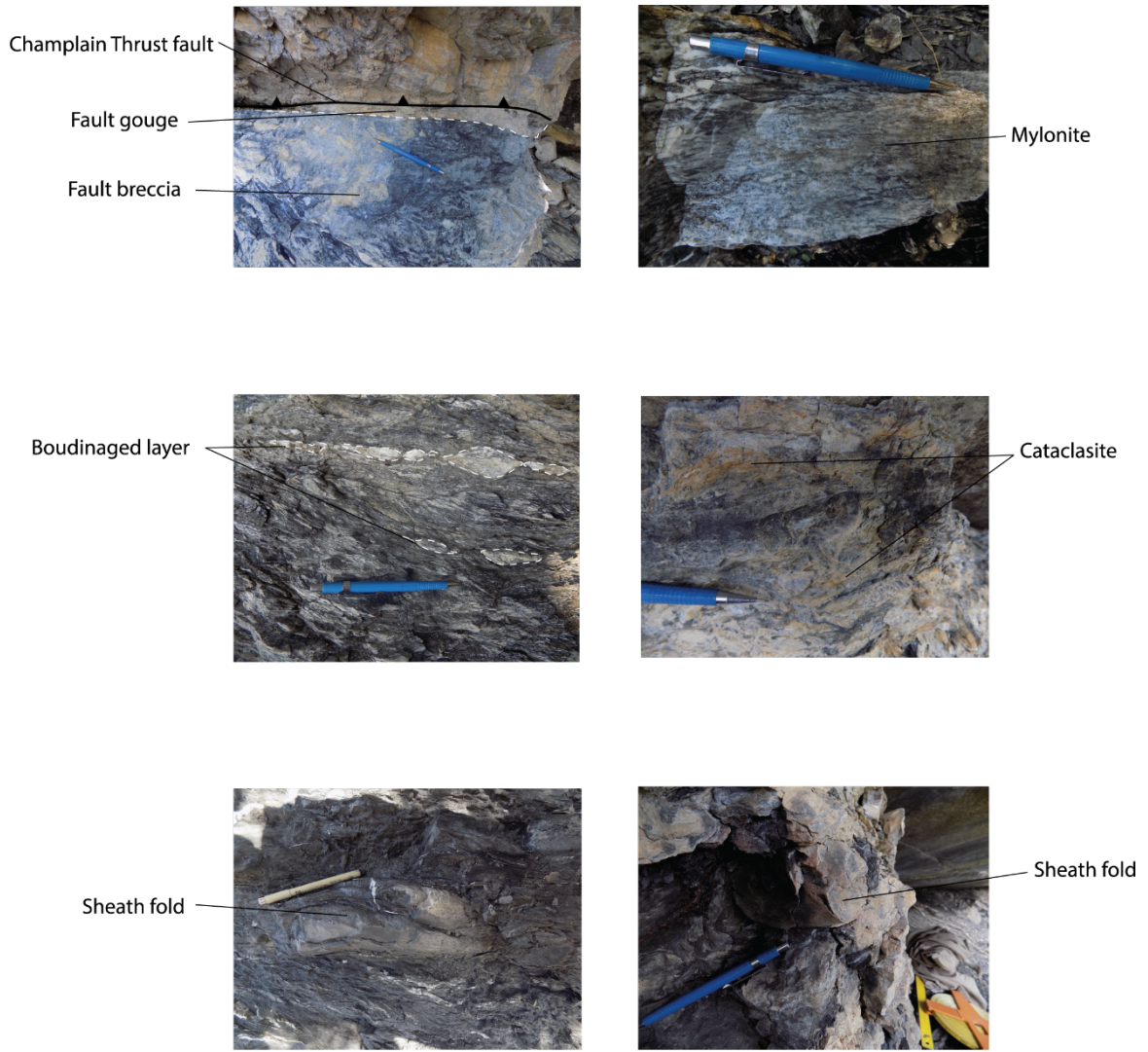


Figure 3.23: Images of various early and late stage 3b structures. Early stage 3b structures include fault breccia, fault gouge, mylonite, and boudin structures. Late stage 3b structures include cataclastic lined faults and sheath folds.

surface, providing the evidence needed to determine sense of shear. The oldest generation of slickenlines record a top-to-the-west slip on the Champlain Thrust (Figure 3.25a), whereas the youngest set records a top-to-the-south slip direction (Figure 3.25b). These slickenline orientations suggest a sharp change in motion direction along the Champlain Thrust fault by approximately 90°.

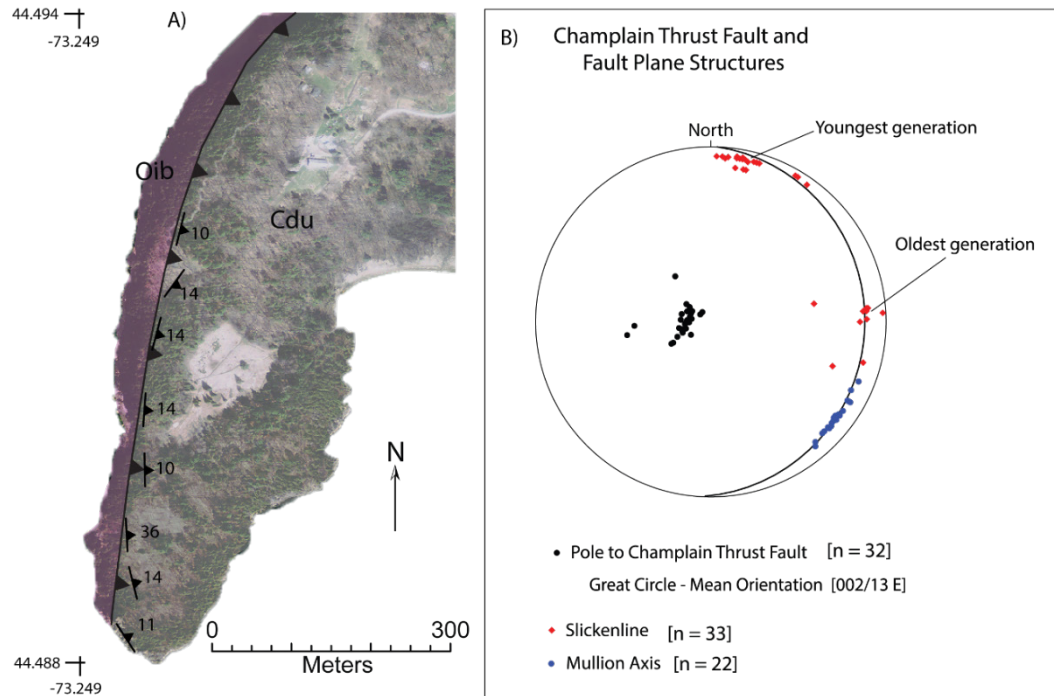


Figure 3.24: A) The slight variations in orientations of the Champlain Thrust fault at Lone Rock Point, Burlington. B) Stereographic projection of Champlain Thrust fault surface with slickenline and mullion orientations. The oldest generation of slickenlines preserved on the Champlain Thrust fault indicate that motion was top-to-the-west, whereas the youngest generation indicates that motion was top-to-the-south. These directions do not match the axes orientations of fault mullions.

Fault mullions are also preserved on the principal slip surface and are best observed along overhanging portions of the slip surface. The mullions have an average wavelength of 162 cm from peak to peak and have axes consistently oriented toward the southeast with a mean plunge of 11° (Figure 3.25b). These fault mullions have previously been used as an indication of motion direction on the Champlain Thrust fault (Stanley, 1987; Mundy et al., 2016). Though the orientation of the mullions matches the orientation of slickenlines preserved on stage 2a, 2b and 3a thrust faults within the footwall, they do not match the orientation of preserved slickenlines along the principal slip surface.

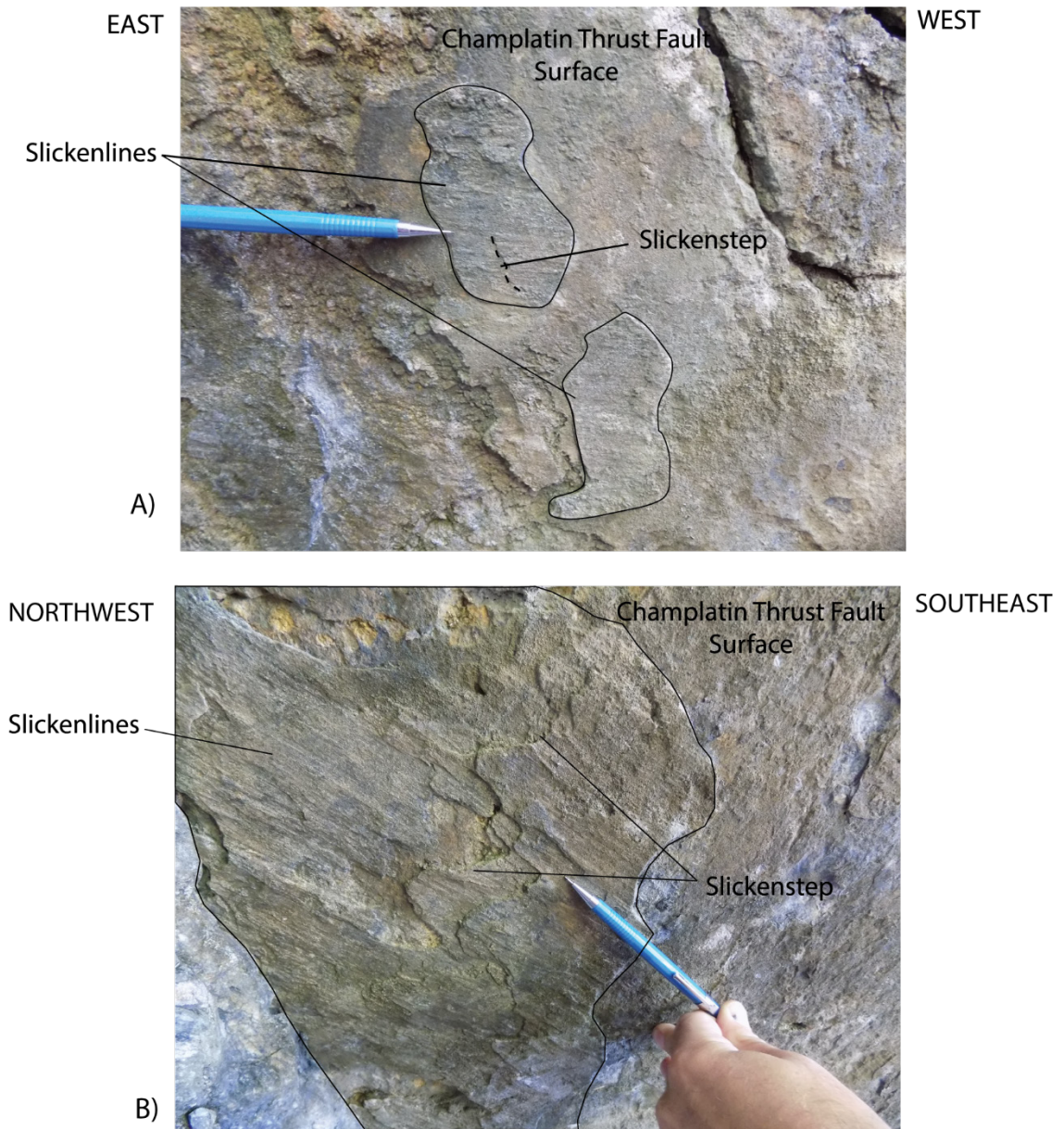


Figure 3.25: Images of slickenlines preserved on the Champlatin Thrust fault surface. A) The oldest generation of slickenlines is highly weathered with a slickenstep indicating that oldest recorded motion is top-to-the-west. B) The youngest generation is less weathered with predominant slickensteps indicating that the youngest recorded motion was top-to-the-south. Both images are looking up at the bottom of the Champlatin Thrust fault surface, and both slickenline sets were separated by ~ 0.5 m.

3.7 Fault Zone Architecture

Combining the data presented in Table 3.1 with the structural maps of each location, I generated a scaled composite diagram of structures observed at all six field sites (Figure 3.26). Lessors Quarry, “the beam”, and the Ferrisburgh Quarry are dominated by early dissolution cleavage planes that are cut and locally folded by late stage 1 faults. At these locations—which correspond to calculated depths of 450 meters and greater below the Champlain Thrust fault surface—late stage 1 thrust faults are not deformed and are the youngest event preserved.

Late stage 1 faults are then incorporated into early stage 2a folds preserved at the “flea market” and “the driveway” outcrops. The early stage 2a folds generated an axial planar cleavage and are later cut by through going late stage 2a thrust faults. It is at these locations that correspond to a minimum calculated depth of 205 m or less below the Champlain Thrust surface that folds contain an axial planar cleavage and older faults are cut and displaced by younger ones.

At Lone Rock Point, early stage 2a folds are preserved and predominately overprinted by late stage 2b faults and duplex style folding. These stage 2b duplexes are preserved at distances greater than 8 m below the Champlain Thrust fault surface and are cut and folded by stage 3a structures. Early stage 3a folds are close folds of bedding and stage 2b faults and folds. These folds are then cut and displaced by late stage 3a thrust faults and normal faults. Stage 3a structures are confined to distances less than 5 m below the Champlain Thrust surface. Early stage 3b mylonite, boudin structures, fault breccia, and fault zone cleavage are cut and transformed by late stage 3b sheath folds, and faults.

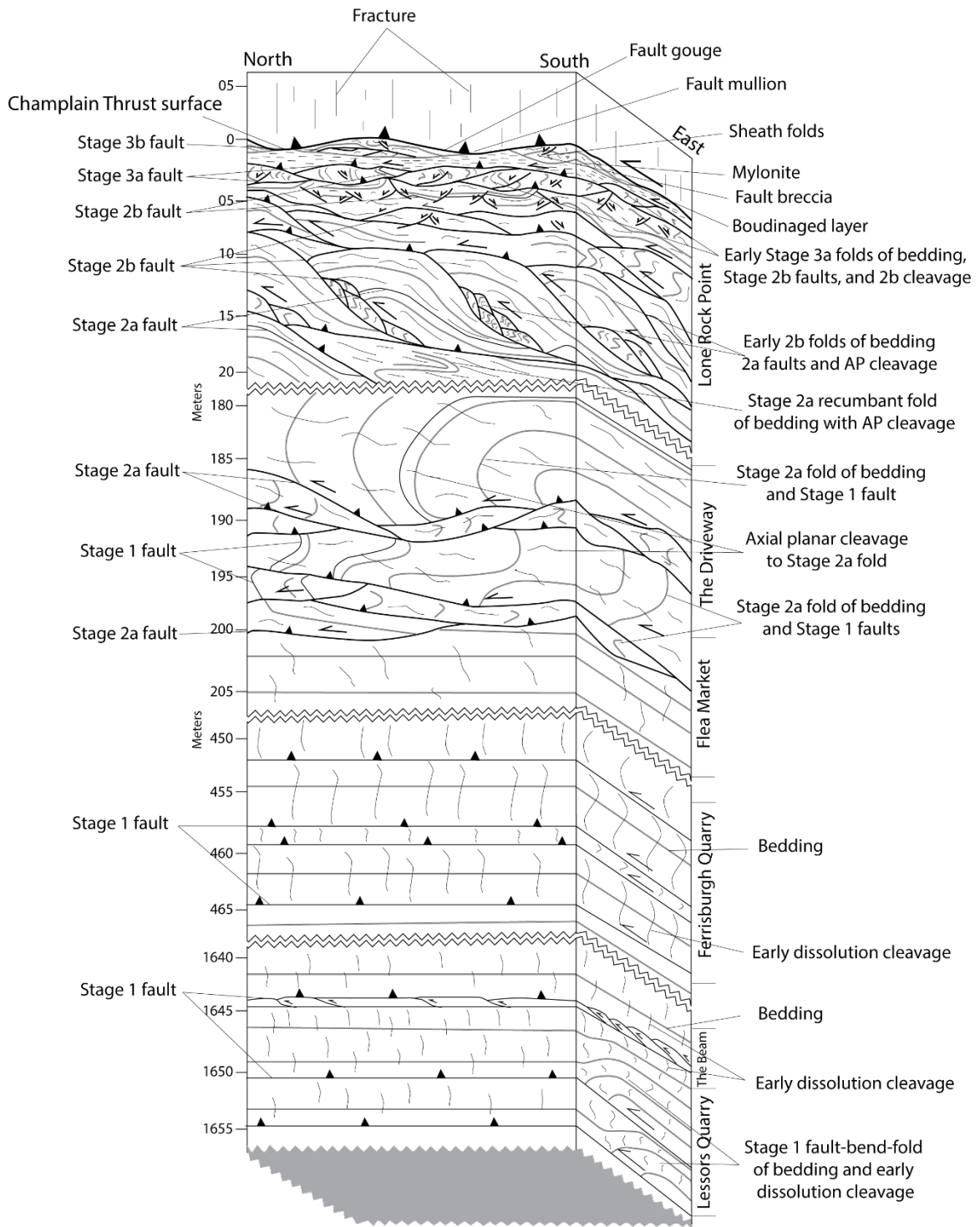


Figure 3.26: A scaled composite diagram of structures preserved within the footwall and hanging wall of the Champlain Thrust fault from each of the six field sites. The distance below the Champlain Thrust fault corresponds to the calculated location of each location (Figure 3.2).

These late stage 3b structures are preserved within 2 m or less from the Champlain Thrust fault surface. Finally, the Champlain Thrust surface cuts all older structures and the motion on the fault generated fault mullions, multiple slickenlines, fault gouge, and mylonite.

Based on these compiled descriptions and datasets, the boundaries of the Champlain Thrust fault zone in northwestern Vermont can be defined (Figure 3.27). The core (which includes the principal slip surface) can be subdivided into upper and lower portions. The upper core is defined by presence of late stage 3b structures and the cleavage intensified zone, whereas the lower core is defined by early stage 3b structures. Overall, the core varies in thickness but can reach up to 8 m in thickness.

The damage zone is observed in both the hanging wall and the footwall. The damage zone in the hanging wall is < 1 m thick and contains micro-faults that cut calcite veins and foliated rocks. The damage zone in the footwall can be subdivided into upper and lower sections. The upper damage zone is defined by the presence of late stage 2b structures including the variable scaled thrust duplexes. The upper damage zone is expressed within the remainder of the Lone Rock Point footwall exposure, therefore constraining the minimum thickness of the upper damage zone to 10 m. The lower damage zone is defined by the presence of early stage 2a folds with axial planar cleavage and late stage 2a thrust faults. This portion of the damage zone is only expressed along the Route 7 exposures, therefore constraining the maximum thickness of the lower damage zone to 430 m. Combined the minimum thickness of the entire damage zone is 197 m with the minimum boundary residing at approximately 205 m below the Champlain Thrust fault surface. The lower boundary of the lower damage zone corresponds to the upper boundary

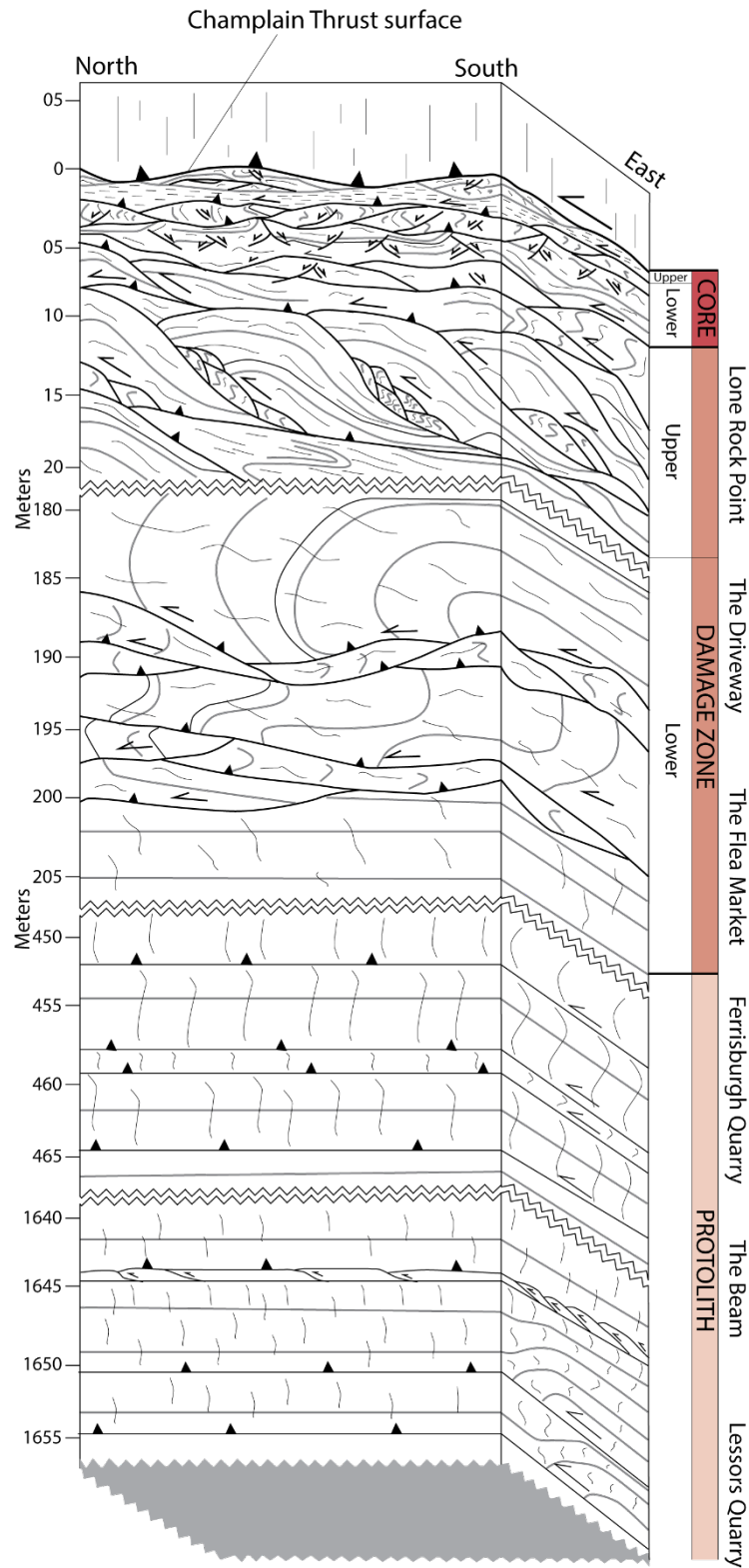


Figure 3.27: Boundaries of the Champlain Thrust fault zone within northwestern Vermont.

of the protolith zone. The protolith zone is therefore defined by locations that contain only stage one structures that are not cut by the younger stage 2 or stage 3 faults or folds.

By defining the boundaries of the fault zone and describing the structures preserved within them, I determined the structural architecture of the Champlain Thrust fault zone exposed in northwest Vermont. The fault zone is predominately preserved within the Champlain Thrust's footwall. Asymmetry is common within other known fault zones (Clausen et al., 2003; Dor et al., 2006; Mitchell et al., 2011; Choi et al., 2016) and can be attributed contrasting rock strength across the fault plane (Berg and Skar, 2005; Choi et al., 2016). An analysis of the fault zone architecture provided insights into the distribution of strain during its evolution.


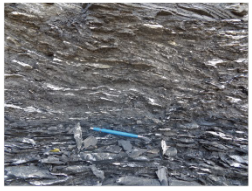



3.8 Relative Strain Description and Distribution

A goal of this study was to determine the distribution of relative strain throughout the fault zone. For this study, I use the term strain to reflect a distortion of a material through extension, shortening, volumetric change, translation, rotation, or a combination thereof. Determining the distribution of strain throughout the fault zone provides insight to how strain localized during fault zone development. The localization of strain is indicated by the narrowing of zones that accommodate active deformation as the fault zone developed (Adam et al., 2004; Frost et al., 2009). This information allows for a greater understanding of the spatial and temporal growth of the Champlain Thrust fault zone and will allow for a determination of which fault zone type model the Champlain Thrust fault zone is.

Five relative strain domains were defined based on macroscale observations of the number of deformation stages present, fold tightness, cleavage spacing, and the presence of ductile sheared fabrics (Table 3.2). Low strain is defined by containing: only stage 1 structures, continuous bedding planes, dispersed layer parallel veins, spaced dissolution cleavage planes greater than 4.5 cm apart, bedding parallel faults, and gentle to open folds of bedding, cleavage, and earlier faults with interlimb angles greater than 100° . Intermediate strain is defined by: zones containing two deformation stages—stage 2a structures that modify stage 1—continuous bedding, an increase in vein density, close to tight folds of bedding or earlier structures with interlimb angles $\sim 20^\circ$ – 40° , and an axial planar cleavage that is spaced less than 10 cm. High strain is defined by: zones containing three deformation stages—stage 2a structures that are modified by stage 2b which are modified by stage 3a—axial planar cleavage planes that are altered by later stages and spaced 0.5–5 cm apart, a predominant presence of veins, continuous bedding up to ~ 10 m, and close folds of bedding, cleavage, veins, and earlier faults with interlimb angles $\sim 50^\circ$ – 60° . Very high strain is defined by: zones of intensified cleavage that is spaced sub-millimeter, discontinuous bedding, and discontinuous veins. Finally, ultra-high strain is defined by: zones containing stage 3b structures, fault zone cleavage with less than 1-cm spacing, tight to close folds with interlimb angles $\sim 30^\circ$ – 50° , and the presence of sheared or boudinaged layers, mylonite, fault gouge, cataclasite, and sheath folds.

Using these various strain zone criteria, I mapped the distribution of these relative strain zones at each of the six field locations. Lessors Quarry, “the beam”, and the Ferrisburgh Quarry are dominated by low strain, constraining the upper boundary of the

Table 3.2: Defining characteristics and examples of relative strain zones within the Champlain Thrust fault zone

Strain Domain	Example	Deformation Stages	Cleavage Spacing	Fold Tightness	Other Characteristics
Ultra-High		Early and Late 3b	< 1 cm	30° - 50°	Sheared or boudinaged layers Mylonite Cataclasite Fault Gouge Sheath folds
Very-High		Deforms all older stages	< 1 mm	N/A	Discontinuous cleavage planes Discontinuous veins Extremely crushed and friable texture No measurable structures
High		Early and late stage 2a deformed by early and late stage 2b Early and late stage 2b deformed by early and late stage 3a	Modified Axial planar 0.5 - 5 cm	50° - 60°	Predominant presence of veins Continuous bedding and cleavage up to 10 meters
Intermediate		Late stage 1 deformed by early and late stage 2a	Axial planar sub-cm to 10 cm	20° - 40°	Continuous bedding Moderate presence of veins
Low		Early and late Stage 1	Dissolution ≥ 4.5 cm	> 100°	Continuous bedding planes Dispersed veins

low strain zone to 205–450 meters below the Champlain Thrust surface. The “flea market” and “the driveway” are dominated by intermediate strain, suggesting the thickness of this intermediate strain zone is between 187–430 meters. At Lone Rock Point, the distribution of strain is much more heterogeneous (Figure 3.28, 3.29). High strain is the dominant

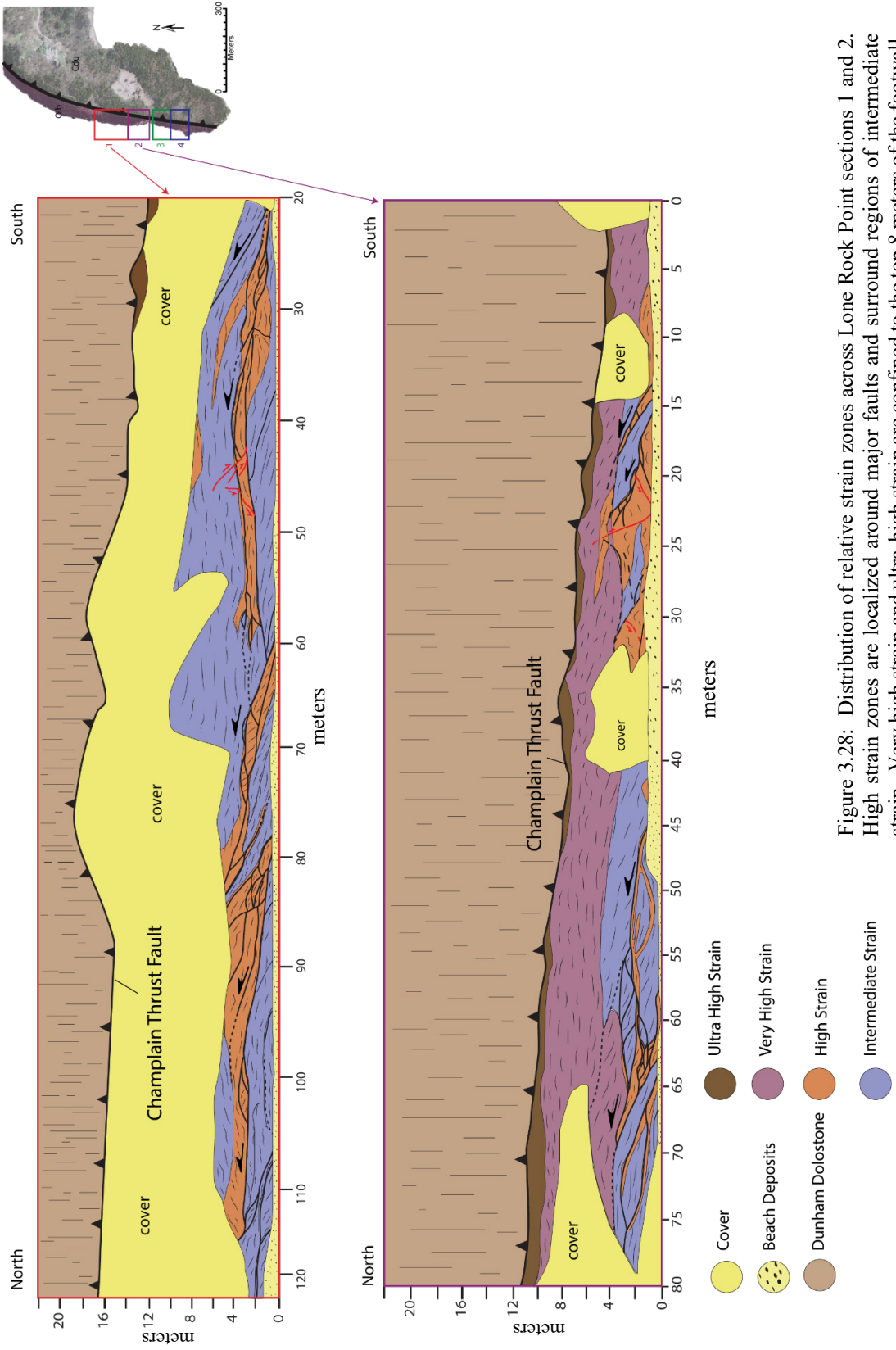
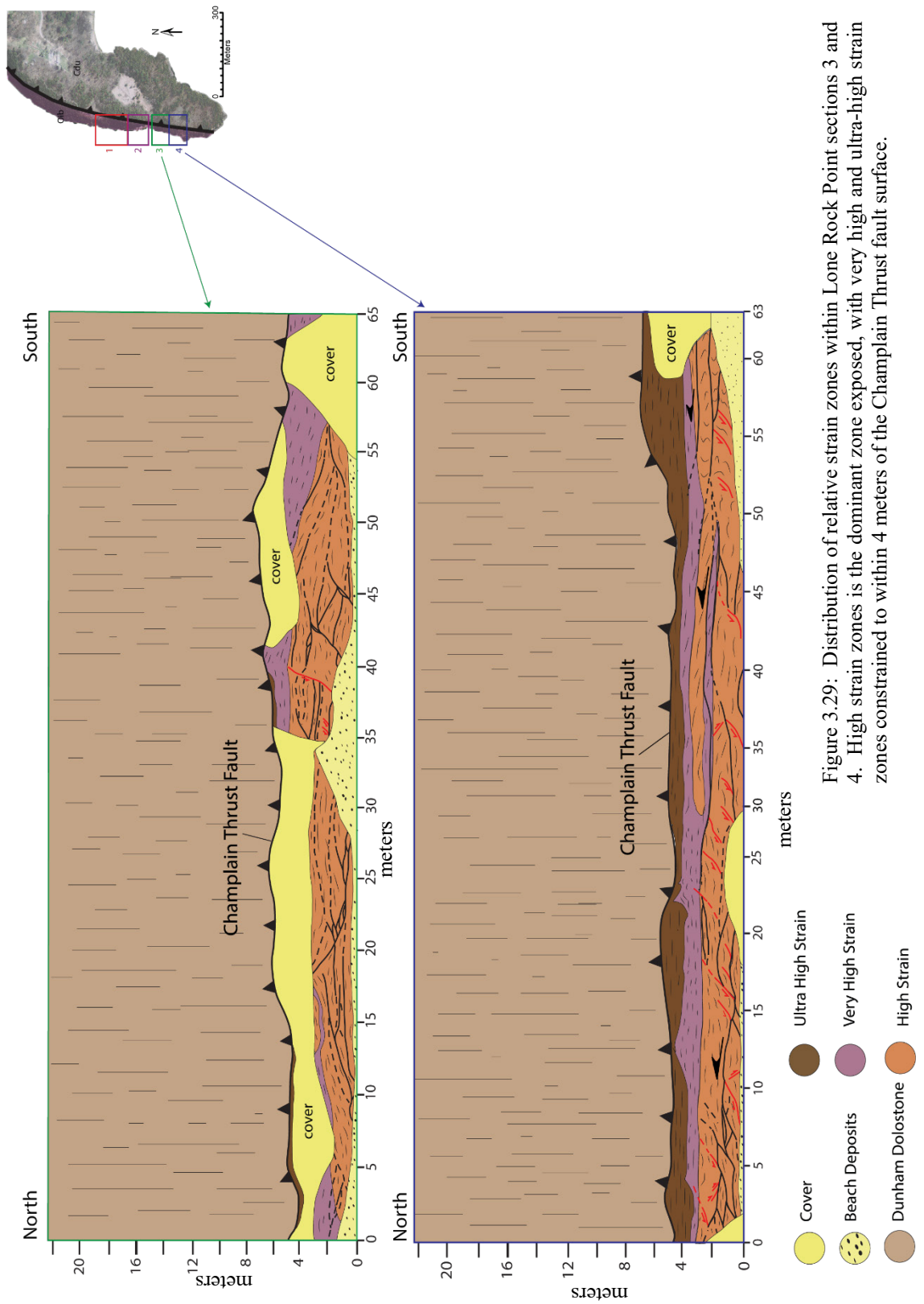


Figure 3.28: Distribution of relative strain zones across Lone Rock Point sections 1 and 2. High strain zones are localized around major faults and surround regions of intermediate strain. Very high strain and ultra-high strain are confined to the top 8 meters of the footwall.



strain zone observed and is between 14–176 meters thick. Very-high strain is focused to the cleavage intensification zone and can be up to 3 m thick. Ultra-high strain is always observed in contact with the Champlain Thrust fault surface and can be up to 2 m thick.

Within the Champlain Thrust fault zone relative strain increases from low to ultra-high strain from the protolith to the upper core (Figure 3.30). The changes in strain intensity also correlate to the relative age of structures preserved within each zone—low strain zones include the oldest structures, whereas ultra-high strain zones include the youngest. The changes in strain intensity also corresponds to a narrowing of strain zone thickness. These spatial and temporal changes of relative strain zones record a progressive localization of strain upwards in the footwall of the Champlain Thrust fault zone.

3.9 Conclusion

Through a structural analysis of the six field sites, I was able to determine three previously undescribed aspects of the Champlain Thrust fault zone which include: (1) the structural based characteristics of the fault core, damage zone, and protolith; (2) the spatial extent of the core, damage zone, and protolith boundaries within northwestern Vermont; and (3) the stages of development preserved within the fault zone. The final architecture of the Champlain Thrust fault zone documented here provides two new aspects of its evolution including: (1) the progressive localization of strain; and (2) the reactivation of the Champlain Thrust fault after localization had occurred. These aspects and the processes that drove them will be discussed in Chapter 4 and used to develop a model of the structural evolution of The Champlain Thrust fault zone.

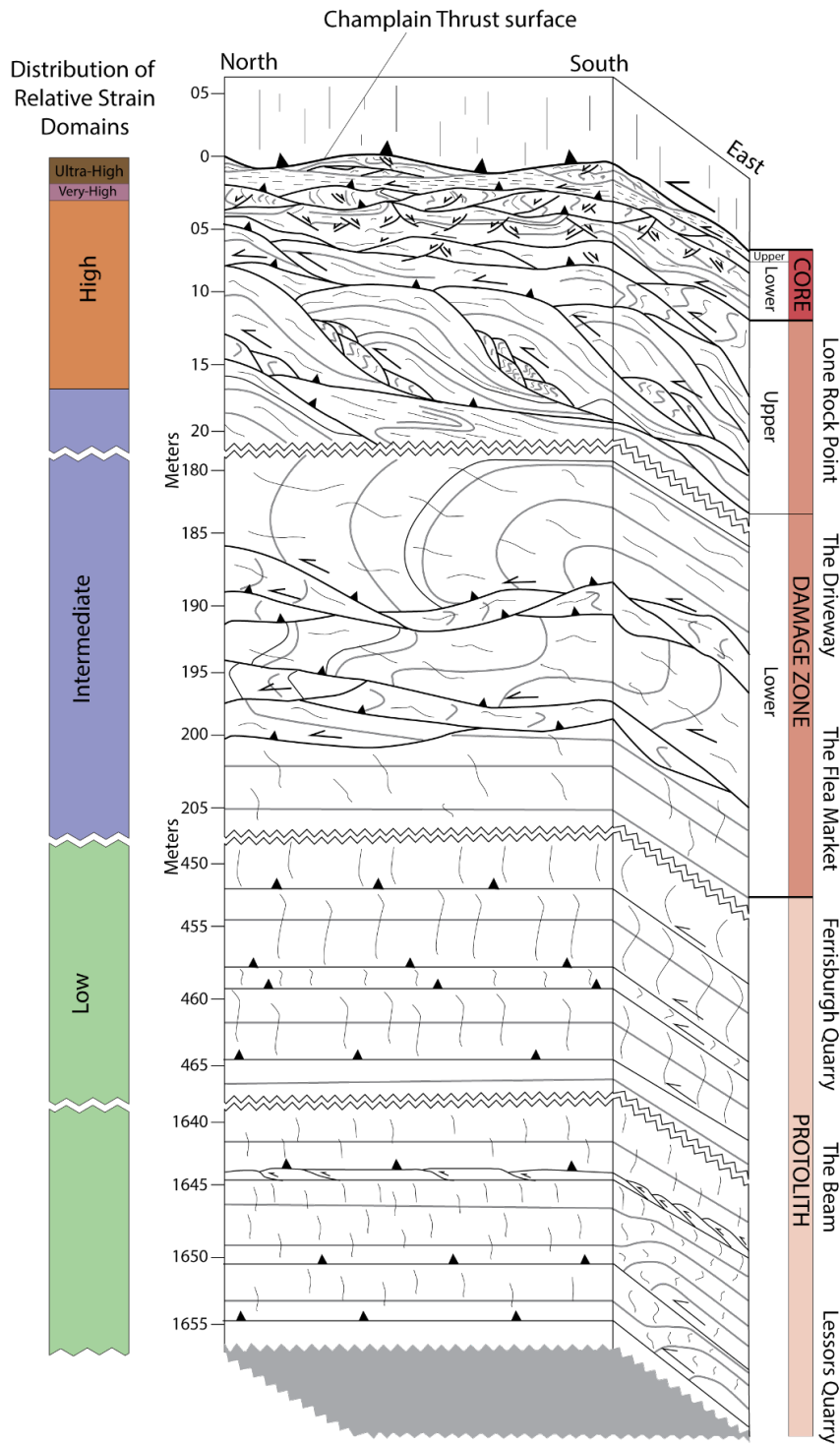


Figure 3.30: Composite diagram of Champlain Thrust fault zone with relative strain distribution. Strain increases as the Champlain Thrust is approached from the protolith in the footwall. Strain zone thickness decreases towards the fault surface indicating a progressive localization of strain.

CHAPTER 4: THE PROGRESSIVE EVOLUTION OF THE CHAMPLAIN THRUST FAULT ZONE

4.1 Introduction

Progressive evolution describes the repeated process of altering one type of pre-existing structure, or a zone of structures, through younger deformational events. Within the Champlain Thrust fault zone, structures of similar type, style, orientation, and relative age can be traced across the boundaries of the protolith, damage zone, and core. With each stage, older structures become increasingly altered, or completely overprinted, by younger structures as distance to the Champlain Thrust surface decreases. The two main aspects that record this progression within the Champlain Thrust fault zone are the localization of strain and the reactivation of the Champlain Thrust fault.

The progressive localization of strain within the fault zone is characterized by (1) a change in motion along minor faults from top-to-the-west, -northwest, -south, -north, and -southwest, and (2) a change in structural style from bedding-parallel faults with open folds, to duplex-forming thrust faults and close folds, to anastomosing faults and close to tight folds. The reactivation of the Champlain Thrust fault was determined from multiple slickenline orientations indicating a change in motion from top-to-the-west to top-to-the-south.

In the following sections, I strive to use the descriptions of fault architecture (Chapter 3) to interpret how the Champlain Thrust fault zone evolved through space and time. I will separately describe the various aspects of progressive deformation including: strain localization, changes in motion direction, changes in structural style, and fault

reactivation. I will briefly explore previously understood mechanisms that contribute the various aspects of progressive deformation in fault zones to determine which ones were likely contributing to the evolution of the Champlain Thrust fault zone. Although I separate these aspects to simplify my description of fault zone evolution, it is not assumed that these aspects of progressive deformation acted independently. Rather, the Champlain Thrust fault zone likely evolved as a dynamic system so that a change in one aspect influenced or reflected changes within another aspect.

4.2 Fault Zone Evolution

Within the footwall, deformation temporally and spatially localized towards the principal slip surface during fault zone evolution. The total thickness of the fault zone was developed during early evolutionary stages, whereas the active thickness of the fault zone diminished—or localized—over time. Of the four different types of shear zone models (Figure 1.2), the Champlain Thrust fault zone evolved as a modified type 2 shear zone (Figure 4.1).

Within a type 2 shear zone, strain localizes toward its center during time transgressive evolution (Hull, 1988; Vitale and Mazzoli, 2008; Fossen and Cavalcante, 2017). This localization of strain without the widening of the fault zone indicates strain softening (White et al., 1980). Several mechanisms have been described that can generate strain softening in a shear zone (Cobbold, 1977; White et al., 1980) and include grain-size reduction (Herwegh, 2005; Warren and Hirth, 2006; Platt, 2015), mineral recrystallization

Passchier and Trouw, 2005), preferred crystallographic orientation (Ji et al., 2004), shear heating (Platt, 2015), and the influence of fluids (Hirth and Tullis, 1992; Finch et al., 2016).

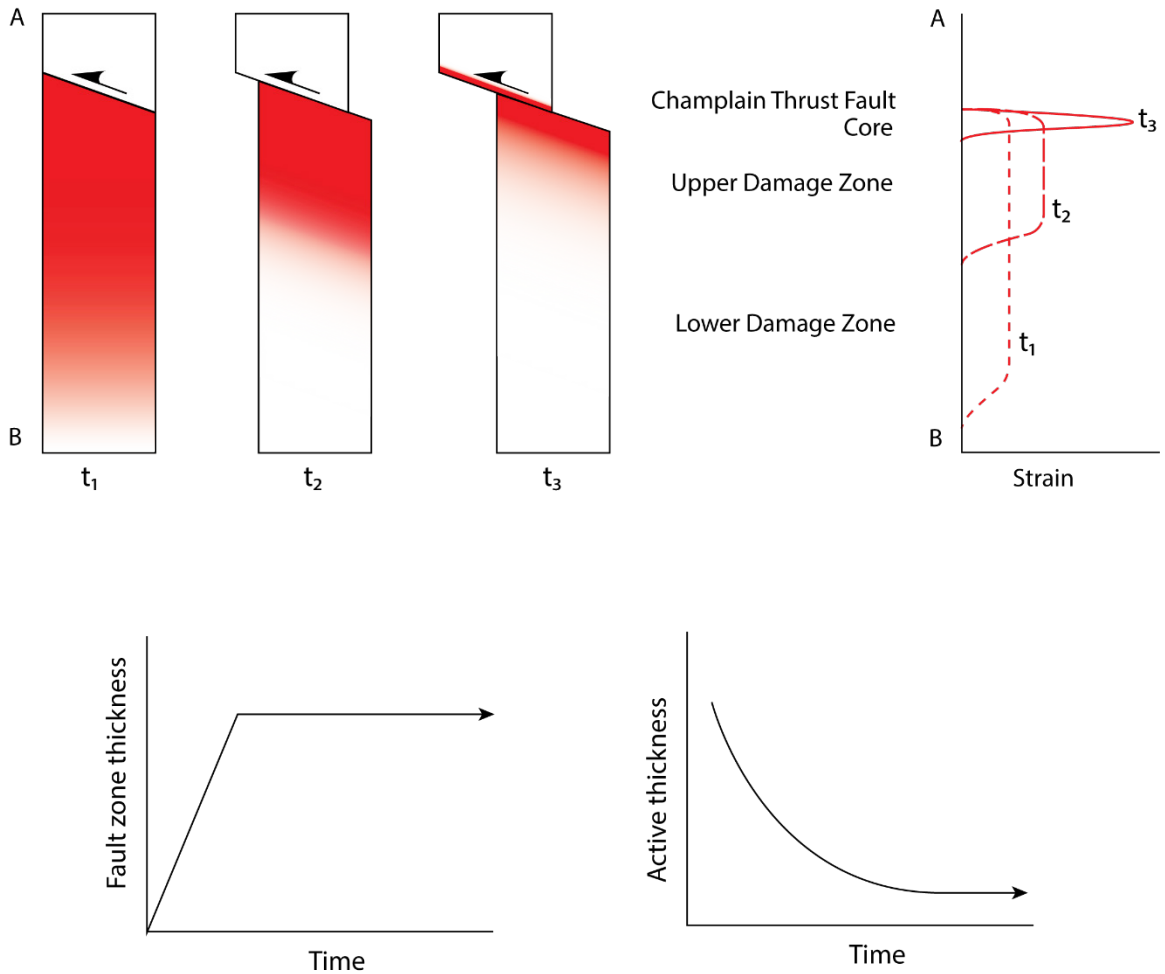


Figure 4.1: A modified model of the Champlain Thrust fault zone as a type 2 shear zone. This type of shear zone records a time progressive localization of strain towards the active slip surface. In this model for the Champlain Thrust, strain localizes into narrower zones over time and increases in intensity. Adapted from Fossen and Cavalcante (2017).

Most of these mechanisms are preserved at the microscale. For this project, I did not conduct a microstructural analysis, therefore cannot interpret how the Champlain Thrust fault zone evolved at the grain scale. However, I did observe calcite veins at each

of the of the six field sites and used an increase in apparent density as a criterion for determining relative strain zones (Table 3.2). Calcite veins, which are evidence for mobilized fluid flow through the fault zone, can further accommodate strain softening within a shear zone as they may be weaker and easier to deform than their surrounding rock (Davis et al., 2012). This increase in calcite vein density through the fault zone suggests that the Champlain Thrust fault zone evolved as a modified type 2 shear zone through the process of strain softening. Mechanisms preserved at the microscale are presumed to have played a critical role in strain softening as well, yet the microstructural investigation to determine which specific mechanism(s) is beyond the scope of this project.

The progressive strain localization that defines type 2 shear zones is characterized in the Champlain Thrust fault zone by (1) changes in slip direction along faults and (2) changes in structural style.

4.3 Change in Slip Direction Along Faults

Using slickenline orientations in conjunction with offset layers, asymmetric cleavages, shear bands, or slickensteps, I determined there are five distinct motion directions recorded throughout the Champlain Thrust fault zone (Figure 4.2). These changes in slip direction are recorded on faults of varying relative ages. Stage 1 thrust faults preserved in the protolith zone and the lower damage zone record a top-to-the-west slip. Stage 2a thrust faults preserved in the lower and upper damage zone record top-to-the-northwest slip. Stage 2b thrusts preserved within the upper damage zone also record top-to-the-northwest slip. Within the lower core, stage 3a thrust faults record top-to-the-

northwest slip and stage 3a normal faults record top-to-the-north and top-to-the-south slip. Within the upper core, stage 3b thrust faults record top-to-the-southwest slip. Finally, the Champlain Thrust records two distinct episodes of slip. The oldest recorded motion is top-to-the-west and the youngest is top-to-the-south (Figure 4.2).

Changes in slip direction along faults within a fault zone reflect changes in local principal stress orientations attributed to mechanical heterogeneities (Gudmundsson et al., 2010) or changes in elastic properties of deformed rocks (Faulkner, 2006). Mechanical heterogeneities are the result of a fault zone that contains multiple rock types with variable mechanical properties. Changes to lithology, bedding thickness, rock strength, and pre-existing structures such as older faults or cleavages all contribute to the mechanical heterogeneity within a fault zone. Gudmundsson (et al., 2010) described how mechanical heterogeneities within a fault zone allow for local principal stresses to differ in magnitude and orientation than regional stresses. Faulkner (et al., 2006) quantitatively modeled how local stresses within a damage zone will rotate as deformation changes the elastic properties of the material.

The Champlain Thrust fault zone incorporates different lithologies with varying bedding thickness and strength. Within this project, field sites attributed to the protolith were predominately exposures of centimeter thick beds of limestone, micrite, and some shale. Here, motion was predominately top-to-the-west. Exposures of the damage zone consisted of 0.5–35-centimeter-thick beds of alternating dolostone and calcareous shales. Here motion direction along faults was predominately top-to-the-west. Within the lower core, bedding consists of centimeter to millimeter thick beds of intensely cleaved

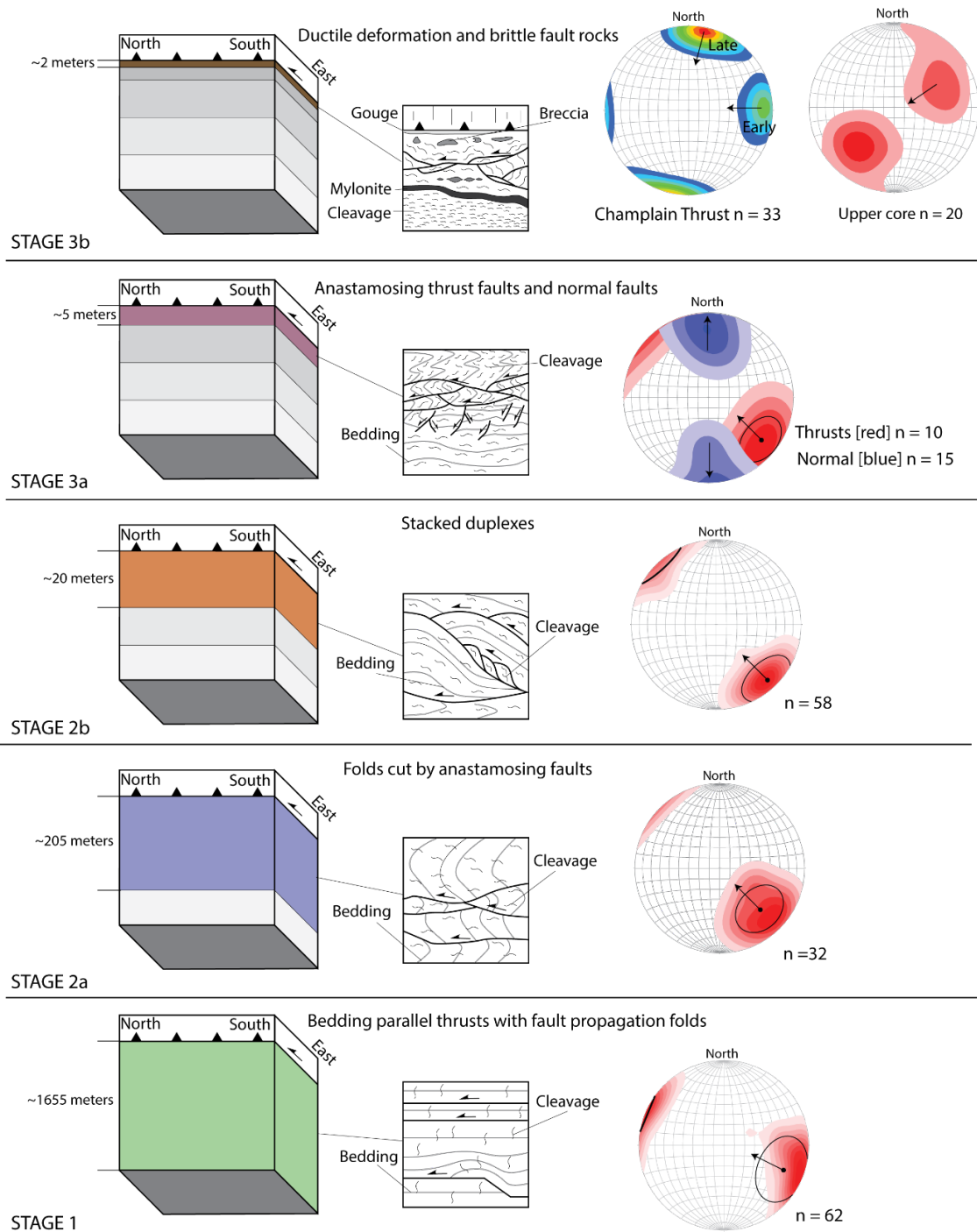


Figure 4.2: Simple models for each stage of Champlain Thrust fault zone evolution. Colors in block diagram indicate zone of active deformation and relative strain intensity at that stage. Center squares indicate type of structures that formed during that stage. Equal area lower hemisphere stereonets of slickenline orientations preserved on thrust faults (or normal where indicated). Contours are generated using Kamb contour method with intervals of 2. Mean vectors are plotted for slickenlines clusters with a 95% confidence interval.

calcareous shale, Here, motion on thrust faults was top-to-the-northwest and normal faults record motion top-to-the-north and -south. The upper core consists of centimeter to millimeter thick beds highly deformed phyllitic shales, mylonite, and breccia. Here motion on thrust faults is top-to-the-southwest.

Major changes in motion direction along faults within the fault is consistent with changes in rock type, bedding thickness, and increased deformation. This suggests that local stress orientations were likely to have rotated during the progressive evolution of the fault zone due to the mechanical heterogeneities and changes in deformation intensity from the protolith through the core. These rotations in local stress orientations could have caused slip to occur in varying direction along faults.

4.4 Change in Structural Style

The three most common classes of structures observed within the Champlain Thrust fault zone are dissolution cleavages, thrust faults, and folds of bedding and cleavage. As the Champlain Thrust surface is approached from the footwall protolith, faults change in style, folds become tighter, and cleavage spacing decreases (Figure 4.2). Within the protolith, thrust faults are bedding parallel and dissolution cleavages are perpendicular to bedding with spacing ≥ 4.5 cm. Folds preserved in the portions of the protolith analyzed for this project were localized fault-bend-folds with tightness $> 100^\circ$. In the damage zone, bedding parallel faults are incorporated into folds of bedding and cleavages and cut by younger through going faults. These folds, which have a tightness from 20° – 60° , generated a dominant axial planar cleavage that is spaced from 0.5–10 cm. Within the core, cleavage

becomes intensified to sub-millimeter spacing in the lower portions, whereas a fault zone cleavage with sub-centimeter spacing is preserved in the upper portions. Folds of bedding and cleavage have a tightness of 30° – 50° , and ductile structures such as mylonite, sheath folds, boudins, and fault gouge are present. Faults within the core vary from tightly spaced thrust faults to normal faults. Within the hanging wall, a < 1 -m thick damage zone is present and contains minor faults that cut veins and foliations within the rock. The remainder of the hanging wall consists of vertical fractures with no apparent offset—a structural style unique only to the hanging wall.

Previous studies have determined that in general, the heterogeneity of structures within a fault zone can be attributed to pre-existing structures, changes in pressure and temperature conditions, changes in stress field orientations, interaction or linkage of structures during development, and changes in rock type throughout the fault zone (Wibberley et al., 2008). Furthermore, complexity in fault zone architecture has also been attributed to the rheologic differences and mechanical anisotropy of multilayered rock types within the fault zone (Carreras et al., 2013). Mechanical anisotropy is defined as the ratio of a rock's ability to resist compression to the rock's ability to resist shear (Biot, 1965). Factors that attribute to mechanical anisotropy include bedding planes, schistosity, and cleavage formation (Carreras et al., 2013).

As with changes in motion direction along faults, changes in structural style within the Champlain Thrust fault zone occur in conjunction with changes in lithology (Figure 4.2). The thicker bedded limestones of the protolith preserve bedding parallel faults and open folds of bedding and cleavages, whereas the thinner bedded calcareous shales of the

damage zone preserve anastomosing thrust faults and close folds of bedding and cleavages. The hanging wall observed at Lone Rock Point, which consist of massive bedded dolostone, consists primarily of vertical fractures with no observable faults or folds. This indicates that rock strength played a key role in how structures developed within the Champlain Thrust fault zone. The thicker bedded and rheologically stronger hanging wall unit did not deform as easily, nor in the same style, as the thinner bedded and weaker shales and limestones within the footwall.

Within the Champlain Thrust fault zone, the variability of bedding thickness not only influences the strength of the rock, but also contributes to mechanical anisotropies. Within the protolith, bed thickness ranges of ~8 to tens of cm thick. Within the lower damage zone, beds range from 0.5–35 cm thick, whereas within the upper damage zone, beds are <10 centimeters thick. Bedding thickness within the core ranges from centimeter to millimeter scale, whereas bedding within the hanging wall is massive. This decrease in bedding thickness as the Champlain Thrust fault surface is approached through the footwall correlates to an increase in mechanical anisotropies within the upper portions of the fault zone.

Another contributing factor to the increase in mechanical anisotropy is dissolution cleavages (Table 3.2). Within the protolith, dissolution cleavages are discontinuous and spaced ≥ 4.5 centimeters apart. These cleavages are also oriented perpendicular to bedding and thrust faults within the protolith. In the lower damage zone, cleavage is axial planar to large scaled folds with spacing ranging from sub-centimeter up to 10 cm apart. In the upper damage zone, cleavages are axial planar to early folds and modified by younger folds

and faults. Spacing of these modified cleavages decrease to 0.5–5 cm apart. Finally, within the lower core, cleavage is intensified to sub-millimeter spacing, and in the upper core, cleavage is sub-centimeter spaced. This progressive change in cleavage spacing throughout the fault zone allows of greater mechanical anisotropy in the upper portions of the fault zone.

If regional pressure and temperature conditions remained constant throughout the development of the Champlain Thrust fault zone, changes in structural style can be attributed to changes in rock strength and the progressive increase in mechanical anisotropy. Increases in mechanical anisotropy is attributed to the changes in bedding thickness and cleavage spacing throughout the fault zone.

In summary, strain localized within the Champlain Thrust fault zone because of strain softening. Characterizing this strain localization at the macroscale are changes in motion direction along faults and changes in structural style. The changes in motion directions can be attributed to local stress rotation influenced by changes in rock type, bedding thickness, and increased deformation. Changes in structural style can be attributed to changes in rock strength, bedding thickness, and cleavage spacing (Wojtal and Mitra, 1986). Combined, this indicates that the heterogeneous layering of rocks within the fault zone influence the localization of strain within the Champlain Thrust fault zone towards the principal slip surface.

4.5 Champlain Thrust Fault Reactivation

Holdsworth (et al., 1997) defined fault reactivation as separate motion events along a pre-existing fault plane with intervals of inactivity greater than 1 Ma. For this project, fault reactivation is defined as a slip surface that accommodated active slip more than once and in more than one direction. This applies directly to the Champlain Thrust fault as two separate sets of superimposed slickenlines, each recording a different direction of slip, are preserved on the principal slip surface (Figure 4.2). The oldest set of slickenlines on the Champlain Thrust surface indicates that motion on the fault was top-to-the-west, whereas the youngest set of slickenlines, preserved a few centimeters away from the older, indicate that motion was also top-to-the-south (Figure 3.25).

The cause of this change in motion direction along the Champlain Thrust is unknown. Here I present three hypotheses that could explain this change in motion direction during fault reactivation.

First, this reactivation could represent deformation associated with younger orogenic events such as the Salinic (ca. 450–410 Ma) or the Acadian (ca. 380–370 Ma). The Salinic orogeny defines the docking of Ganderia against Laurentia, whereas the Acadian orogeny marks the accretion of Avalonia onto the composite Laurentian margin (Tremblay and Pinet, 2016). Deformation associated with both orogenic events migrated through New England and southeast Canada towards the north west (Bradley et al., 2000; Tremblay and Pinet, 2016). In Vermont, Salinic deformation is attributed to large backthrusts and later normal faults in the Green Mountain belt, and Acadian deformation is attributed to polyphase folding within the Connecticut Valley trough and the formation

of the Green Mountain anticlinorium (Tremblay and Pinet, 1994). Due to no apparent or observable structures associated with these younger orogenic events deforming the Champlain Thrust fault surface within this project's field locations, I propose that the reactivation recorded on the Champlain Thrust was during the Taconic orogeny. Although the history of motion recorded on the Champlain Thrust is complex, multiple orogenic deformation is not needed to generate such complexities.

Second, the reactivation on the Champlain Thrust and the change in hanging wall units along strike of the fault may indicate the presence of a lateral ramp. A lateral ramp is defined as an inclined portion of the fault plane that cuts beds within the footwall and has a strike orientation parallel to thrust transport direction (Butler, 1982) (Figure 4.3). Due to the parallel orientation of the ramp to the thrust fault, strike-slip displacement becomes dominant (Boyer and Elliott, 1982), yet the motion direction does not change (Figure 4.3). If the Champlain Thrust fault interacted with a lateral ramp, then slickenline orientations should be consistent, yet this is not the case (Figure 4.2). The presence of a lateral ramp may explain the change in the Champlain Thrust hanging wall lithology from Dunham Dolostone in the north to the stratigraphically higher Monkton Formation in the south. However, a simple interaction with a lateral ramp does not include the change of motion direction that occurred along the Champlain Thrust surface (Figure 4.3). Therefore, I suggest a lateral ramp did not cause the reactivation along the Champlain Thrust surface.

Finally, this reactivation could represent the complexities associated with basin inversion. Basin inversion is defined as the shortening of extensional basins (Bonini et al.,

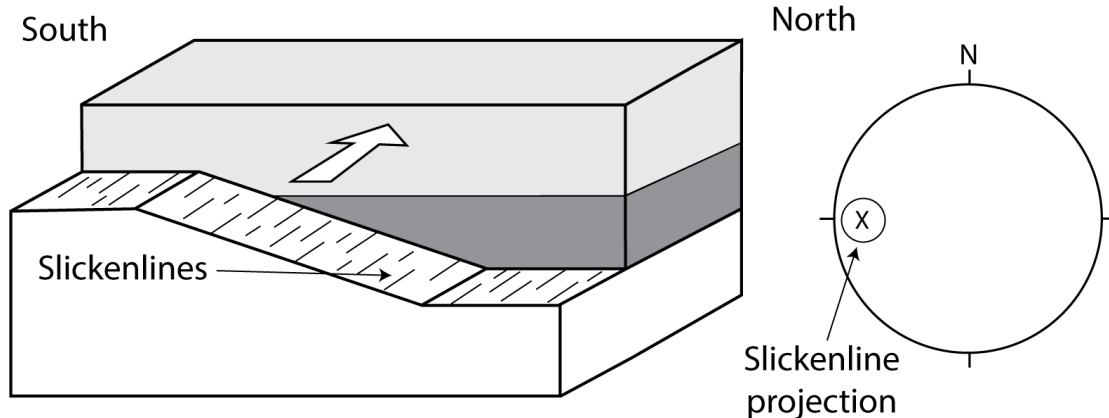


Figure 4.3: A block diagram of a lateral ramp along a thrust fault. A lateral ramp is defined as a portion of a fault plane that cuts bedding and has a strike direction parallel to transport direction (Boyer, 1982). Along a lateral ramp, faults exhibit strike-slip components, yet slickenlines preserved on the fault plane should be a consistent orientation. Slickenlines along the Champlain Thrust fault record motion in two distinct orientations, therefore suggesting reactivation was not due to a lateral ramp.

2012) and contribute to a wide variety of internal deformation patterns during shortening (Turner and Williams, 2004; Bonini et al., 2012). Through the results of sandbox experiments, Ventisette et al. (2006) describes that variations in deformation during shortening is directly controlled and influenced by pre-existing extensional structures. Furthermore, Ventisette et al. (2006) also modeled that thrust faulting can occur with variable displacement patterns when compression is oriented obliquely to extensional structures.

Although most basin inversion models indicate the direct reactivation of normal faults as thrust faults—also known as positive inversion (Cooper and Williams, 1989)—some models indicate that thrust faults can propagate over or cut through pre-existing normal faults (Figure 4.4a). Thrust faults that develop in the overriding sedimentary cover of extensional basins may reflect kinematic changes that are controlled by pre-existing

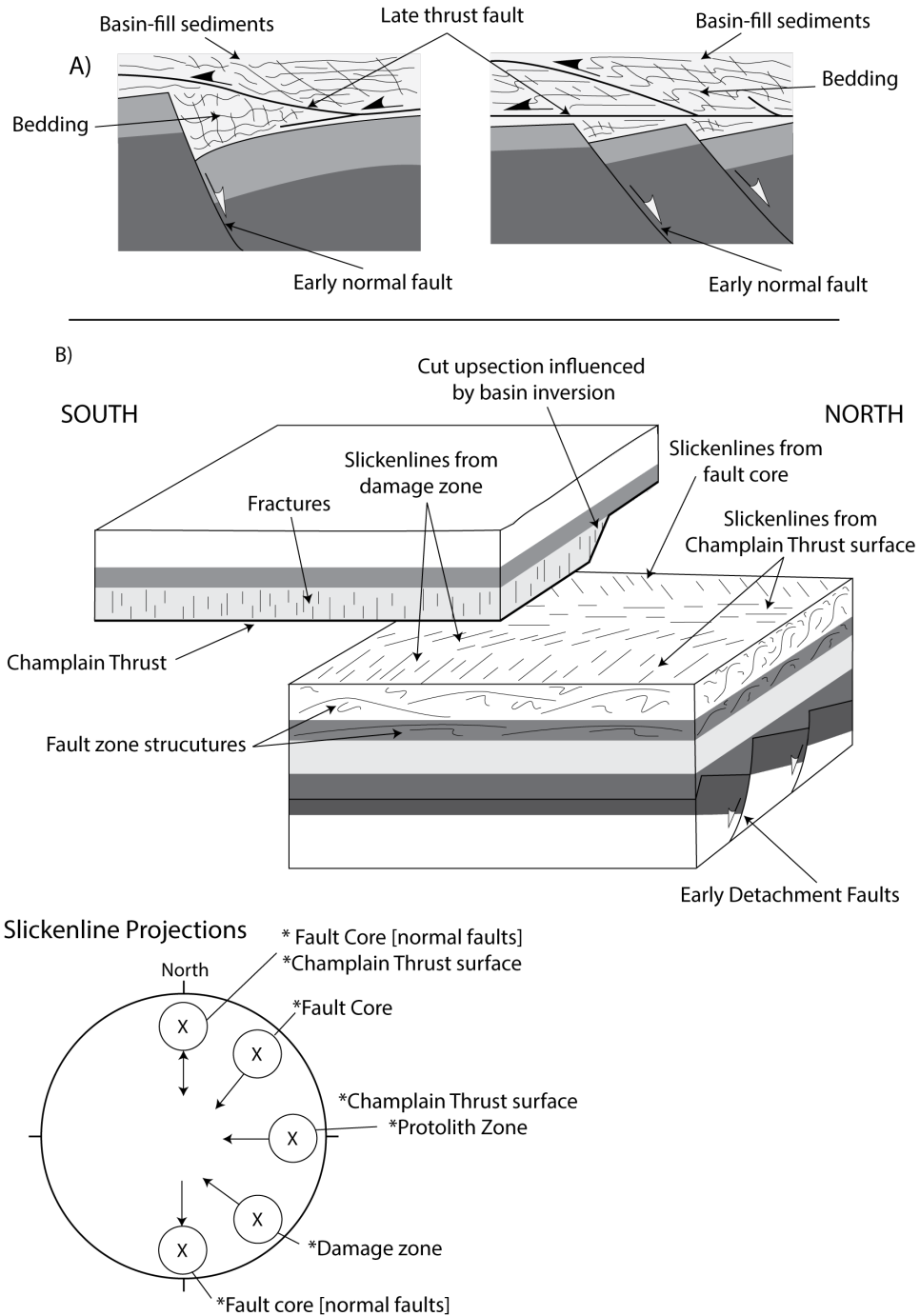


Figure 4.4: A) During basin inversion, newly formed thrust faults can propagate through rift-basin sediments over pre-existing extensional structures. Both images depict complex deformation within the thrust fault's footwall and hanging wall. Modified from Bonini et al. (2012). B) Block diagram of proposed Champlain Thrust evolution as a result of basin inversion. Reactivation of the Champlain Thrust fault surface, and heterogenous motion recorded in the fault zone, was likely influenced by buried pre-existing extensional structures. Slickenline projections mimic orientations from measured data.

extensional structures (Scisciani, 2009). I suggest that this model of kinematic control that pre-existing extensional features exert on newly formed thrust faults that propagate through sedimentary cover of rift basin be applied to the Champlain Thrust fault.

The Neoproterozoic–Cambrian sedimentary rocks associated with the Champlain Thrust fault were deposited in pre-Taconic rift-basins (Figure 4.4b). These basins formed through low-angle detachment faults associated with Laurentia-Rodinia rifting (Allen et al., 2009). Although there is no direct evidence that the Champlain Thrust fault is a reactivated pre-existing normal fault, the change in motion direction recorded on the Champlain Thrust surface is likely influenced by buried extensional structures. This hypothesis of basin inversion is supported not only by the multiple motions recorded on the fault surface, but also the complex changes in structural style and motion directions within the fault zone, and the change in hanging wall units (Figure 4.4b).

This process of thrust fault interaction with an unknown buried structure has been suggested to have occurred on the Morgan's Corner Fault in the Quebec Appalachians (Sejourne and Malo, 2007). The Morgan's Corner Fault is the eastward bounding fault to the Saint-Dominique carbonate slice in southeast Quebec. The Saint-Dominique slice is bound to the west by the Champlain Thrust fault (known as Logan's Line in Quebec) (Sejourne and Malo, 2007). Within the Morgan's Corner fault zone Sejourne and Malo (2007) document three different deformation stages that also record changes in motion including: (1) dextral strike-slip faults in the footwall; (2) top-to-the-northwest thrusting of the main fault; and (3) sinistral reactivation of the thrust fault. Because of these kinematic changes, the Morgan's Corner fault is interpreted to have developed over an oblique ramp

that greatly influenced the geometry of structures within its fault zone (Sejourne and Malo, 2007). Sejourne and Malo (2007) also note that seismic time-structures built by SOQUIP (1982, 1984) indicate the presence of a possible normal fault extending from underlying Grenvillian basement into the autochthonous sedimentary cover.

The data within this project confirm the reactivation of the Champlain Thrust, and suggest that the change in motion recorded along the fault surface was influenced by a buried pre-existing extensional structure. The complexity of motion recorded on the Champlain Thrust surface and within the fault zone suggest oblique compression during basin inversion.

CHAPTER 5: SUMMARY AND FUTURE WORK

5.1 Introduction

The results of this study demonstrate how deformation is accommodated at the forefront of a fold-and-thrust belt. I utilized fault, fold, and cleavage plane data collected from six separate exposures of the Champlain Thrust fault footwall to define and evaluate the architecture of the core, damage zone, and protolith of the Champlain Thrust fault zone. I also used this data to determine the progressive spatial and temporal evolution of this fault zone in northwestern Vermont. This section summarizes several key discoveries made regarding the Champlain Thrust fault zone architecture and evolution, and concludes with suggestions for future research regarding the fault zone

5.2 Fault Zone Architecture Summary

The architecture of the Champlain Thrust fault zone is asymmetric across the principal slip surface (Figure 3.27). The deformation and development of the fault zone occurred predominately within the carbonate rich Ordovician units of the footwall. The internal boundaries of the fault zone were determined using (1) changes in the relative age of faults, folds, and cleavages, (2) changes in structural style of faults, folds and cleavages, and, (3) the intensity of strain preserved within each region.

The fault zone core records the youngest evolutionary stage. The Champlain Thrust fault surface is the youngest preserved feature of the fault zone as it cuts all older structures within its footwall. Stage 3a and 3b faults within the core are observed as anastomosing thrust faults and normal faults. Variations of cleavage within the core range from altered

axial planar cleavage, to a zone of very strong cleavage, to localized fault zone cleavage. The core also includes ductile structures such as mylonite, boudinaged layers, and sheath folds. The core, which is dominated by ultra-high and very high strain zones, can be subdivided into upper and lower portions with a combined thickness of ~8 meters.

The damage zone contains the second youngest stage of faults and folds—stage 2a and 2b—which vary in style from duplex forming faults and associated folds to anastomosing faults that cut inclined folds. Cleavage within the damage zone is axial planar to the inclined folds and is deformed by thrust duplexes. The damage zone can also be subdivided into upper and lower portions with a combined thickness of ~197 to 430 m.

The protolith zone contains the oldest observed stage of faults and associated folds—stage 1. Faults within the protolith are bedding parallel that generated localized fault-bend-folds. Cleavage within the protolith are weak dissolution cleavages that are normal to bedding planes. The protolith is dominated by low relative strain with its upper boundary constrained to ~205–450 m below the Champlain Thrust fault surface.

5.3 Fault Zone Evolution Summary

The Champlain Thrust fault zone evolved as a modified type 2 shear zone (Figure 4.1). Type 2 shear zones record a progressive localization of strain toward the slip surface with the zone of active deformation narrowing over time (Fossen and Cavalcante, 2017). The Champlain Thrust fault zone records the progressive localization of strain towards the principal slip surface through time. However, strain was predominately accommodated within the footwall, therefore making the Champlain Thrust fault zone a modified type 2

shear zone (Figure 4.1). I determined the presence of five relative strain zones based on the number of deformational stages preserved, cleavage spacing, and fold tightness (Table 3.2). The progressive localization of strain zones was determined by the spatial narrowing of the strain zone through the fault zone (Figure 3.30).

The progressive localization of strain within the Champlain Thrust fault zone was determined to be the result of strain softening during fault zone development. Strain softening was interpreted by the apparent increase in calcite vein density moving towards the fault surface from the protolith. The apparent increase in calcite vein density towards the fault surface indicates the increase in fluid flow towards the fault surface. Calcite veins can may have accommodated deformation easier than their surrounding host rock (Davis, 2012). This process was one of the mechanisms that drove strain softening within the fault zone. The progressive localization of strain was characterized by changes in motion direction along faults within the fault zone and changes in structural style.

The recorded direction of motion on faults changed from: (1) top-to-the-west in the protolith; (2) to top-to-the-northwest in the damage zone and lower core; (3) to top-to-the-north and -south within the core; (4) to top-to-the-southwest in the upper core; and (5) to top-to-the-west then top-to-the-south along the Champlain Thrust surface (Figure 4.2). These changes in motion recorded along faults was the result of local changes in principal stress orientation and fault reactivation. Changes in rock type, rock strength, bedding thickness, and increased deformation all contribute to mechanical heterogeneities within the fault zone and can contribute to the rotation of local principal stress orientations during active deformation. The reactivation of the Champlain Thrust surface, specifically

reactivation with a change in motion direction, also contributed to changes in motion within the fault zone.

The style of cleavage, folds, and faults also change as the Champlain Thrust fault is approached from the protolith zone within the footwall (Figure 4.2). These changes in structural style can be attributed to changes in rheologic differences throughout the fault zone and the progressive increase in mechanical anisotropy. Rheologic differences are evidenced by the changes in rock type from limestones in portions of the protolith, to carbonate-rich shales of the damage zone and core, to dolostones in the hanging wall. The increases in mechanical anisotropy is attributed to: (1) the changes in bedding thickness from tens of centimeters in the protolith and lower damage zone, to <10 centimeters in the upper damage zone, to sub-centimeters in the core, and to massive within the hanging wall; and (2) changes in cleavage spacing throughout the fault zone from ≥ 4.5 centimeters within portions of the protolith, to <10 centimeters within the damage zone, to sub-centimeter within the core.

Finally, the Champlain Thrust fault surface records a reactivation with a change in slip direction from an early top-to-the-west to a later top-to-the-south direction (Figure 4.2). This reactivation likely occurred during the Taconic orogeny as there is no apparent deformation associated with later orogenic events deforming the Champlain Thrust fault surface. This reactivation of the Champlain Thrust fault was the likely response to interaction with a pre-existing structure during oblique basin inversion (Figure 4.4b). Kinematic complexities commonly occur on thrust faults that propagate through rift-basin sediments and over buried extensional structures (Figure 4.4a) (Bonini et al., 2012). The

Champlain Valley and Green Mountain bedrock belts in Vermont are both associated with the Champlain Thrust and fault and deposited in rift basins along the passive Laurentian margin (Kim et al., 2011). The reactivation of the Champlain Thrust fault was likely influenced by a buried pre-existing extensional structure as it propagated through the sedimentary cover of a rift basin. The presence of a buried fault influencing the kinematics of an overriding thrust fault was reported along the Morgan's Corner Fault within the southern Quebec Appalachians (Sejourne and Malo, 2007).

5.4 Future Work

This project and the results presented within have been a continuation of previous studies on the Champlain Thrust fault and the preserved deformation associated with its fault zone (Keith, 1923; Keith, 1932; Clark, 1934; Cady, 1945; Welby, 1961; Stanley and Sarkisian, 1972; Stanley, 1987; Stanley, 1990; Kim et al., 2011; Mundy et al., 2016). Though I was able to determine characteristics regarding its architecture and temporal evolution, there is still much work to be done to understand the mechanisms that drove the progressive deformation and fault reactivation within this fault zone. Here, I propose where future work should be focused to increase the understanding of the Champlain Thrust fault zone.

The most intriguing mystery associated with the Champlain Thrust fault zone is the cause of reactivation along the fault surface. I suggested that this reactivation was a result of the fault surface propagating over a pre-existing structure during oblique basin inversion. I would suggest a detailed transect of all exposures of the Champlain Thrust surface to

determine if evidence for reactivation is preserved elsewhere apart from Lone Rock Point. I would also suggest the Champlain Thrust fault surface, and the fault core be dated for absolute dates. If the Champlain Thrust fault or core preserve dates younger than the Taconic orogeny, then reactivation can then be suggested to have occurred as a result of younger mountain building events.

Secondly, I would suggest a microstructural analysis of each relative strain zone as well as each evolutionary stage. This would allow for a greater understanding of the fault zone's temporal and structural changes at the microscale. This analysis would also provide information regarding grain-scale deformation mechanisms that aided in fault zone development. If recrystallization is preserved, this analysis may provide information regarding pressure and temperature conditions during strain localization.

I would also suggest a detailed study regarding the distribution and chemistry of calcite veins preserved throughout the fault zone. In this study, I suggest that the increase in calcite veins was a mechanism that drove strain softening during fault zone growth. I suggest that the chemistry of these calcite veins be analyzed to determine if they were precipitated from fluids internal to the fault zone or external.

Finally, I would suggest a structural analysis of other Taconic thrust faults that are to the east of the Champlain Thrust (e.g. the Hinesburg Thrust and Underhill Thrusts). Comparing fault zone architecture and evolution of other Taconic thrust faults with that of the Champlain Thrust may provide greater insight to progressive deformation at the tectonic scale.

COMPREHENSIVE BIBLIOGRAPHY

- Adam, J., Urai, J.L., Wieneke, B., Oncken, O., Pfeiffer, K., Kukowski, N., Lohrmann, J., Hoth, S., Van Der Zee, W. and Schmatz, J., 2005. Shear localization and strain distribution during tectonic faulting—New insights from granular-flow experiments and high-resolution optical image correlation techniques. *Journal of Structural Geology*, 27(2), pp.283-301.
- Allen, J.S., Thomas, W.A. and Lavoie, D., 2009. Stratigraphy and structure of the Laurentian rifted margin in the northern Appalachians: A low-angle detachment rift system. *Geology*, 37(4), pp.335-338.
- Allen, J.S., Thomas, W.A., Lavoie, D., Tollio, R.P., Bartholomew, M.J., Hibbard, J.P. and Karabinos, P.M., 2010. The Laurentian margin of northeastern North America. From Rodinia to Pangea: the lithotectonic record of the Appalachian Region. Edited by R. Tollo, J. Bartholomew, J. Hibbard, and P. Karabinos. *Geological Society of America Memoir*, 206, pp.71-90.
- Alvarez, W., Engelder, T. and Geiser, P.A., 1978. Classification of solution cleavage in pelagic limestones. *Geology*, 6(5), pp.263-266.
- Anderson, E. I., and Bakker, M., 2008. Groundwater flow through anisotropic fault zones in multiaquifer systems. *Water resources research*, 44(11).
- Bastesen, E. and Braathen, A., 2010. Extensional faults in fine grained carbonates—analysis of fault core lithology and thickness—displacement relationships. *Journal of Structural Geology*, 32(11), pp.1609-1628.
- Bense, V. F., Gleeson, T., Loveless, S.E., Bour, O., Scibek, J., 2013. Fault zone hydrogeology. *Earth Science Reviews*. 127, 171-192.
- Bense, V. F., Pearson, M., Chaundhary, K., You, Y., Cremer, N., Simon, S., 2008. Thermal anomalies as indicator of preferential flow along faults in an unconsolidated sedimentary aquifer system. *Geophysical Research Letters*. 35, L24406.
- Berg, S.S. and Skar, T., 2005. Controls on damage zone asymmetry of a normal fault zone: outcrop analyses of a segment of the Moab fault, SE Utah. *Journal of Structural Geology*, 27(10), pp.1803-1822.
- Bonini, M., Sani, F. and Antonielli, B., 2012. Basin inversion and contractional reactivation of inherited normal faults: A review based on previous and new experimental models. *Tectonophysics*, 522, pp.55-88.
- Boyer, S.E. and Elliott, D., 1982. Thrust systems. *Aapg Bulletin*, 66(9), pp.1196-1230.
- Bradley, D.C., 2000. Migration of the Acadian orogen and foreland basin across the northern Appalachians of Maine and adjacent areas (No. 1624). US Department of the Interior, US Geological Survey.
- Brandes, C. and Tanner, D.C., 2014. Fault-related folding: A review of kinematic models and their application. *Earth-Science Reviews*, 138, pp.352-370.
- Butler, R.W., 1982. The terminology of structures in thrust belts. *Journal of structural Geology*, 4(3), pp.239-245.
- Cady, W.M., 1945. Stratigraphy and structure of west-central Vermont. *Geological Society of America Bulletin*, 56(5), pp.515-588.

- Caine, J.S., Evans, J.P. and Forster, C.B., 1996. Fault zone architecture and permeability structure. *Geology*, 24(11), pp.1025-1028.
- Caine, J.S., Ridley, J. and Wessel, Z.R., 2010. To reactivate or not to reactivate—Nature and varied behavior of structural inheritance in the Proterozoic basement of the eastern Colorado Mineral Belt over 1.7 billion years of Earth history. *Field Guides*, 18, pp.119-140.
- Calamita, F., Di Domenica, A. and Pace, P., 2018. Macro-and meso-scale structural criteria for identifying pre-thrusting normal faults within foreland fold-and-thrust belts: Insights from the Central-Northern Apennines (Italy). *Terra Nova*, 30(1), pp.50-62.
- Carreras, J., Cosgrove, J.W. and Druguet, E., 2013. Strain partitioning in banded and/or anisotropic rocks: Implications for inferring tectonic regimes. *Journal of Structural Geology*, 50, pp.7-21.
- Chester, F.M. and Logan, J.M., 1986. Implications for mechanical properties of brittle faults from observations of the Punchbowl fault zone, California. *Pure and Applied Geophysics*, 124(1-2), pp.79-106.
- Choi, J.H., Edwards, P., Ko, K. and Kim, Y.S., 2016. Definition and classification of fault damage zones: A review and a new methodological approach. *Earth-Science Reviews*, 152, pp.70-87.
- Clark, T.H., 1934. Structure and stratigraphy of southern Quebec. *Bulletin of the Geological Society of America*, 45(1), pp.1-20.
- Clausen, J.A., Gabrielsen, R.H., Johnsen, E. and Korstgård, J.A., 2003. Fault architecture and clay smear distribution. Examples from field studies and drained ring-shear experiments. *Norwegian Journal of Geology/Norsk Geologisk Forening*, 83(2).
- Cobbold, P.R., 1977. DESCRIPTION AND ORIGIN OF BANDED DEFORMATION STRUCTURES. 2. RHEOLOGY AND GROWTH OF BANDED PERTURBATIONS. *Canadian Journal of Earth Sciences*, 14(11), pp.2510-2523.
- Cooper, M.A., Williams, G.D., De Graciansky, P.C., Murphy, R.W., Needham, T., De Paor, D., Stoneley, R., Todd, S.P., Turner, J.P. and Ziegler, P.A., 1989. Inversion tectonics—a discussion. *Geological Society, London, Special Publications*, 44(1), pp.335-347.
- Davis, G.H. and Reynolds, S.J., 2012. Structural geology of rocks and regions. In *Structural geology of rocks and regions*. 3rd edition. Wiley.
- De Souza, S., Tremblay, A. and Ruffet, G., 2014. Taconian orogenesis, sedimentation and magmatism in the southern Quebec–northern Vermont Appalachians: Stratigraphic and detrital mineral record of Iapetan suturing. *American journal of science*, 314(7), pp.1065-1103.
- Del Ventisette, C., Montanari, D., Sani, F. and Bonini, M., 2006. Basin inversion and fault reactivation in laboratory experiments. *Journal of Structural Geology*, 28(11), pp.2067-2083.
- Del Ventisette, C., Montanari, D., Sani, F. and Bonini, M., 2006. Basin inversion and fault reactivation in laboratory experiments. *Journal of Structural Geology*, 28(11), pp.2067-2083.

- Dor, O., Ben-Zion, Y., Rockwell, T.K. and Brune, J., 2006. Pulverized rocks in the Mojave section of the San Andreas Fault Zone. *Earth and Planetary Science Letters*, 245(3-4), pp.642-654.
- Dorsey, R.L., Agnew, P.C., Carter, C.M., Rosencrantz, E.J., and Stanley, R.S., 1983, Bedrock geology of the Milton quadrangle, northwestern Vermont: Vermont Geological Survey Special Bulletin No. 3, p. 14.
- Eichhubl, P., Bole, J., 2000. Focused fluid flow along faults in the Monterey Formation, coastal California. *GSA Bulletin*. 11, 1167-1679.
- Ellsworth, W.L., 2013. Injection-induced earthquakes. *Science*, 341(6142), p.1225942.
- Faulkner, D.R., Jackson, C.A.L., Lunn, R.J., Schlische, R.W., Shipton, Z.K., Wibberley, C.A.J. and Withjack, M.O., 2010. A review of recent developments concerning the structure, mechanics and fluid flow properties of fault zones. *Journal of Structural Geology*, 32(11), pp.1557-1575.
- Faulkner, D.R., Mitchell, T.M., Healy, D. and Heap, M.J., 2006. Slip on 'weak' faults by the rotation of regional stress in the fracture damage zone. *Nature*, 444(7121), p.922.
- Finch, M.A., Weinberg, R.F. and Hunter, N.J., 2016. Water loss and the origin of thick ultramylonites. *Geology*, 44(8), pp.599-602.
- Finch, M.A., Weinberg, R.F. and Hunter, N.J., 2016. Water loss and the origin of thick ultramylonites. *Geology*, 44(8), pp.599-602.
- Fossen, H. and Cavalcante, G.C.G., 2017. Shear zones—A review. *Earth-Science Reviews*, 171, pp.434-455.
- Fossen, H., 2016. *Structural geology*. Cambridge University Press.
- Frost, E., Dolan, J., Sammis, C., Hacker, B., Cole, J. and Ratschbacher, L., 2009. Progressive strain localization in a major strike-slip fault exhumed from midseismogenic depths: Structural observations from the Salzach-Ennstal-Mariazell-Puchberg fault system, Austria. *Journal of Geophysical Research: Solid Earth*, 114(B4).
- Gudmundsson, A., Simmenes, T.H., Larsen, B. and Philipp, S.L., 2010. Effects of internal structure and local stresses on fracture propagation, deflection, and arrest in fault zones. *Journal of Structural Geology*, 32(11), pp.1643-1655.
- Harding, T.P., 1985. Seismic characteristics and identification of negative flower structures, positive flower structures, and positive structural inversion. *AAPG Bulletin*, 69(4), pp.582-600.
- Hayman, N.W. and Kidd, W.S.F., 2002. Reactivation of prethrusting, synconvergence normal faults as ramps within the Ordovician Champlain-Taconic thrust system. *Geological Society of America Bulletin*, 114(4), pp.476-489.
- Hennings, P., Allwardt, P., Paul, P., Zahm, C., Reid, R., Alley, H., Kirschner, R., Lee, B. and Hough, E., 2012. Relationship between fractures, fault zones, stress, and reservoir productivity in the Suban gas field, Sumatra, Indonesia. *AAPG bulletin*, 96(4), pp.753-772.
- Herwegh, M. and Handy, M.R., 1996. The evolution of high-temperature mylonitic microfabrics: evidence from simple shearing of a quartz analogue (norcamphor). *Journal of Structural Geology*, 18(5), pp.689-710.

- Hirth, G. and Tullis, J., 1992. Dislocation creep regimes in quartz aggregates. *Journal of Structural Geology*, 14(2), pp.145-159.
- Holdsworth, R.E., Butler, C.A. and Roberts, A.M., 1997. The recognition of reactivation during continental deformation. *Journal of the Geological Society*, 154(1), pp.73-78.
- Hull, J., 1988. Thickness-displacement relationships for deformation zones. *Journal of Structural Geology*, 10(4), pp.431-435.
- Hussey, A.M., Bothner, W.A. and Aleinikoff, J., 2010. The tectono-stratigraphic framework and evolution of southwestern Maine and southeastern New Hampshire. *Geological Society of America Memoir*, 206, pp.205-230.
- Ji, S., Jiang, Z., Rybacki, E., Wirth, R., Prior, D. and Xia, B., 2004. Strain softening and microstructural evolution of anorthite aggregates and quartz–anorthite layered composites deformed in torsion. *Earth and Planetary Science Letters*, 222(2), pp.377-390.
- Julien, P.S. and Hubert, C., 1975. Evolution of the Taconian orogen in the Quebec Appalachians. *American Journal of Science*, 275, pp.337-362.
- Karabinos, P., Macdonald, F.A. and Crowley, J.L., 2017. Bridging the gap between the foreland and hinterland I: Geochronology and plate tectonic geometry of Ordovician magmatism and terrane accretion on the Laurentian margin of New England. *American Journal of Science*, 317(5), pp.515-554.
- Karabinos, P., Samson, S.D., Hepburn, J.C. and Stoll, H.M., 1998. Taconian orogeny in the New England Appalachians: collision between Laurentia and the Shelburne Falls arc. *Geology*, 26(3), pp.215-218.
- Keith, A., 1923. Cambrian succession of northwestern Vermont. *American journal of science*, (26), pp.97-139.
- Keith, A., 1932. Stratigraphy and structure of Northwestern Vermont.—I. *Journal of the Washington Academy of Sciences*, 22(13), pp.357-379.
- Keranen, K.M., Weingarten, M., Abers, G.A., Bekins, B.A. and Ge, S., 2014. Sharp increase in central Oklahoma seismicity since 2008 induced by massive wastewater injection. *Science*, 345(6195), pp.448-451.
- Kim, J., Klepeis, K., Ryan, P., Glae, M., McNiff, C., Ruksznis, A., Webber, J., 2011. A Bedrock Transect Across the Champlain and Hinesburg Thrusts in West-Central Vermont: Integration of Tectonics with Hydrogeology and Groundwater Chemistry: in West, D., editor, *New England Intercollegiate Geological Conference: Guidebook for Field Trips in Vermont and adjacent New York*, 103rd Annual Meeting, Middlebury, Vermont, Trip B1, p. B1-1 – B1-35.
- Kim, Y.S., Peacock, D.C. and Sanderson, D.J., 2004. Fault damage zones. *Journal of structural geology*, 26(3), pp.503-517.
- Macdonald, F.A., Karabinos, P.M., Crowley, J.L., Hodgins, E.B., Crockford, P.W. and Delano, J.W., 2017. Bridging the gap between the foreland and hinterland II: Geochronology and tectonic setting of Ordovician magmatism and basin formation on the Laurentian margin of New England and Newfoundland. *American Journal of Science*, 317(5), pp.555-596.

- Macdonald, F.A., Ryan-Davis, J., Coish, R.A., Crowley, J.L. and Karabinos, P., 2014. A newly identified Gondwanan terrane in the northern Appalachian Mountains: Implications for the Taconic orogeny and closure of the Iapetus Ocean. *Geology*, 42(6), pp.539-542.
- Means, W.D., 1995. Shear zones and rock history. *Tectonophysics*, 247(1-4), pp.157-160.
- Mitchell, T.M. and Faulkner, D.R., 2009. The nature and origin of off-fault damage surrounding strike-slip fault zones with a wide range of displacements: A field study from the Atacama fault system, northern Chile. *Journal of Structural Geology*, 31(8), pp.802-816.
- Mitchell, T.M., Ben-Zion, Y. and Shimamoto, T., 2011. Pulverized fault rocks and damage asymmetry along the Arima-Takatsuki Tectonic Line, Japan. *Earth and Planetary Science Letters*, 308(3-4), pp.284-297.
- Montési, L.G., 2013. Fabric development as the key for forming ductile shear zones and enabling plate tectonics. *Journal of Structural Geology*, 50, pp.254-266.
- Mundy, E.M., Dascher-Cousineau, K., Gleeson, T., Rowe, C.D. and Allen, D.M., 2016. Complexity of hydrogeologic regime around an ancient low-angle thrust fault revealed by multidisciplinary field study. *Geofluids*, 16(4), pp.673-687.
- Muñoz, J.A., 2017. Fault-related folds in the southern Pyrenees. *AAPG Bulletin*, 101(4), pp.579-587.
- O'Brien, T.M. and van der Pluijm, B.A., 2012. Timing of Iapetus Ocean rifting from Ar geochronology of pseudotachylytes in the St. Lawrence rift system of southern Quebec. *Geology*, 40(5), pp.443-446.
- O'Hara, A.P., Jacobi, R.D. and Sheets, H.D., 2017. Predicting the width and average fracture frequency of damage zones using a partial least squares statistical analysis: Implications for fault zone development. *Journal of Structural Geology*, 98, pp.38-52.
- Oliot, E., Goncalves, P. and Marquer, D., 2010. Role of plagioclase and reaction softening in a metagranite shear zone at mid-crustal conditions (Gotthard Massif, Swiss Central Alps). *Journal of Metamorphic Geology*, 28(8), pp.849-871.
- Passchier, C.W. and Trouw, R.A., 2005. *Microtectonics* (Vol. 1). Springer Science & Business Media.
- Paul, P.K., Zoback, M.D. and Hennings, P.H., 2009. Fluid flow in a fractured reservoir using a geomechanically constrained fault-zone-damage model for reservoir simulation. *SPE Reservoir Evaluation & Engineering*, 12(04), pp.562-575.
- Platt, J.P., 2015. Influence of shear heating on microstructurally defined plate boundary shear zones. *Journal of Structural Geology*, 79, pp.80-89.
- Rankin, D.W., Coish, R.A., Tucker, R.D., Peng, Z.X., Wilson, S.A. and Rouff, A.A., 2007. Silurian extension in the Upper Connecticut Valley, United States and the origin of middle Paleozoic basins in the Quebec embayment. *American Journal of Science*, 307(1), pp.216-264.
- Ratcliffe, N.M., Stanley, R.S., Gale, M.H., Thompson, P.J., Walsh, G.J., Rankin, D.W., Doolan, B.L., Kim, J., Mehrtens, C.J., Aleinikoff, J.N. and McHone, J.G., 2011. Bedrock geologic map of Vermont (No. 3184). US Geological Survey.

- Riley, P.R., Goodwin, L.B. and Lewis, C.J., 2010. Controls on fault damage zone width, structure, and symmetry in the Bandelier Tuff, New Mexico. *Journal of Structural Geology*, 32(6), pp.766-780.
- Rowley, D.B., 1982. New methods for estimating displacements of thrust faults affecting Atlantic-type shelf sequences: With an application to the Champlain Thrust, Vermont. *Tectonics*, 1(4), pp.369-388.
- Rowley, D.B., 1983. Contrasting fold-thrust relationships along northern and western edges of the Taconic allochthons; Implications for a two-stage emplacement history. In *Geological Society of America Abstracts with Programs* (Vol. 15, p. 174).
- Ryan, P.C., Kim, J.J., Mango, H., Hattori, K. and Thompson, A., 2013. Arsenic in a fractured slate aquifer system, New England, USA: influence of bedrock geochemistry, groundwater flow paths, redox and ion exchange. *Applied geochemistry*, 39, pp.181-192.
- Savage, H.M. and Cooke, M.L., 2003. Can flat-ramp-flat fault geometry be inferred from fold shape?: A comparison of kinematic and mechanical folds. *Journal of Structural Geology*, 25(12), pp.2023-2034.
- Scisciani, V., 2009. Styles of positive inversion tectonics in the Central Apennines and in the Adriatic foreland: Implications for the evolution of the Apennine chain (Italy). *Journal of Structural Geology*, 31(11), pp.1276-1294.
- Séjourné, S. and Malo, M., 2007. Pre-, syn-, and post-imbrication deformation of carbonate slices along the southern Quebec Appalachian front—implications for hydrocarbon exploration. *Canadian Journal of Earth Sciences*, 44(4), pp.543-564.
- Sibson, R.H., 1977. Fault rocks and fault mechanisms. *Journal of the Geological Society*, 133(3), pp.191-213.
- Stanley, R.S. and Ratcliffe, N.M., 1985. Tectonic synthesis of the Taconian orogeny in western New England. *Geological Society of America Bulletin*, 96(10), pp.1227-1250.
- Stanley, R.S., 1987. The Champlain thrust fault, lone rock point, Burlington, Vermont. *Northeastern Section of the Geological Society of America: Geological Society of America Centennial Field Guide*, 5, pp.225-228.
- Stanley, R.S. and Sarkisian, A., 1972. Analysis and chronology of structures along the Champlain Thrust west of the Hinesburg synclinorium, New England *Intercollegiate Geological Conference Guidebook*. BL Doolan, RS Stanley, pp.117-149.
- Stanley, R.S., 1990. The evolution of mesoscopic imbricate thrust faults—an example from the Vermont Foreland, USA. *Journal of structural geology*, 12(2), pp.227-241.
- Stanley, R. and Wright, S., 1997, The Appalachian foreland as seen in northern Vermont, *in* Grover, T.W., Mango, H.N., and Hasenohr, E.J., eds., *Guidebook to field trips in Vermont and adjacent New Hampshire and New York: New England Intercollegiate Geological Conference*, v. 89, p. B1, 1-33.

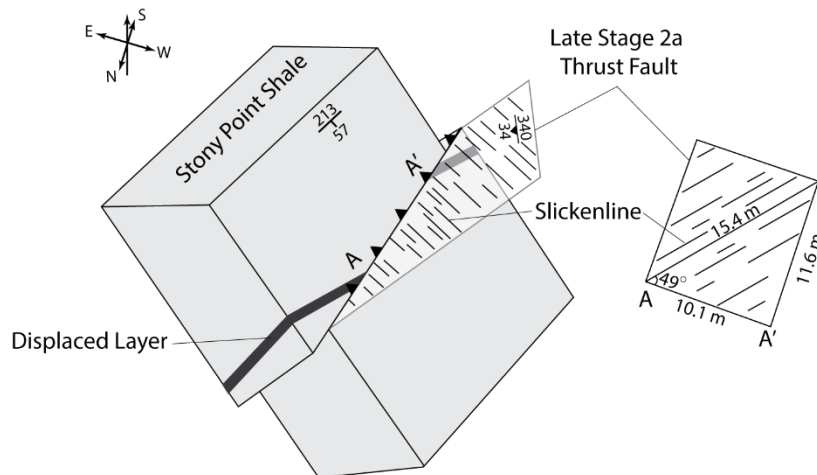
- Suppe, J., 1983. Geometry and kinematics of fault-bend folding. *American Journal of science*, 283(7), pp.684-721.
- Thompson, P.J. and Thompson, T.B., 2003. The Prospect Rock thrust: western limit of the Taconian accretionary prism in the northern Green Mountain anticlinorium, Vermont. *Canadian Journal of Earth Sciences*, 40(2), pp.269-284.
- Treagus, S.H., 1988. Strain refraction in layered systems. *Journal of Structural Geology*, 10(5), pp.517-527.
- Tremblay, A. and Pinet, N., 2005. Silurian to early Devonian tectonic evolution of the northern Appalachians (Canada and northeastern USA) and the origin of the Connecticut Valley-Gaspé and Merrimack troughs. *Geological Magazine*, 142, pp.1-16.
- Tremblay, A. and Pinet, N., 2016. Late Neoproterozoic to Permian tectonic evolution of the Quebec Appalachians, Canada. *Earth-science reviews*, 160, pp.131-170.
- Turner, J.P. and Williams, G.A., 2004. Sedimentary basin inversion and intra-plate shortening. *Earth-Science Reviews*, 65(3-4), pp.277-304.
- Twiss, R.J. and Moores, E.M., 1992. *Structural geology*. Macmillan.
- van Staal, C.R., Barr, S.M. and Percival, J.A., 2012. Lithospheric architecture and tectonic evolution of the Canadian Appalachians and associated Atlantic margin. *Tectonic styles in Canada: the LITHOPROBE perspective*. Edited by JA Percival, FA Cook, and RM Clowes. Geological Association of Canada, Special Paper, 49.
- Van Staal, C.R., Dewey, J.F., Mac Niocaill, C. and McKerrow, W.S., 1998. The Cambrian-Silurian tectonic evolution of the northern Appalachians and British Caledonides: history of a complex, west and southwest Pacific-type segment of Iapetus. *Geological Society, London, Special Publications*, 143(1), pp.197-242.
- Ventissette, C., Montanari, D., Sani, F. and Bonini, M., 2006. Basin inversion and fault reactivation in laboratory experiments. *Journal of Structural Geology*, 28(11), pp.2067-2083.
- Vitale, S. and Mazzoli, S., 2008. Heterogeneous shear zone evolution: the role of shear strain hardening/softening. *Journal of Structural Geology*, 30(11), pp.1383-1395.
- Wall, B. R. G., 2006. Influence of depositional setting and sedimentary fabric on mechanical layer evolution in carbonate aquifers. *Sedimentary Geology*, 184(3-4), 203-224.
- Walsh, G.J. and Aleinikoff, J.N., 1999. U-Pb zircon age of metafelsite from the Pinney Hollow Formation; implications for the development of the Vermont Appalachians. *American Journal of Science*, 299(2), pp.157-170.
- Warren, J.M. and Hirth, G., 2006. Grain size sensitive deformation mechanisms in naturally deformed peridotites. *Earth and Planetary Science Letters*, 248(1-2), pp.438-450.
- Welby, C.W., 1961. Occurrence of *Foerstephyllum* in Chazyan rocks of Vermont. *Journal of Paleontology*, pp.391-394.
- West, D., Kim, J., Klepeis, K., Webber, J., 2011, Classic Bedrock Teaching Localities in the Champlain Valley between Middlebury and Burlington, Vermont: in West, D., editor, *New England Intercollegiate Geological Conference: Guidebook for Field*

- Trips in Vermont and adjacent New York, 103rd Annual Meeting, Middlebury, Vermont, Trip B1, p. C51-C523.
- White, S.H., Burrows, S.E., Carreras, J., Shaw, N.D. and Humphreys, F.J., 1980. On mylonites in ductile shear zones. *Journal of Structural Geology*, 2(1-2), pp.175-187.
- Wibberley, C.A., Yielding, G. and Di Toro, G., 2008. Recent advances in the understanding of fault zone internal structure: a review. Geological Society, London, Special Publications, 299(1), pp.5-33.
- Williams, H., 1979. Appalachian orogen in Canada. *Canadian Journal of Earth Sciences*, 16(3), pp.792-807.
- Wojtal, S. and Mitra, G., 1986. Strain hardening and strain softening in fault zones from foreland thrusts. *Geological Society of America Bulletin*, 97(6), pp.674-687.
- Yeck, W.L., Weingarten, M., Benz, H.M., McNamara, D.E., Bergman, E.A., Herrmann, R.B., Rubinstein, J.L. and Earle, P.S., 2016. Far-field pressurization likely caused one of the largest injection induced earthquakes by reactivating a large preexisting basement fault structure. *Geophysical Research Letters*, 43(19).

APPENDIX I

Approximate net displacement on late stage 2a thrust faults observed at “the driveway” was calculated to be 15–29 meters. This approximation was determined by the following steps:

1. I first located a stage 2a thrust fault that could be traced for an extended distance.
2. I located a unit that was cut by the fault and located portions of this unit in both the hanging wall and the footwall of the fault.
3. I measured the distance of apparent offset between these layers. For this fault it was 10.1 m. I also included the maximum apparent displacement of 21.8 m.
4. I measured the orientation of the fault – 340/34 NE
5. I measured the orientation of the outcrop face – 213/57 NW
6. I measured the orientation of the slickenlines – 27-110
7. I determined the rake of the fault against the outcrop face at 49°
8. Using trigonometry, I calculated the approximate net displacement of this fault to be 15.4 meters [minimum] and 29 meters [maximum].



Approximate minimum displacement - 10 meters [apparent]
15 meters [net]

Approximate maximum displacement - 19 meters [apparent]
29 meters [net]

APPENDIX II

The following table provides information regarding thin sections cut from samples collected from Lone Rock Point, Burlington, Vermont. Sample R7-02-17 was collected from “The Driveway”.

Sample ID	Single Arrow	Face	Purpose	S/D of Sample	Notes
R7-02-17	48-108	198	Lith; Kin	108/85	Cut along fault in line with slicks. Bottom of sample is fault
CT-HW-01A-17	06-185 Arrow points to 005	264	Lith; Normal Fault	005/86	Normal faults within vein? From hanging wall. Bottom of hand-sample is CT
CT-HW-01B-17	06-185 Arrow points to 005	264	Lith; Kin	005/86	Cut next to HW-01A. No apparent faults. Vein cuts mineral below.
CT-HW-02-17	06-175 Arrow points to 355	265	Lith; Fault Rocks; Kin	348/90	From hanging wall. Bottom of hand sample is CT. Veins are folded? Or thrust faults?
CT-HWF-01A-17	NA	NA	Lith; Fault Rocks	NA	What is the black vein? Bottom of hand sample is CT.
CT-HW-03A-17	260-05	170	Lith; Fault Rocks; Kin	260/85	Hanging wall rock. Black fault rock to top. Normal fault top right. Unknown Lith.
CT-HW-03C-17	350-10 Arrow points to 170	80	Lith; Fault Rocks; Kin	170/85	Hanging wall rock. Micro faults with unknown lith and fault rocks
CT-HW-04-17	100/05 Arrow points to 280	190	Lith; Kin	280/90	Hanging wall fault rock. Black vein at top? Sheared lithology, with micro-faults
CT-C-01-17	175-35	275	Lith; Kin	170/75	Core Rock . Slicks on opposite side of arrow. Micro faults and folds.

CT-C-02-17	SOUTH	Unknown sample destroyed	Lith; Kin, Fold Characteristics	Unknown	Folded shale and veins. From S3 High strain zone.
CT-C-02.3-17	185-32 Arrow point to 005	270	Lith; Kin; Fold	185/90	High strain rock. Folds of shale? Very deformed.
CT-C-03A-17	110-00	200	Lith; Mylonite	110/90	Mylonite. Unknown Lth. Fault within it
CT-C-03B-17	110-00	200	Lith; Mylonite	110/90	Mylonite. Unknown Lth. Folded.
CT-C-03C-17	145-00	235	Lith; Kin	145/90	Mylonite of unknown lith
CT-C-03D-17	145-00	235	Lith; Kin	145/90	Mylonite of unknown lith
CT-HW-06A-17	108-15	18	Lith; Vein	288/85	Dunham Dolostone. Look at lith. Vein is offset - steeply
CT-HW-06B-17	108-15	198	Lith; Vein	288/85	Dunham Dolostone. Vein is not offset but cut another vein.
CT-HW-07A-17	104-14	194	Lith; Fault Rock; Kin	104/90	Hanging wall. Bottom of sample is CT. Unknown Lith of fault rock
CT-HW-07B-17	000-00	95	Lith; Fault Rock; Kin	185/80	Hanging wall. Bottom of sample is CT. Unknown Lith of fault rock. Normal fault is present.
CT-C-10-17	155-25	60	Lith	350/70	Core Rock from S4 Outcrop Just below cataclasite in contact with CT

CT-C-11A-17	BOTTOM	Unknown	Lith	Unknown	Cataclasite. Top is in contact with CT
CT-C-11B-17	BOTTOM	Unknown	Lith	Unknown	Cataclasite. Top is in contact with CT
CTF-01-16	NA	NA	Lith	Float	Unknown Lith. What is the black stuff?
CTF-02-16	NA	NA	Lith	Float	Unknown Lith. What is the black stuff?
CTF-03-16	NA	NA	Lith	Float	Unknown Lith.
CTF-04-16	NA	NA	Lith	Float	Unknown Lith.
CTF-05-16	NA	NA	Lith	Float	Unknown. Folded
CTF-06-16	NA	NA	Lith	Float	Unknown. Folded
PST-01X	NA	NA	Lith	Float	PST. Perpendicular (apparent) to bedding. Is it PST. What is host rock?
PST-01A	NA	NA	Lith	Float	PST.
PST-01B	NA	NA	Lith	Float	PST.
PST-01C	NA	NA	Lith	Float	PST.